UNIVERSITY OF OKLAHOMA

GRADUATE COLLEGE

THE USE OF RECYCLED MATERIAL BACKFILLS TO MITIGATE THE EFFECTS OF EXPANSIVE SOILS ON SUBTERRANEAN STRUCTURES

A THESIS

SUBMITTED TO THE GRADUATE FACULTY

in partial fulfillment of the requirements for the

Degree of

MASTER OF SCIENCE

By

JENNA JACOBY
Norman, Oklahoma
2016

THE USE OF RECYCLED MATERIAL BACKFILLS TO MITIGATE THE EFFECTS OF EXPANSIVE SOILS ON SUBTERRANEAN STRUCTURES

A THESIS APPROVED FOR THE
SCHOOL OF CIVIL ENGINEERING AND ENVIRONMENTAL SCIENCE

BY

_____
Dr. Amy Cerato, Chair

_____
Dr. Gerald Miller

_____
Dr. K.K. Muraleetharan

This Thesis is dedicated to my parents, Jim and Deanna, and sister Rachel, for this wouldn't be possible without your full support. Thank you.

Acknowledgements

First, I would like to thank my advisor and mentor, Dr. Amy Cerato. You were the one to first get me interested in geotechnical work, and without your influence, guidance, and support over the past few years, I would not be in the position I am today. I am very grateful for you taking me on as your student and always helping me along the way.

I would also like to thank Mike Schmitz for his tremendous help in the construction of the test setup and for answering my many questions along the way. You always knew how to carry out and improve my ideas, and for that I am appreciative.

Thank you to Dr. Gerald Miller and Dr. Kanthasamy Muraleetharan for being on my committee and for always providing me with valuable feedback. Additionally, thank you to Dr. Kianoosh Hatami for providing guidance in the computer modeling portion of this project.

A huge thank you to Michelle Basham for helping me in all aspects of the project, and for picking up the slack when I was having trouble doing it on my own. In addition, thanks to Rodney Collins for always being patient while answering my many questions.

Lastly, a big thank you to my friends Austin, Jason, Nate, and Jake for keeping me sane this past year. Without all of you, this past year would have been significantly less fun. I am very thankful I had you to complain to when I needed it, the ability to count on you when I needed help, and for always providing a laugh.

Table of Contents

List of Tables

List of Figures

Abstract

The extreme annual weather patterns of the Midwest United States have created a demand for basements as emergency shelters in both residential and commercial structures. However, with the majority of the Midwest experiencing vast changes in the weather patterns between seasons while simultaneously being underlain by expansive soils, the associated shrink and swell generates a significant problem for basement design. As traditional backfill materials can be costly and of limited availability, this study looks at using recycled backfills to mitigate the effects of expansive soils on basements as a possible solution to both issues. This project includes a review of the current literature describing the effects of expansive soils on basements and the traditional mitigation methods used. Specifically, the review focused on the different types of backfill materials used and their effectiveness on mitigating the effects of shrink and swell.

Three recycled materials – crumb rubber, glass cullet, and shredded plastic – were evaluated for desirable characteristics prior to bench scale tests, and one material, crumb rubber, was used for bench scale tests. The crumb rubber was not treated outside of compaction efforts. The evaluated recycled backfill materials had material properties that reflected traditional backfill properties, such as particle size and consistency. Laboratory experiments were conducted to analyze the effects of shrink and swell on small scale basement walls in K_0 conditions without any backfill. Various thicknesses of recycled backfill were tested to determine the optimal thickness in reducing the effects of the shrink and swell. The results of this investigation provided information on the effectiveness of recycled materials as an alternate solution to traditional backfills for

subterranean structures built in expansive soils. Recycled materials will simultaneously provide an environmentally conscious option. This paper discusses the testing procedures, interpretation of the acquired data, and recommendations for the use of recycled materials as an alternate means to customary backfill materials.

Three bench scale tests were run using crumb rubber, and one additional test was run with soil only. The three tests with crumb rubber were compared to the test with soil only. It was determined that a 1:6 backfill height to total height ratio produced at maximum a 66% decrease in swell pressure at 80% soil compaction. However, at 90% soil compaction, the percent reduction decreased to 27%. It was also found that there is a strong correlation between compaction percentage and reduction in swell pressure when using the same backfill height to total height ratio, with a linear regression value of 0.9918 when comparing the three tests that used crumb rubber. Using this correlation and extrapolating the data to 95% compaction, the swell pressure would only be reduced 12% if a 1:6 backfill height to total height ratio is used. When comparing crumb rubber cost to sand fill cost, the cost of crumb rubber is approximately 1.1 to 8.7 times more expensive than sand, when normalizing for the amount needed.

Looking at the finite difference modeling, the FLAC results are somewhat comparable to the actual tests completed. The general patterns are overall correct, with the displacement occurring in the expected direction and the greatest stresses on the bottom of the box towards the center. However, some of the actual values are much greater than what was actually seen in the bench scale tests.

Chapter 1: Introduction

Expansive soils are found across the United States, but are most prevalent in the Midwest region. A major problem with expansive soils is their physical tendency to have large amounts of shrink and swell with changes in moisture content. Constructing subterranean structures in these types of soils can be difficult given the extreme swell pressures that expansive soils can exhibit under changing moisture conditions. These swell pressures need to be quantified and mitigated given the need for underground emergency shelters. If the subterranean structure is built in expansive soils, the soil can exert extreme pressures on the walls of basements or storm shelters, for example, causing the walls to deform and crack. The current methods of mitigating the effects of shrink and swell include complete removal and replacement with select fill, which is expensive and using a sand backfill surrounding the underground structure. Using a sand backfill can be expensive if a nearby source of clean sand is not available. With the goal of creating a sustainable and resilient foundation system to be constructed in expansive soils, it is necessary to investigate alternative materials to alleviate expansive soil pressures around subterranean structures.

This project will focus on using recycled rubber as backfill for basements and other subterranean structures. This research will focus on the recycled rubber's effectiveness in mitigating the shrink and swell pressures exerted on basement walls in relation to a typical non-swelling soil. The project will be completed in two main stages: a literature review on the current types of mitigation methods used and typically used backfills followed by bench-scale laboratory testing to measure the effects of the type and thickness of recycled

rubber backfill on expansive soil pressures exerted on rigid (K_0) walls. The ultimate goal is to determine which, and how much, recycled material is both efficient in mitigating shrink and swell effects while simultaneously being a cost efficient option.

Chapter 2: Literature Review

2.1 Problems with Expansive Soils

Clays are typically problematic foundation materials due to their low shear strength, high compressibility potential and, depending on mineralogy, being highly expansive. Additionally, low shear strength is only worsened with the addition of water [1]. Highly expansive soils are found primarily throughout the Midwest, with a large concentration in Oklahoma. When these soils swell, significant swelling pressures are exerted on foundations and subterranean structures. These pressures can reach 30,000 pounds per square foot (psf) at their maximum [2]. During the dry season, these same soils can shrink significantly, resulting in differential movement of the soil itself. These differential movements create an uneven distribution of pressure for the structure, resulting in cracking in the foundations and walls, as well as wall deformations [2]. Because of this, basements throughout the Midwest are very uncommon.

Apart from the issue of safety for the building occupants, engineers working in areas underlain by expansive soils run the risk of being sued if foundation failures occur [3]. With approximately 2.3 billion dollars (in 1988) of damage caused annually in the United States alone, expansive soils create a monetary risk situation [4]. While an engineer can recommend the best foundation design, there is no obligation of the client to pay for the top design. Though there are regulations on foundation design, such as those found in the International Building Code (IBC), these are only minimum requirements and are often vague stipulations. For example, as stated under the 2012 IBC, “deflection and racking of the supported structure shall be limited to that which will not interfere with the usability

and serviceability of the structure" [5]. While this is technically a regulation, there is still room for interpretation. However, when failures do occur, there is a risk that the client will choose to seek reparations for the failures. By providing safe foundations at a lower cost, the liability risk is lowered [3].

2.2 Mitigation Methods

2.2.1 Typical Mitigation Methods

There are various mitigation methods currently used throughout the United States to reduce damage caused to structures from expansive soils. These include removing the expansive soil and replacing it with a non-expansive soil, utilizing non-expansive backfills, chemical stabilization with fly ash [1], lime, and cement, and heat treatments [6], with all methods proving highly effective. Based on the results presented by Al-Rawas et al., adding 6% lime reduced the swell percent and swell pressure to zero [6]. Additionally, calcination of the soil at 740 °C and 780 °C reduced the swelling potential to zero [6]. However, while these methods are effective, they are not always inexpensive. In a study comparing costs for chemical soil stabilization versus cut and fill techniques, chemical stabilization was significantly cheaper, averaging $2.45 per square yard for Portland cement and fly ash versus $23.50 per square yard for cut and fill [7]. Yet, for a typical structure, the additional cost can still extend into the thousands of dollars. Research has also been done on stabilizing clays using granulated blast furnace slag (GBFS) [8]. As detailed in the article, the addition of GBFS resulted in an overall decrease in the swell percentage. With additional curing time, the swell percentage decreased by up to 10 times the original percentage [8]. While there has been extensive research on

expansive soil properties and chemical soil stabilization, there is limited research on non-chemical mitigation methods.

2.2.2 Non-Swelling Backfill

Katti et al. performed an extensive study on the effectiveness of using cohesive non-swelling (CNS) soil to mitigate shrink and swell of a highly expansive clay [9]. In the study, Katti performed several large scale swell tests with varying amounts of non-swelling soil. The test setup involved four large tanks, two made of concrete and two made of steel, with a thin coating of grease coating the inside to minimize side friction, and with lateral pressure measuring units placed approximately every 60cm. The soil was placed inside the box and compacted in 14 different layers. Air dry pluviated sand, air dry compacted sand, compacted saturated sand, air dry pluviated CNS, compacted saturated CNS, air dry pluviated expansive soil, air dry compacted expansive soil and compacted saturated expansive soil were each tested to know how that soil would swell in its natural state. All of the soils in the pluviated condition were pulverized to pass a B.S. Sieve No. 7 and then dropped from a height of 30cm for every 7.5cm layer. There were three main testing arrangements using various expansive soil/CNS combinations: expansive soil with varying amounts of CNS backing and no CNS on top, expansive soil with varying amounts of CNS on top and no CNS backing, and expansive soil with varying amounts of CNS backing with varying amounts of CNS on top. The various testing arrangements were allowed to saturate for a period of at least 60 days, during which water was filtered through the system through small layers of sand lining the perimeter of the steel box. During saturation, the lateral swelling pressures were measured

and the vertical change in height was measured using probe plates. It was found that the lateral pressure at the surface was almost 0, and increased rapidly until approximately 1.2 – 1.5 meters below the surface. At this point, the lateral pressure remained approximately constant. This pattern can be seen in Figures 1-3, recreated after Katti et al. 1983.

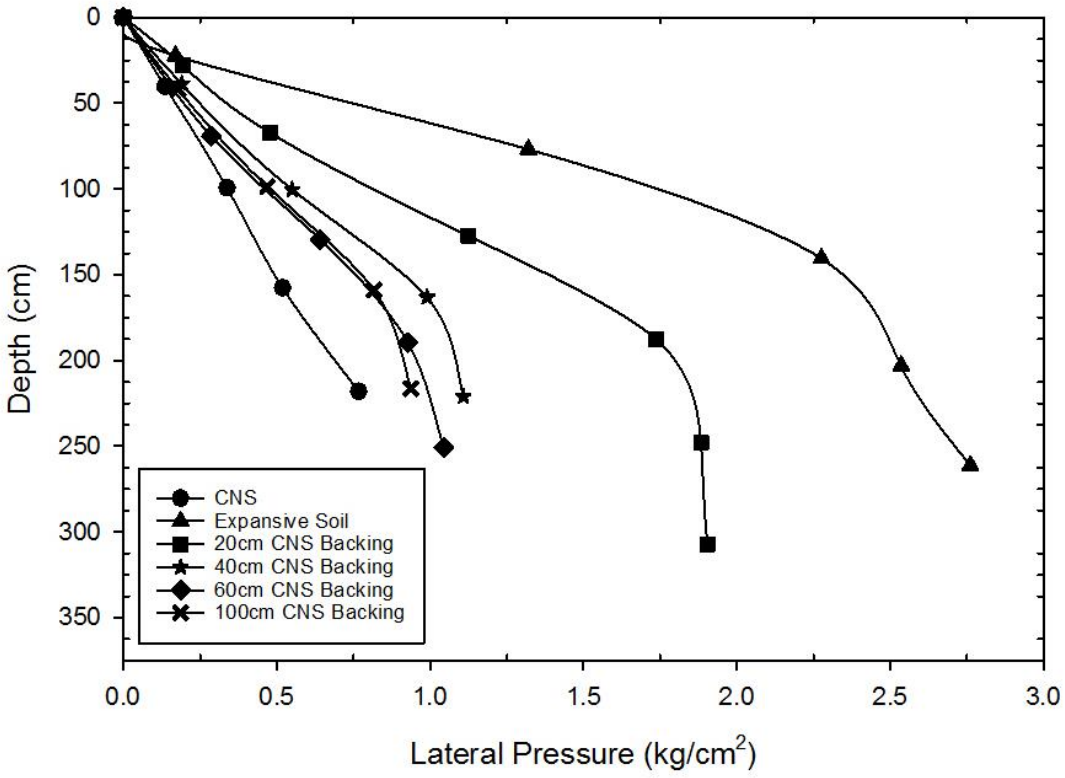

Figure 1. Variation of Lateral Pressure with Depth after Compaction and Saturation for Expansive Soil with Varying Amounts of CNS Backing and no CNS on top (after Katti et al. 1983)

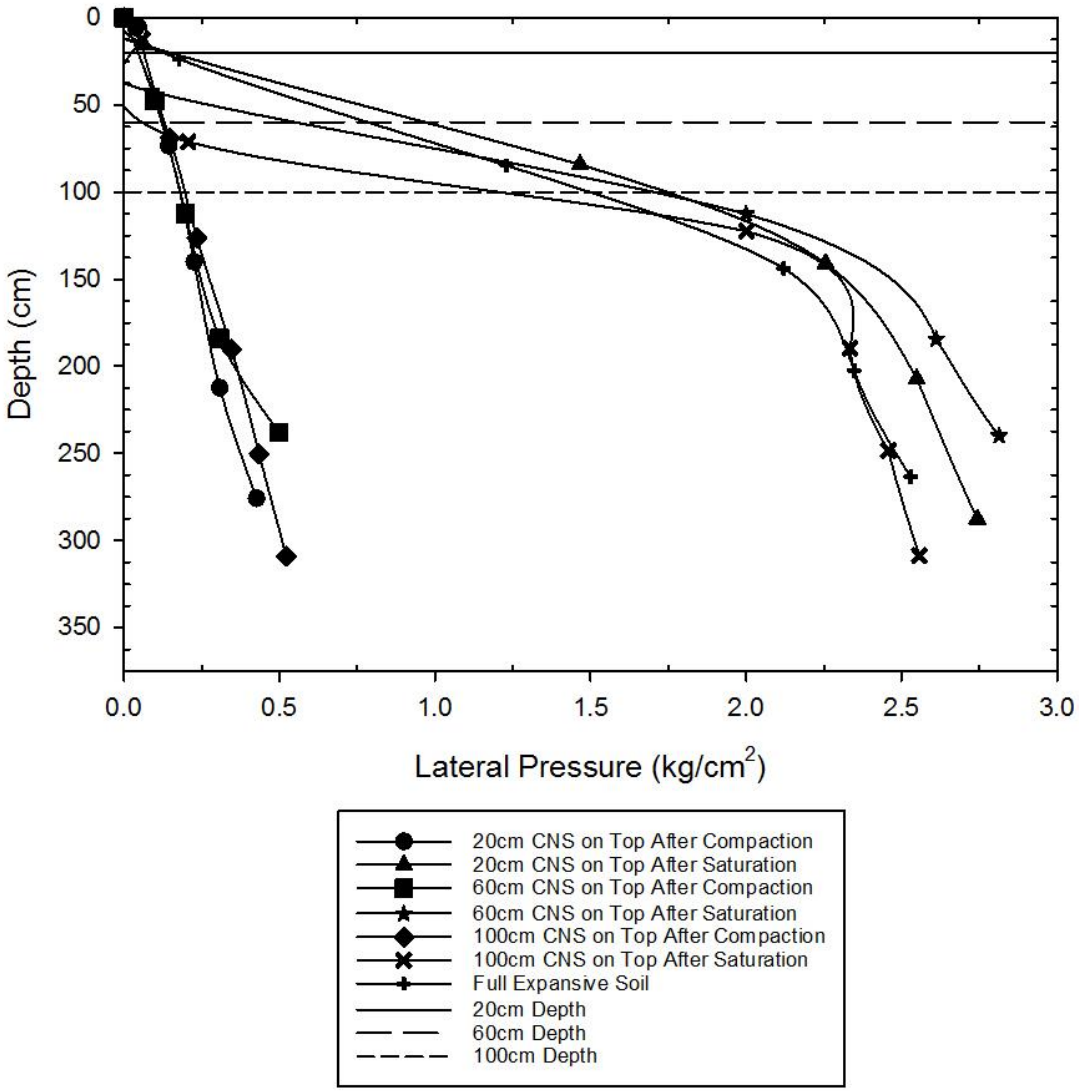

Figure 2. Variation of Lateral Pressure with Depth after Compaction and Saturation for Expansive Soil with Varying Amounts of CNS on top and no CNS Backing (after Katti et al. 1983)

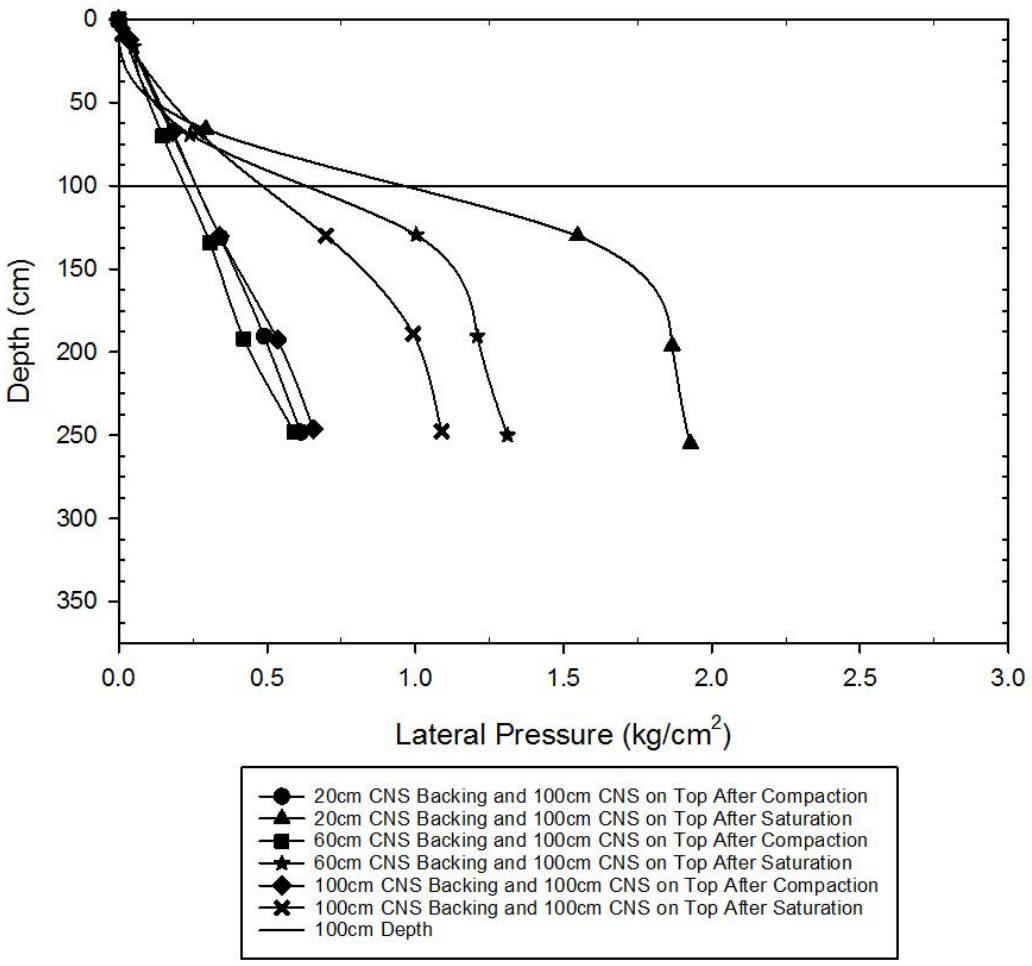

Figure 3. Variation of Lateral Pressure with Depth after Compaction and Saturation of Expansive Soil with Varying Amounts of CNS Backing and 100cm CNS on top (after Katti et al. 1983)

As shown in the preceding figures, reduction in lateral pressures is mostly dependent on the amount of CNS backing. Comparing the combination of CNS backing and 100cm CNS on top with CNS backing and no CNS on top, it can be seen that having no CNS on top reduces the lateral pressures more. However, it was noted that when there was CNS on top of the expansive soil, there was little to no upward heave. Comparisons of the percent reduction, as well as the equations for determining percent reduction for each scenario, can be seen in Table 1.

Table 1. Percent Reduction in Lateral Pressure

Depth of Backing (cm)	Depth of CNS on Top (cm)	Percent Reduction	Equation to Determine Percent Reduction*
20	0	48.0	$100\left(\frac{\text{L EXPO - L BACKING}}{\text{L EXPO - L CNS}}\right)$
40	0	81.67	
60	0	86.26	
100	0	90.0	
20	100	38.88	$\frac{\text{L EXPO - L BACKINGS 100}}{\text{L EXPO 100 - L CNS}}$
60	100	72.98	
100	100	87.92	

*L EXPO = lateral pressure in expansive soil; L BACKING = lateral pressure with various CNS backings; L CNS = lateral pressure in CNS alone at corresponding depths; L EXPO 100 = lateral pressure in expansive soil underlying the 100cm CNS thickness; L BACKINGS 100 = lateral pressures with various CNS backings with 100cm CNS on top of expansive soil

2.2.3 Alternative Backfill

2.2.3.1 Geofoam

Geofoam, made of expanded polystyrene (EPS) or extruded polystyrene (XPS), is a lightweight engineered material used as a fill material in many different applications. Geofoam has become a popular fill material because of its lightweight and low density properties while still having high compressive strength. Geofoam blocks typically have densities ranging from 11 to 30 kg/m^3 and can be handled without the use of machines, therefore reducing cost during construction [10]. While being a low density material, EPS blocks still have high compressive strengths. Based on the ASTM standard, an EPS block with a density of 12 kg/m^3 (the lowest density block typically used) has a compressive strength 35 kPa at a 10% strain [10]. As well as having desirable engineering properties, geofoam is effectively used as a fill material to help reduce swelling pressures exerted on structures. In a study conducted by Ikizler et al., varying thicknesses of EPS geofoam were tested to see what thickness was required to minimize the swelling pressure

produced by a highly expansive clay [11]. In the study, a steel box with dimensions of 250mm x 250mm x 300mm was filled with expansive clay. Three geofoam thicknesses were tested, as well as expansive soil with no geofoam fill. It was found that geofoam reduced both the lateral and vertical swelling pressures, and the percent reduction increased as the thickness of geofoam increased. Furthermore, it was found that a ratio of 1:5 (thickness of EPS geofoam to height of the steel testing box) proved most effective in reducing the swelling pressure [11].

2.2.3.2 Rubber

In a study conducted on the effect of shredded waste tire on various clay properties, three types of clay were used, each with five different percentages of shredded tire ranging from 0% to 20% mixed together, to create fifteen soil-tire mixtures. Physical property tests and compaction tests were then run on each mixture [12]. The study concluded that with an increase in the percentage of shredded tires, the plasticity index and permeability of the soil will decrease, while the shear strength will increase. In all three soils, the compression index decreased as the amount of shredded tire increased. Furthermore, the study found that an increase in shredded tire decreased both the swelling pressure and swelling potential of each clay material.

In an investigation done on the effects of specimen and rubber particle sizes in soil-rubber mixtures, multi-scale (small scale, large scale, and field scale) testing was done on samples with varying soil-rubber ratios [13]. Small scale testing was done with an oedometer 19mm in height, while large scale testing was done with a triaxial machine

with a sample 152mm in height. Field scale tests were 102mm in height, with a total volume of 0.19 m^3. Across each scale, it was determined that the most significant factor in the swell percentage and swelling pressure was the water content, followed by relative compaction and rubber content. It was also found that an increase in nominal rubber particle size resulted in an increase in swell percentage and pressure. Overall, it was found that an increase in specimen size resulted in a decrease in swell percentage and pressure, though it was noted that this could be due to different diameter ratios or variations in saturation. Furthermore, the specimen size did not have a significant effect on compressibility parameters.

2.2.3.3 Plastic

A case study performed at the University of Alabama looked at the effectiveness of using recycled plastic bottles as a lightweight fill for geotechnical applications [14]. The study used varying sized plastic bottles held together with a polyurethane adhesive to form a 2' x 2' x 2' sample. Small samples were also tested for compressive strength. Tests showed that the plastic bottle samples have approximately half of the compressive strength of geofoam materials, but are still stronger than many soils typically used in geotechnical applications. A field study was also completed, where the lightweight plastic blocks were used behind a retaining wall along a bike trail. Blocks made from the plastic bottles and foam were placed behind the wall, as well as loose bottles being placed around the blocks "to achieve the desired final gradient of the site." Urethane foam was used to hold the loose bottles in place, and was given 24 hours to cure. Finally, a geotextile was used to cover the fill to keep soil particles out. As indicated in the article, the fill is still

"performing above expectations and cannot be distinguished from the surrounding natural material."

2.2.3.4 Glass

A study completed in Victoria, Australia looked at the application of recycled crushed glass in roadway applications [15]. Glass of coarse, medium, and fine particle size was analyzed. Compaction curves for fine and medium grain sizes showed that they exhibited typical curves as those of a poorly graded sand, and coarse grained glass did not present a typical curve. Both durability and abrasion resistance were tested for each type of glass, where the Los Angeles (LA) abrasion test and post-compaction sieve analysis were used. The LA abrasion test indicated that fine and medium grained glass have values similar to that of crushed rock, while the sieve analysis indicated that post compaction, there is not a significant change in the gradation curve. Hydraulic conductivity tests indicated that the fine and coarse grained glass have comparable hydraulic conductivity values of sand and gravel mixtures. Overall, the study concluded that fine and medium grained glass could be a suitable geotechnical material as it produced similar results to that of a sand or gravel, while coarse grained glass did not present desired properties (i.e. poorly sized/shaped particles after compaction, high segregation potential, and lack of absorption).

In order to bring non-swelling material backfill into mainstream construction as a method to mitigate expansive soil pressures on basement walls (K_0 conditions), it is necessary to fully understand the pressures exerted on the basement walls. A Finite Element Model or Finite Difference Model is needed to be able to predict K_0 pressures in a certain clay

type and show a design engineer the non-swelling backfill thickness required, based on the type chosen, to mitigate the expected pressures. In order to calibrate this model, data from carefully controlled physical experiments are needed. While there have been pressure measurements made with varying thicknesses and backfill materials, such as non-swelling cohesive soil (Katti et al. 1983) and geofoam (Ikizler et al.), as previously mentioned, the studies on the recycled materials including rubber, plastic, and glass, have not specifically measured the pressures along wall height or varied thicknesses of backfill. The studies mentioned were primarily concerned with how the existence of these materials affected the original soil properties, i.e., how was strength changed with the addition of a certain percentage of recycled material. Therefore, this study aims to fill that knowledge gap and provide pressure measurements along a rigid wall with varying thicknesses of the recycled material, rubber. The results from this study, along with the non-swelling cohesive soil and geofoam experiments, will be used for model calibration.

2.3 Testing Methods

2.3.1 Lateral and Vertical Swelling

When testing the swell pressure of a soil, both vertical and lateral swelling can be significant. However, the lateral swelling of soil is not understood as well as the vertical swelling. The purpose of a study conducted in Turkey was to get a better concept of lateral swelling behavior of an expansive soil [16]. In the study, a modified oedometer was used to measure lateral swelling pressure at the midpoint of the ring. Vertical swelling pressures were also measured. Both the initial water content and initial dry density were modified for different tests. It was found that the lateral swelling pressures

were smaller than the vertical swelling pressures. Furthermore, it was determined that for samples with the same initial dry density, the swell ratio increased with initial water content.

2.3.2 Evaluating Swell Pressure

There are several methods in which swelling pressures can be measured. The most common is the constant volume swell test or one dimensional swell test. Other methods include free swell test and triaxial test. Triaxial tests have the benefit of providing a variation of confining stress situations and drainage conditions. For example, as detailed in Powell et al., the triaxial swelling tests were conducted in two stages. Stage one involved isotropic consolidation and stage two involved adding water to the system while keeping a constant volume and constant mean stress [17]. The free swell test provides a reference of the soil's expansion potential. In free swell tests, the swelling pressure is defined as "the pressure that is required to recompress a completely swollen soil sample to its original unloaded volume" [18].

A general correlation for swelling pressure based on the initial water content and initial dry unit weight was found and noted as giving a good relationship between the predicted and measured swelling potential [18]. Another strong correlation has been identified between measured and predicted swell pressures. Erzin and Erol identified that this correlation is primarily dependent on the initial dry density and plasticity index, and less dependent on initial water content [4]. Though it is not exact, it is a simple way at identifying how much a particular soil with known parameters should swell. The

following tables outline the equations used to estimate the swell pressure, where P_s = swell pressure (kg/cm^2), ρ_{dry} = initial dry density (g/cm^3), w = initial water content (%), LI = liquidity index (%), and R = coefficient of multiple determination.

Table 2. Predicted Swell Pressure as a Function of Initial Water Content

PI (%)	Equation	R (%)	Standard Deviation (%)
30	log(Ps) = -5.424 + 3.084ρdry - 0.0247w	85.3	15.6
50	log(Ps) = -4.785 + 2.862ρdry - 0.0215w	91.6	11.4
68	log(Ps) = -3.689 + 2.310ρdry - 0.0150w	96.0	6.1
84	log(Ps) = -3.083 + 2.033ρdry - 0.0128w	98.1	3.7
97	log(Ps) = -2.681 + 1.853ρdry - 0.0117w	98.8	2.7

Table 3. Predicted Swell Pressure as a Function of Liquidity Index

PI (%)	Equation	R (%)	Standard Deviation (%)
30	log(Ps) = -5.914 + 3.082ρdry - 0.736LI	85.2	15.7
50	log(Ps) = -5.210 + 2.859ρdry - 1.077IL	91.4	11.5
68	log(Ps) = -3.995 + 2.315ρdry - 0.989IL	95.7	6.3
84	log(Ps) = -3.357 + 2.315ρdry - 1.072IL	98.0	3.8
97	log(Ps) = -2.929 + 1.854ρdry - 1.116IL	98.6	2.8

Another study determined a way to estimate a soil's swell potential and shrinkage potential using two different methods [19]. The first method is based on a soil's plasticity index using the equation

$$S=2.16x10^{-3}(PI)^{2.44}$$

where S is the volumetric shrinkage and PI is the plasticity index. The second method bases the shrinkage potential on the coefficient of linear extensibility (COLE), a test run

to determine the “linear strain of a soil clod when dried from 5 psi to oven dry suction,” as defined by Brasher et al. [20]. The volumetric shrinkage potential can be estimated using the following equation.

$$VS=[(COLE+1)^3 - 1]100$$

It was also found that the shrinkage potential can also be estimated using the plasticity index with the following equation.

$$VS=3.28(PI) - 33.48$$

In this study, the soil pressure generated by the expansive soil using pressure will be measured directly using transducers. These direct measurements will be compared with some of the empirical formulations presented above to see which are most accurate and useful.

2.3.3 Measuring Compressibility of Backfill Material

Measuring the compressibility of the backfill material is important to understand how much it will deform under expansive soil pressure and be able to calculate what thickness is necessary to fully mitigate the pressures at the basement wall. Compressibility is a material property that depends on particle size, among other parameters, and therefore, once known, can be input into the model and chosen by the design engineer depending on what material is available for the job. In this way, the design engineer can specifically

check the thickness of the backfill against the soil pressures to ensure that enough of the soil pressure has dissipated at the basement wall.

A study completed in Kingston, Ontario looked at using post-consumer glass as a binder in concrete mixes as well as the strength of the glass as a binder [21]. It was anticipated that if the glass may act as a pozzolan, or a material that has "very little or no cementing properties" but that may have a cementing reaction if introduced to lime or other chemicals. The glass used consisted of mainly household glasses, such as jars and liquor bottles and was ground down so that at least 85% of it passed a No. 325 Canadian Standard Sieve. The glass was then combined with mill tailings from three different mines, sand, Normal Portland cement (which acted as the lime addition in these experiments) and water. Binder percentages ranged between 3% and 4%, which incorporated the replacement of Portland cement with glass with values ranging from 0 to 65%. Uniaxial and triaxial compression tests were then run on the samples at 7, 14, 28, 56, 112, 224 days. It was found that in certain cases, the post-consumer glass could increase the strength of the concrete and act as an efficient binder. However, this was dependent on each mine, the curing time, and may also be affected by the percentage of Portland cement used. Furthermore, it was noted that if more than one pozzolan was used, the strength may be dominated by the more reactive pozzolan.

An investigation done on the immediate and time-dependent compression of tire derived aggregates (TDA) tested both TDA, TDA-sand mixtures, and sand for compressibility [22]. The aggregates were made of automobile and small truck tires, and processed into

tire shreds (average length of approximately 18 cm) and tire chips, that when a sieve analysis was run on the samples, classified as a poorly graded gravel. Because of the large particle sizes, special testing devices were constructed – an oversize oedometer and a large cantilever test system (similar to a traditional gravity consolidation test frame). Isotropic compression tests were also run using a triaxial machine. Both immediate and time-dependent compression were tested using the oversize oedometer and the cantilever test system. The triaxial tests were performed "to determine how reductions in pore volume during compression contribute to overall volume change in the specimen." It was found that tire derived aggregates are subject to large immediate and time-dependent compression. The study also concluded that immediate compression is most heavily influenced by tire particle size, TDA content, and applied stress while time-dependent compression is mostly a function of TDA content and time.

As discussed earlier, another study was completed involving recycled tire material, but used shredded tire and clayey soil mixtures. Three different clays were used with five different percentages of shredded tire used for each clay. The study indicated that as the amount of shredded tires was increased, the compression index increased [12].

This study will calculate the compressibility of the rubber backfill used with two main goals. First, by determining the compressibility of the rubber, we can narrow down what thicknesses of rubber should be used for the physical tests by knowing how much the fill will reduce in thickness when introduced to significant pressures. Second, compressibility tests will allow us to characterize the rubber for future tests and for the Finite Element

Model (FEM) analyses. As stated previously, the properties of the materials used in the finite element analyses are necessary to have before the analyses are carried out to accurately calibrate the simulations.

2.4 Environmental Impacts

With the use of recycled materials, or typical construction materials, environmental impacts should be considered. In comparing the environmental effects of various materials, there are two different approaches. Approach one is a Life Cycle Assessment (LCA) comparison, in which the entire life cycle is compared, from raw materials to the end of a material or object's life. Approach two, a "direct analysis," looks at only one aspect of the timeline, such as leaching of contaminants into the groundwater after the material has been placed. In both scenarios, it is desirable to limit the variables and to compare similar situations. As there has not been much use of recycled materials for backfills, other building uses should be evaluated and compared. For our purposes, we will assume that the environmental effects would be comparable to these other uses.

2.4.1 Life Cycle Assessment

An evaluation on the environmental impacts of two different asphalt wearing courses was completed in Slovenia in 2015 [23]. Both conventional construction aggregates and carbon steel slag aggregates were evaluated using the Life Cycle Assessment method. The study only looked at the production and placement of the wearing course, under the assumption that "during the operation and maintenance stage, the environmental burdens do not differ significantly for the two different types of asphalt wearing course." The

energy it takes to produce each asphalt mix and the transportation impact for each type of mix were taken into consideration. However, the energy used in placing both asphalt mixes was considered to be the same. Furthermore, the assessment was taken as an ideal situation in which materials for both mixes were coming from relatively close locations and therefore this impact was considered to be minimal. In the analysis, the steel slag aggregate had some distinct advantages to the typical asphalt mix, with an overall impact reduction of about 20%, with some areas of the analysis being reduced more or less. For example, the impact on human toxicity was greater than 20%, while the impact on abiotic depletion was lower. The impact on global warming is also considered variable, with it "depending on the delivery distance of steel slag aggregate."

A study done in Stockholm looked at the use of bottom ash from incineration of municipal waste for road construction as a replacement to traditional rock aggregates [24]. The study uses an environmental systems analysis (ESA) approach, where resource use and emissions are the main focus. In the analysis, two different scenarios were evaluated; the first scenario used crushed rock as the subbase material whereas the second scenario used bottom ash as the subbase. Both scenarios used crushed rock as the base layer. It was determined that the traditional crushed rock subbase would use more energy than the bottom ash alternative, and would also lead to greater emissions of all types except metals. It was noted that the greatest difference in the energy use was caused by the fuel and electricity required to produced crushed rock. However, a significant boundary condition in the assessment is the travel distance necessary to get the bottom ash to the site. It was

determined that “if the MSWI bottom ash had to be transported more than 140 km, alternative 2 would use more energy than alternative 1.”

2.4.2 Direct Analysis

Several studies have been conducted on the environmental effects of recycled material in different construction applications. As these materials have already been processed and used in other applications previously, there are different aspects then introducing a new material into the system, such as fly ash or lime, that must be evaluated. A study on field site leaching of recycled concrete aggregates in Oslo, Norway looked at the change in pH value for both covered and uncovered subbase aggregates in roadways [25]. The project consisted of different sections where different materials were used as subbases. All of the sections were covered with asphalt, except two that were left open to the atmosphere. Samples were collected from pipes leading directly from the sub-base and tested. It was found that recycled aggregates with an asphalt cover resulted in a pH reduction slower than aggregates without an asphalt cover. Furthermore, this study showed that the leaching of elements from the aggregates did not exceed the acceptable criteria when the elements were mixed with surface water and groundwater.

A 2012 study conducted in Australia looked at the environmental impacts of using recycled glass in construction [26]. The investigation used recycled glass from a recycling site stockpile and soaking the glass in water, 1 mol L^{-1} HNO_3 solution (acid), and 1 mol L^{-1} KOH solution (base) for approximately 24 hours. The glass was also studied for its organic content prior to testing. . It was found that conductivity, pH values, most heavy

metals (specifically lead, copper, and zinc, with magnesium and manganese not having specified limits), and organic and inorganic material contents were not problematic and stayed within the allowable criteria. However, it was noted that iron content in acid-extracted samples was above the allowable limits, though it was acceptable when water was used.

Disfani et al. (2012) also examined the environmental risks of using recycled glass in roadway applications [27]. Two types of glass were used, fine recycled glass and medium recycled glass (maximum particle size of 4.77mm and 9.5mm, respectively). Leaching tests were run in accordance with Australian Standard Leaching Procedure guidelines and were compared to EPA Victoria standards. It was determined that contaminant concentrations were significantly less than the allowable limit for both types of glass, even when accounting for acid rain being the main leaching fluid. However, it was noted that the total amount of chromium (chromium III + chromium VI) did exceed limits, but "the EPA Victoria requirement presented…as the threshold for fill material is on hexavalent chromium (chromium VI)." Therefore, unless all of the chromium present is chromium VI, which did not appear to be the case in these tests, the glass is still within the allowable boundaries.

In 2013, an analysis on the health effects of artificial turf was conducted in Italy [28]. The project looked at three routes of contact – direct skin contact, skin contact with rainwater runoff, and dust and gas inhalation. Both turf and soil samples were collected for six sporting fields, with four artificial turf fields having recycled rubber products on their

fields, one artificial turf field whose infill consists of a thermoplastic elastomer that is specifically designed for turf fields, and one consisting of natural turf. Results showed that of the four fields with recycled rubber, BTX (benzene, toluene, and xylene) and PAH (polycyclic aromatic hydrocarbons) were detected in the leachate, and had higher concentrations in the newer fields compared to the older fields. However, when compared to the natural turf field, the concentrations were similar. Furthermore, all of the fields were within the allowed limits for the cumulative carcinogenic risk and the non-carcinogenic risk for all routes assessed.

In a study completed for lateritic soils found in Northeast India stabilized with fly ash and lime, the leaching of heavy metals was evaluated [29]. Two methods were used for evaluating the leaching of heavy metals, the single batch leaching test and the column leaching test. Fly ash only, combinations of fly ash and soil, and soil only were tested. Varying amounts of lime were used in the soil and fly ash combinations. Overall, it was determined that with less than approximately 20% fly ash, the leaching potential decreases. However, if the content of fly ash is increased beyond 20%, the leaching potential begins to increase. Furthermore, the results of mixes with lime varied more than the results without. With lime treatment, the leaching potential for Fe, Ni, Mg, Mn and Al increase, the leaching potential for Hg, Zn and Na decrease, and the leaching potential for Cd, Cr and K remain relatively similar to the mixes without lime. It was also concluded that the concentrations of metals do not exceed the allowable limits for any of the tested combinations, though the leaching behavior is affected by fly ash and lime content.

Olsson, Kärrman, and Gustafsson also looked at the leaching of metals when using bottom ash as a subbase layer in road construction [24]. Two methods were used in estimating the amount of leachate present. The first method estimated the amount of metal in the leachate using CEN tests with a liquid/solid (L/S) ratio of 2 while the second method ran tests using the available content of metals and arsenic. An L/S ratio was used in conjunction with the assumption that water infiltration was approximately 15 mm per year, which would result in an estimate that is approximately the same as the accumulated leaching in a 100 year period. The analysis found that the L/S method would considerably underestimate the amount of contaminants leaching from the road when compared to the tests run on the available content. However, in almost all of the tests run, the bottom ash leachate had approximately equal or greater amounts of metals than the crushed rock leachate.

The leaching behavior and mechanisms of soil stabilized with fly ash was examined, with a focus on the effect of pH [30]. Soil, fly ash, and soil-fly ash combinations were all tested. Four fine-grained soils and one sand were used, as well as three different fly ashes. Leaching tests were run on samples with a pH ranging from 3 to 13. The study found that the leachate in the soil samples were neutral to slightly alkaline, whereas the leachate from the fly ash samples were very alkaline, with pH values greater than 9. However, the soil-fly ash mixtures ranged from slightly alkaline to extremely alkaline, indicating that the fly ash can greatly affect the leachate pH despite its relatively low percentage in the mixture (20%). It was also found that there is a similarity in the leaching behavior for a given element for all scenarios presented, despite the variations in mixtures.

2.5 Modeling Earth Pressures Acting on Structures

In an early study (1989), Bhatia and Bakeer used the finite element method to model a static earth pressure problem [31]. In the test, a 10m high reinforced concrete basement wall was tested in the at-rest condition, as well as when it was rotated about its hinged base. Three backfill materials were used (two types of slag and a silty-sand). ABAQUS was used for the analyses. A two-dimensional finite element mesh was used to model the wall. To model the backfill, a non-linear elastic/perfectly plastic model with von Mises yielding criteria was used. No external loads were considered. In the analyses, both the magnitude of the lateral earth pressure and the ratio of the lateral to vertical earth pressure were considered. Some of the conclusions from the analyses are as follows: 1) the finite element model and experimental test gave very similar results, with the modeled values being within 4 percent of the measured earth pressure values and 3 percent for the location of the resultant earth pressure, 2) the magnitude of the earth pressure can be affected by as much as 16.5 percent if the nodes of the wall elements are restrained; however, if the nodes were not restrained, the wall is free to move to a different position which will change the earth pressure magnitude and distribution. Therefore, to adequately model the wall, a final wall displacement of negligible magnitude can be specified, and 3) when considering the condition of a free lateral boundary of the backfill, a backfill distance of 4H from the wall results in the best analysis; this condition can be applicable to the field in the case of a sloped edge at an angle smaller than the angle of repose of the soil.

In 1995, Karpurapu and Bathurst looked at simulating the behavior of geosynthetic reinforced soil retaining walls using finite element modeling [32]. Two reinforced

retaining walls were constructed using different building methods, but with the same dimensions and using a dense sand as backfill. After construction, surcharge loads were applied in increments using airbags between the backfill soil and the top of the wall until failure (collapse). The walls were loaded until failure. Each increment was applied for a minimum of 100 hours. Finite element analyses were completed to simulate each wall and its respective loading to compare the results. The constitutive models used were nonlinear and developed for soil-polymeric reinforcement interaction analyses. To model the soil, eight-noded quadrilateral elements were used and a modified hyperbolic stress-strain model was used to model the stiffness behavior. During the analysis, the soil dilation angle was set to 0° and 15° to see how the dilatancy angle affected the results. It was determined that the analysis using an angle of 0° predicted much greater panel displacements in the wall and larger reinforcement strains. Overall, the models successfully modeled the behavior of the walls and also verified that the different construction techniques can be efficiently modeled. It is also important to recognize that the strength and stiffness properties of different components can be determined from common independent laboratory tests.

In a project done by Loukidis and Salgado, the active pressure on gravity walls was modeled with a finite element program based on critical state soil mechanics [33]. The goals of the analysis were to accurately model the change of the friction angle during shearing rather than assume a constant friction angle until failure and to model the active earth pressure (K_A) between the critical and minimum active earth pressure. The constitutive model used was originally created for sands in 1997 and has been

subsequently modified to overcome drawbacks of earlier models. The most recent model, modeled by Loukidis and Salgado, takes into account four distinct surfaces: bounding surface, dilatancy surface, critical state surface, and yield surface. This model considers the anisotropy of sands. In the analysis, the wall dimensions were varied, and the unit weight of both the sand and wall was held constant. The at rest earth pressure (K_0) was set to 0.5 in all simulations and there was no surcharge placed on the backfill. The analysis indicated that to reach the minimum K_A value, wall crest displacements of approximately 0.001H-0.010H were required, where H is the height of the wall. Furthermore, to achieve $K_{A,\,min}$, a mobilized wall-soil interface friction angle is approximately 1.0 (loose sand) to 1.3 (dense sand) times greater than the critical state interface friction angle. Additionally, for dense and medium dense sands to reach the wall limit state, the crest displacement is approximately 0.013H-0.026H. At this point, the mobilized interface angle has already reached the critical state value.

A study conducted on the use of finite element analysis of earth pressures for narrow retaining walls looked at both at-rest and active conditions [34]. The goal of the analysis was to determine if the same mechanics that apply in a typical retaining wall would be the same for a narrow retaining wall. Plaxis (version 8) was used to model the narrow retaining walls. To maintain the at-rest condition, “a horizontal fixity is superposed on facial structure to prevent it from horizontal movement.” The finite element analyses were compared to centrifuge tests to determine their accuracy. It was concluded that for both the at-rest and active conditions, the FEM simulations can effectively predict the earth pressures.

This project will provide the data for calibrating a finite element model that should be able to simulate soil pressures on rigid concrete basement walls. The following sections discuss available Finite Element and Finite Difference software and their constitutive models, followed by a recommendation based on the needs of this project.

2.5.1 Available Select Finite Element Modeling Software

Currently, there are several Finite Element or Finite Difference programs available, each with their own set of capabilities. Seven different modeling programs were reviewed, as follows: Abaqus, FLAC 2D/3D, PLAXIS, Ansys, ZSoil, OpenSees, and DEEPSOIL. The various aspects compared were user friendliness, availability and cost, and each model's soil modeling capabilities. Each model is discussed in the following sections, with their major components described and what constitutive model or models are used. The constitutive models are discussed in the following section (2.5.2 Constitutive Models).

2.5.1.1 ABAQUS

ABAQUS uses several different constitutive models, with the most prominent being Mohr-Coulomb, extended Drucker-Prager, modified Drucker-Prager/cap model, and volumetric hardening model based on the modified Cam-Clay model. However, it is possible for a user to implement different constitutive models if they are more appropriate [35].

2.5.1.2 FLAC 2D/3D

FLAC uses several constitutive models, including null, elastic, plastic, creep, dynamic, and thermal models. These models include the more well-known constitutive models, such as an isotropic model, Mohr-Coulomb, modified Cam-Clay, and Drucker-Prager. User defined constitutive models are also able to be implemented in FLAC, and constitutive models created by individual users are available to others through Itasca. In addition to the models mentioned above, FLAC 2D 8.00 has a new 'swell' constitutive model, which is based on the Mohr-Coulomb model. Though FLAC does have an initial purchasing fee, demo versions are available to students for free, with program restrictions.

2.5.1.3 PLAXIS

PLAXIS is both a two-dimensional and three-dimensional modeling software that implements the Plaxis constitutive model. There is an initial purchasing fee and then a yearly license fee. However, it is considered one of the better modeling programs for reasons discussed in section 2.5.2 Constitutive Models.

2.5.1.4 Ansys

Ansys utilizes the Drucker-Prager constitutive model, as well as the Cap Drucker-Prager model. The cap model is a new addition to the Extended Drucker-Prager model and is applicable in modeling soils. The cap model includes cap hardening as well as shear envelope hardening, and implement cap for both tension and compression.

2.5.1.5 ZSoil

ZSoil implements Mohr-Coulomb, Rankine, Cap Drucker-Prager, Cam-Clay, Hardening small strain, and densification models. Other constitutive models can also be employed if these are not adequate.

2.5.1.6 OpenSees

OpenSees uses an elasto-plastic constitutive model [36]. OpenSees allows for existing material models to be used, as well as the development of new elasto-plastic models. This is done by combining yield functions, plastic flow directions, and evolution laws (such as hardening and softening) into a working elasto-plastic model. OpenSees is free to download and use.

2.5.1.7 DEEPSOIL

DEEPSOIL is a one-dimensional linear and nonlinear model created at the University of Illinois. It implements its own constitutive model, which is a continuation of the Clough and Duncan model [37]. This model is a modified hyperbolic model. DEEPSOIL is free to download and use.

2.5.2 Constitutive Models

As mentioned above, each of the discussed programs uses one or more constitutive models. In comprehensive papers done by Ti et al. and Brinkgreve, the most common constitutive models used for geotechnical engineering were summarized by their basic aspects, capabilities, and limitations. These parameters are discussed below.

2.5.2.1 Hooke's Law

Hooke's Law is not a constitutive model, but rather the basis for the elastic portion of more advanced elastoplastic models [38]. However, it is often not sufficient to accurately describe soil behavior on its own. Hooke's Law is based on two parameters, Young's modulus and Poisson's ratio. Despite its crude nature, it is possible to model stiff materials in soil, such as thick concrete walls or rock layers.

2.5.2.2 Mohr-Coulomb Model

As discussed by Ti et al., the Mohr-Coulomb model is a first order (linear), elastic-perfectly plastic model [39]. The failure criteria are defined by the friction angle and cohesion values. The Mohr-Coulomb model is one of the simpler models, using only two strength parameters to describe the plastic behavior, and effectively describes the strength behavior of the soil. It is typically used to analyze the stability of dams, slopes, embankments, and shallow foundations. However, one of the major drawbacks of this model is that the effective stress path may diverge largely from observations in undrained materials. Furthermore, the stiffness behavior, and thus deformation, before reaching local shear is poorly modeled. This model, compared to some of the following models, does not account for strain hardening or softening.

2.5.2.3 Drucker-Prager Model

The Drucker-Prager model is pretty consistent with the capabilities and limitations of the Mohr-Coulomb model, with the exception of the shape of the failure cone [38]. In a Mohr-Coulomb model, the shape is hexagonal, whereas in the Drucker-Prager model, the shape

is a simple cone. However, this can lead to issues when modeling failure. If a problem includes multiple different stress paths, the Drucker-Prager model is incapable of successfully modeling a friction parameter for all of these different stress paths. Therefore, the Mohr-Coulomb model is typically preferred over the Drucker-Prager model.

2.5.2.4 Modified Cam-Clay Model

The Modified Cam-Clay model is a first order elastic plastic strain hardening model [39]. In this model, the non-linear behavior is modeled through hardening plasticity. This model most effectively models normally or near normally consolidated clays. One of the limitations of this model lies in how the linear elastic behavior is modeled. Because it is only modeled before yielding and is on a log-linear scale, it may produce unreasonable results of Poisson's ratio. The type of modeling being done may also be considered a drawback, as it is better for modeling deformation than failure. Likewise, this model is best for modeling loading scenarios, such as embankments or foundations. Still, the Modified Cam-Clay model is better at predicting the undrained shear strength of a soil when compared to the Mohr-Coulomb model. However, though the standard Cam-Clay model has been modified over the years, there are still some major disadvantages to this model. The Modified Cam-Clay model is based on Critical State theory. When modeling soils on the 'dry side,' many critical state models considerably overestimate the failure stresses. This was especially noticed when compared to undrained tests on loose sand and normally consolidated (undisturbed) clays. Furthermore, critical state models do not

effectively model granular materials. It was noted that critical state models are typically limited to saturated clays and silts.

2.5.2.5 Duncan-Chang (Hyperbolic) Model

Ti et al. defines the Duncan-Chang model as a first order incremental nonlinear stress-dependent model, which is also known as the hyperbolic model. It is applicable to both clay and sand, and is based on drained triaxial test stress-strain curves. The failure criteria comes from the Mohr-Coulomb failure criteria, which is a function of friction angle and cohesion. One of the most important characteristics of the Duncan-Chang model is that it defines the three important qualities of soil: non-linearity, stress dependent, and inelastic behavior of both cohesive and cohesionless soil. Another important aspect of this model is that the necessary parameters can be directly obtained from a triaxial test. For these reasons, this model is typically preferred over the Mohr-Coulomb model. However, because of the framework, dilatancy cannot be described. Drawbacks of this model include the inability to distinguish between loading and unloading consistently (when compared to a purely hypo-elastic model) and it is not suited for collapse load computations in the fully plastic range. If implemented in three-dimensional stress space, an improvised solution must be applied [39]. Despite the disadvantages of this model, it is typically the preferred first order model for geotechnical applications [38].

2.5.2.6 Plaxis Soft Soil Model

The Plaxis Soft Soil model is a second order (quadratic) model similar to the Modified Cam-Clay model, but with some improvements [38]. The Soft Soil model failure criteria

is based on Mohr-Coulomb failure, and therefore does not over-predict the shear strength for overconsolidated states of stress like the Modified Cam-Clay model. Furthermore, the friction constant can be selected independently of the friction angle and cohesion, which allows for a more realistic K_0 value to be determined. This model also does not require an initial void ratio input. In comparison to the Mohr-Coulomb model, both models are effective at modeling unloading conditions.

2.5.2.7 Plaxis Hardening Soil Model

The Hardening Soil model is a second order model that is considered appropriate for any type of application [39]. The model implements two types of hardening to model different types of strain. The first, friction hardening, is used for the plastic shear strain during deviatoric loading while the second, cap hardening, is used for plastic volumetric strain during primary compression. As with previous models, the failure is defined by Mohr-Coulomb failure criteria. An important capability of this model is its ability to model a reduction of mean effective stress while simultaneously modeling the mobilization of shear strength. This is particularly important in excavation and retaining wall problems. Another significant aspect of this model is its ability to accurately model dilatancy and neutral loading when compared to the Duncan-Chang model. This is due to the Hardening Soil model being based on hardening plasticity (whereas Duncan-Chang used a non-linear elastic approach). However, it is limited in that is does not incorporate anisotropic strength of stiffness and does not model time-dependent behavior such as creep.

2.5.2.8 Hyperelastic Model

The Hyperelastic Model, also known as the Green model, is used when modeling a material that is "characterized as a material which does not depend on the history of the deformation process" [39]. Therefore, only the current stress is relevant. This is typically used to model polymer materials with rubbery behavior, and can also be used for concrete and rock in proportional loading, with limitations. The greatest drawback of the Hyperelastic model is the large amount of required parameters. For example, in a fifth-order isotropic hyperelastic model, 14 parameters are required. This would generally require a large number of tests to acquire the parameters, reducing this model's practicality.

2.5.2.9 Hypoelastic Model

A hypoelastic model would be appropriate to model materials that displays nonlinear, but reversible, stress strain behavior [39]. It is most typically used to model the behavior of a material once it has been loaded beyond the elastic limit. This model is similar to the hyperelastic model in that it only depends on the current loading and not the loading history. There are different ways to implement a hypoelastic model, such as using a nonlinear elastic model as a special form of the hybrid hyperelastic model, modeling the deformation behavior of cohesionless soil, and describing the nonlinear stress-strain behavior of soils loaded in an axisymmetric fashion. However, the downsides of the hypoelastic model include displaying stress induced anisotropy in the nonlinear range and that under the uniaxial stress condition, the distinction between loading and unloading can be unclear.

2.5.2.10 Viscoelastic Model

Viscoelastic materials involve both an elastic element and a viscous element [39]. Viscoelastic materials are defined by three main characteristics: hysteresis, stress relaxation and creep. Viscoelastic materials are commonly modeled using the relationship between strain and the logarithm of time during which creep occurs. The viscoelastic model is very popular when modeling time-dependent behavior.

2.5.2.11 Viscoplastic Model

The Viscoplastic model is a continuation of the viscoelastic model wherein permanent strain is present [39]. In the elasto-viscoplastic model proposed by Adachi and Oka, it is assumed that even after primary consolidation, static equilibrium is never reach for a normally consolidated clay and therefore viscoplastic strain is a hardening parameter. Another elasto-viscoplastic model proposed by Sekiguchi describes the rate sensitive behavior of clay. However, this model depends on state variables and time, and is not considered a reliable model except in the case of a very simple perfectly plastic soil model.

2.5.2.12 Swell Model

The swell model is not one of the basic models, but is specifically designed for the FLAC program. From the Itasca website, this model is based on the Mohr-Coulomb model, with the key difference being that the “wetting-induced deformations are taken into account by means of coupling the wetting strains with the model state prior to wetting.” This model is specifically designed for geotechnical analyses in expansive soil.

2.5.3 Model Recommendations

Based on the availability, cost, and ease of use of the modeling programs available, as well as the constitutive models used by each program, the program recommendations are as follows: 1) PLAXIS, 2) FLAC 2D or 3D, and 3) ABAQUS. PLAXIS is commonly referenced as one the better soil modeling programs, but does have a big drawback when looking at the cost. FLAC is a comparable alternative, though no information on the cost was available, and therefore may not be a good alternative to PLAXIS. Depending on the type of analysis being completed, ABAQUS may be difficult to use, in which case Ansys could be an alternative, though ABAQUS is typically seen as the better model. OpenSees and DEEPSOIL are both free alternatives if cost is a limiting factor, with OpenSees being the preferred program.

In the end, FLAC 2D was chosen for three main reasons. One, a complete older version was already available to students within the department. Two, updated demo versions were available through Itasca, if the older version did not have the necessary modeling capabilities. Three, by starting with FLAC 2D, it was anticipated that the model could later be modeled in FLAC 3D for further analysis. Furthermore, this program has a 'swell' constitutive model, which is very beneficial for modeling this research.

Chapter 3: Experimental Work

To investigate the reduced effects of expansive soils using recycled backfill materials, the experimental work was modeled after Katti et al. and Ikizler et al. An aluminum box of approximately 1 cubic foot was constructed and subsequently tested with no backfill and with varying thicknesses of backfill and compaction percentages to compare the swelling pressure exerted on the walls of the box. Initially, crumb rubber, glass cullet, and shredded plastic were evaluated for testing, but ultimately it was determined that crumb rubber had the most desirable characteristics and therefore only crumb rubber was used in full size tests. Detailed procedures can be found in the following sections.

3.1 Material Selection

3.1.1 Clay

Heiden clay was used for the expansive soil for two primary reasons. One, it is found throughout Oklahoma and Texas, the primary areas of study. Two, it is known to be a highly plastic clay which would indicate high swelling pressures. Only Heiden clay was used in the tests to ensure normalcy between each of the tests. A picture of the air dried clay can be seen in Figure 4.

Figure 4. Heiden Clay

3.1.2 Crumb Rubber

Crumb rubber was of primary interest for several reasons. First, it is a very compressible material and therefore had the potential to act similar to geofoam, which had previously been shown to reduce swelling pressure exerted by highly plastic clay. Second, crumb rubber does not have a high water retention capability, which is desirable as a backfill material. Third, it is a permeable material, which is important in draining water away from structures. However, crumb rubber is not the most easily accessible material of the three materials evaluated. A picture of the crumb rubber can be seen below.

Figure 5. Crumb Rubber

3.1.3 Glass Cullet

Glass cullet, like crumb rubber, is very permeable and does not retain water. Furthermore, glass cullet is the most similar in size, structure, and strength to sand, which would make it a desirable option. Glass is also one of the most recycled materials, making it easy to access. Additionally, glass cullet can be purchased in different particle sizes. For this project, cullet passing a No. 12 mesh was chosen. However, it is not very compressible and therefore may be good for drainage but is not ideal for absorbing the swelling pressure of clay. An image of the glass cullet can be seen below.

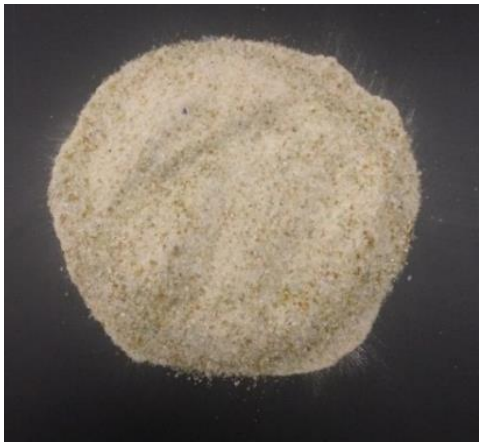

Figure 6. Glass Cullet

3.1.4 Shredded Plastic

Shredded plastic has similar properties to crumb rubber in that it is highly compressible, does not retain water, and is very permeable. However, it is not as easily acquired compared to the other materials. Furthermore, it is not shredded into highly uniform pieces, unlike the crumb rubber and glass cullet. Additionally, it is very lightweight and will float on water, which could lead to problems during placement and compaction, and

could potentially result in being eroded away once it has been placed. The shredded plastic can be seen in the below figure.

Figure 7. Shredded Plastic

3.2 Testing Box

The main testing box was constructed out of six ½" thick aluminum plates, with outside dimensions of 12" x 12" x 13" (length x width x height). The aluminum used was alloy 5086, chosen for its corrosion resistance. The inner dimensions of the box measured 11" x 11" x 12 " (length x width x height). A hole was cut in both the top and bottom plates for the pressure sensors. The sensors fit into the holes so that the sensing area was flush with the wall. Two 4" diameter holes were hollowed out on each side of the box for the porous stones to rest in. This would allow water into the box without losing soil mass. Brass porous stones were used to minimize outward bending and loss of wall strength. Prior to the final test, four additional holes were added in the box lid. This was to allow pipes with holes drilled in them to be placed through the lid and into the soil and crumb rubber for additional water to enter the center of the box. The addition of these pipes is discussed further in section 3.6.4.1 Box Retrofitting. Before assembling the box, each

wall was marked with 1” segments for the entire height of the box. To-scale schematics of the box before and after retrofitting can be seen in Figure 8 and Figure 9. Figure 10 and Figure 11 show the inside and outside of the testing box, respectively.

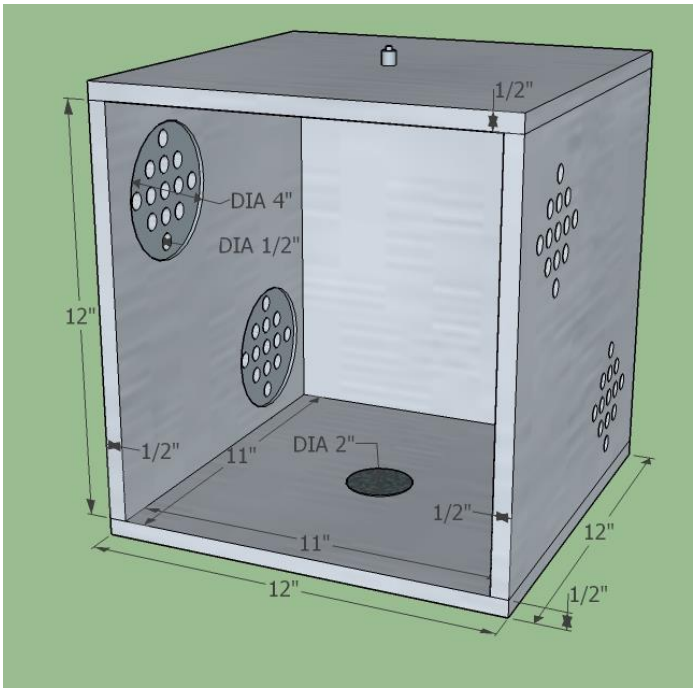

Figure 8. Box Setup Prior to Retrofitting

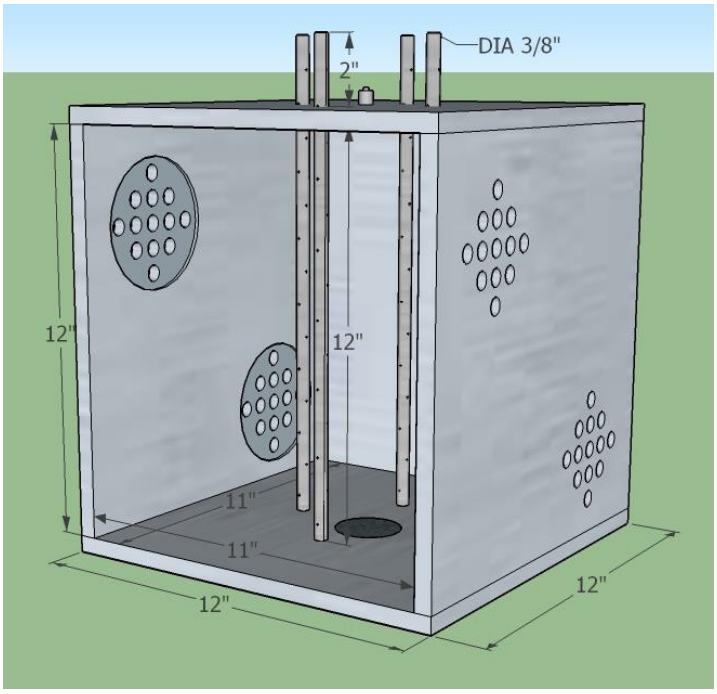

Figure 9. Box Setup After Retrofitting


Figure 10. Inside of Testing Box

Figure 11. Outside of Testing Box

3.3 Data Acquisition

A Somat eDAQ-lite system was used to monitor the swell pressures over the testing period. One KDF-500 kPa soil pressure gauge, produced by Tokyo Measuring Instruments Laboratory Co., Ltd., was mounted on the top (herein known as Sensor T) and bottom (herein known as Sensor B) plates of the box. This would allow one sensor to read the pressure coming directly from the soil and one sensor to read the pressure coming from the backfill material. The sensors measure 50mm in diameter, with a 46mm sensing area diameter (Figure 12). Prior to each box test, the sensors were checked outside of the test box by placing a known load on the sensor and calculating the pressure that should be exerted on the sensor from this load. This was compared to values being read by the data acquisition system to ensure that the sensors were reading accurately. An image of the sensor can be seen in Figure 13.

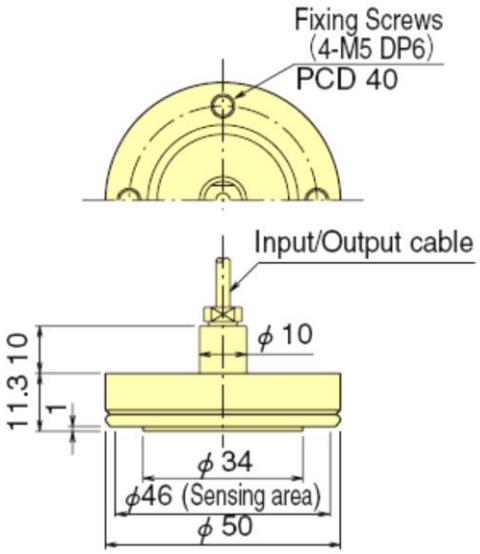

Figure 12. Pressure Sensor Dimensions

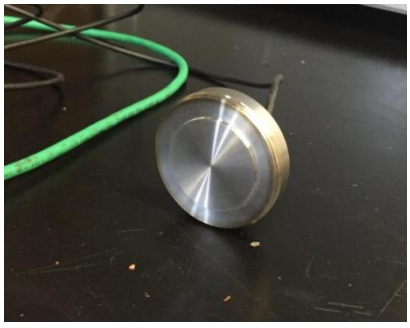

Figure 13. Pressure Sensor

3.4 Characterizing Materials

3.4.1 Heiden Clay

The Heiden clay properties had previously been determined by Lin 2012 [40]. Additional sieve analyses, particle size distributions, Atterberg limits, one dimensional free swell, one-dimensional consolidation, flex wall permeability, and unconfined compression tests were completed in accordance with their respective ASTM standards to ensure that the samples used in these experiments were comparable in their characteristics to those found in Lin's test.

All of the clay used in experimentation was sieved down to pass a No. 4 standard sieve prior to box testing, and three sieve analyses were run on the sieved down sample. The three sieve analyses were averaged to get an average gradation for the sample. A No. 4 sieve was chosen because it was small enough to adequately mix the soil and water to bring the soil to optimum conditions, but was large enough to not be unreasonable in the field. To determine the particle size distribution of the soil, two hydrometers were run on an oven dried sample. The soil was sieved down to pass a No. 40 sieve prior to being tested in the hydrometer. The soil was mixed with a dispersing agent and allowed to sit for at least 16 hours prior to testing, after which readings were taken incrementally for a 24 hour period. Four Atterberg limit determinations were performed for the clay. A 10 point spread was ensured for the blow counts for each liquid limit test. These values were compared to Lin's to determine the anticipated swell.

To evaluate the swell pressure of the clay, two free swell tests were completed. In the first test, the clay was compacted at 80% compaction and -0.2% of the optimum water content directly in the oedometer ring. A seating load of 1 kPa was applied to the specimen, which was then inundated with deionized water and allowed to swell until equilibrium was reached. After reaching equilibrium, incremental loads were placed on the sample until the original sample height was reached. The stress at which the strain is 0% is the swell pressure. The second test was run in the same manner, but at 100% compaction and -2% of optimum water content. This was done to cover the best case scenario (80% compaction at optimum water content) and worst case scenario (90% compaction at optimum water content) seen in the box tests. The measured swell pressures were

compared to correlations of predicted swell pressure based on the correlations presented by [4] and [19]. The correlations presented by [4] were computed for varying plasticity index values. Therefore, to predict the swell pressure of the Heiden clay with a plasticity index of 44, the value was interpolated between the predicted swell pressure for plasticity index values of 30 and 50.

A one-dimensional consolidation test was run on the clay, compacted at maximum dry density and -0.5% optimum water content. Incremental loads were placed on the specimen and the changes in height were recorded at 0, 0.25, 0.5, 1, 2, 4, 8, 15, 30, 60, 120, 240, 480, and 1440 minutes. End of increment stress-strain curves were plotted. From these curves, the maximum past pressure was estimated and subsequently used in the calculations for the elasticity modulus.

To evaluate the permeability of the clay, a sample was compacted at -0.5% optimum water content and 90% maximum dry density. The sample had a 2:1 (height to diameter) ratio. The sample was back saturated until a B value of 0.95 was achieved. After saturation, the test was run as a “falling head, rising tail” test. The cell pressure, back pressure, and head pressure were kept constant for some tests, and increased for other tests. The pressures were set prior to testing, after which the sample was left to permeate, and the change in the headwater and tailwater elevations over a time period were noted for each test. From this, the permeability of the soil was estimated. The permeability of the clay was not reported by Lin, but was compared to values listed on the Web Soil Survey website for Heiden clay taken in the same general location.

Three unconfined compression tests with a 2:1 (height to diameter) ratio were completed to approximate the unconfined compression strength and undrained shear strength of the soil. The samples were compacted at 93%, 93%, and 98% compaction and within +/- 0.5% of the optimum moisture content. The unconfined compression strength was not necessary for the box tests or calculations, but was used in the finite modeling program.

3.4.2 Backfill Materials

3.4.2.1 Sieve Analyses

Sieve analyses were completed for the crumb rubber, glass cullet, and plastic samples. ASTM D5644-01, ASTM D1214-10, and ASTM D1921-12 standards were followed for crumb rubber, glass cullet, and plastic respectively. However, for the crumb rubber and plastic gradations, talc and antistat were not used. Gradation curves were then plotted for each, and can be seen in section 4.1.2.1 Sieve Analyses. Three sieve analyses were run on each material type, and the percent passing was averaged for each sieve size to get an average particle distribution.

3.4.2.2 Compressibility Tests

One-dimensional oedometer tests were completed for the crumb rubber, glass cullet, and shredded plastic samples. Three tests were performed for the crumb rubber to ensure consistent behavior, and one test was run for both the glass cullet and shredded plastic. All tests were run in accordance with ASTM D2435/D2435M-11. For the crumb rubber tests, different stresses and time durations were tested to compare how each would affect the behavior, but maintained a Load Increment Ratio of 2. A semi log stress-strain curve

was plotted for each material, and the compression and recompression index were defined for each. It was assumed that there was no maximum past pressure for the recycled materials. The crumb rubber stress-strain curve was also compared to that of geofoam curves completed in other studies. The curves, as well as the compression and recompression indices, can be found in section 4.1.2.2 Compressibility Tests.

3.5 Material Preparation

3.5.1 Heiden Clay

The clay was sieved down to pass at least a No. 4 standard sieve. Prior to testing, a sieve analysis was completed to determine the grain size distribution. It was decided that the clay would be compacted at the optimum water content of 24.2% and varying percentages of the maximum dry density. To achieve the optimum water content, the soil was split evenly into five trays and three water contents were taken for each tray to get an average water content for each. Water was then added to the soil and allowed to sit for 24 hours, after which three water contents were taken for each tray. More water was added if necessary, or the soil was laid out to dry if it was too wet. After 24 hours, three more water contents were taken. This process was repeated until the three water contents had an average of +/- 0.5% of the optimum water content. All of the soil trays were kept in a humid room wrapped in plastic wrap until it was time for the first box test. One final water content from each tray was taken 24 hours prior to compaction to ensure that the water contents were in the desirable range.

3.5.2 Crumb Rubber

Prior to testing, there was no modification to the crumb rubber. The crumb rubber chosen was comparable in particle size to a fine to coarse grained sand to allow for more analogous results. As the rubber was already processed, it was not rinsed or washed to remove contaminants. Crumb rubber that had not previously been used in the sieve analyses or compressibility tests was used.

3.6 Box Tests

3.6.1 Box Test One – 2 Inch Backfill, 80% Compaction

An initial thickness of 2 inches of crumb rubber was chosen for the first box test, to achieve a 1:6 fill thickness to total height ratio. This was based on the literature findings, where a 1:5 ratio was the most efficient in reducing the swell pressure. The calculated backfill density was based on the compressibility tests done prior to the first box test, as well as the available literature on geofoam. At a density of approximately 550 kg/m^3 in the compressibility test, the crumb rubber presented similar strain behavior to that of the geofoam under similar stresses. Therefore, the same density used in the compressibility tests was used for the box test. The crumb rubber was placed between the clay and top plate rather than between the clay and side walls (as done in Ikizler's tests) for ease of placement and under the assumption that the vertical swelling pressure is greater than or equal to lateral swelling.

The amount of soil and crumb rubber needed for the full size tests were volume based calculations, in which the volume of the box was known and the density of both materials was known, and the mass for each was back-calculated.

Prior to compaction, the box was assembled without the top plate and placed into the poly stock tank. The box was kept elevated off of the floor of the tub so that there was no interference with the swelling on the bottom plate and so that the pressure sensor wiring was not bent. The sides of the box were wrapped with plastic wrap to maintain moisture inside of the box once compaction began. The top plate was wrapped in plastic wrap separately. The bottom plate was not wrapped, but did not have any significant inlets for air.

The clay was compacted in fifteen 2/3” lifts, for a total of 10”. A modified proctor hammer was used to compact each lift. Between the compaction of each lift, a moist paper towel was laid over the top of the box, making sure that it did not come in contact with the soil itself, and was then covered by the plastic wrapped top plate to hold in moisture. The trays with soil wet of optimum were compacted first so that any moisture that was lost would not significantly change the results.

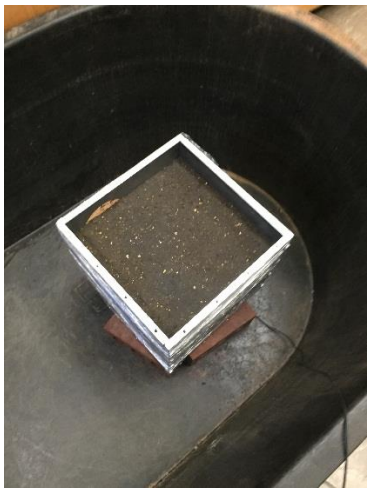

Figure 14. Box with Compacted Soil Prior to Testing

The crumb rubber was placed in a single lift once the clay had been compacted fully. The proctor hammer was not used in the rubber compaction. Instead, the rubber was hand patted and pressed until it was approximately flush with the top of the box. The top plate was screwed onto the box while pressure was applied to the top of the plate to ensure that the rubber was fully flush. Once completely assembled, all screws were tightened as much as possible. The tub was then filled with water until the box was completely submerged, with approximately 1" of additional water coverage. The box setup was kept submerged for 60 days. This time span was chosen based on previous literature that indicated it would be sufficient enough time for complete saturation to occur, and a permeability test was run on the sample to ensure that the permeability values from previous work were comparable. The saturation water content was found by determining the weight and volume of solids put into the initial test, assuming full saturation at the end of the soaking period, and back-calculating what the required water content would be for 100% saturation. Note that the saturation water content may be lower than actual water contents determined at the end of soaking due to three main assumptions made in the saturation

calculations. One, it was assumed that every gram of soil weighed out to be compacted made it into the box, when in reality small amounts may not have. Two, to find the mass and volume of solids in the original test, the initial water content was used in calculations. It was assumed that the initial water content was 24.2%, but in reality it ranged from 23.7% to 24.7%. Three, when finding the saturation water content, it was assumed that the soil mass had the same final volume as the initial volume. While this may be true in the soil only test, it is not accurate in the tests with crumb rubber. The pressure sensors took continuous readings from the beginning of compaction through the 60 day saturation period. After one week the sampling rate of the sensors was lowered from 100 samples/sec to 20 samples/sec, and this was the only time in which they were not taking readings.

Figure 15. Box with Compacted Soil and Crumb Rubber Prior to Testing

Figure 16. Testing Setup with Submerged Box and Somat DAQ System

After 60 days, the rubber and soil were removed from the box. Prior to removal, the tub was drained and the box was once again wrapped in plastic wrap. During the first test, three soil plugs were then taken using a tubular soil sampler, with two taken on opposite corners and one taken in the center. Because of its noncohesive nature, the rubber was not easily removed with the plug and was therefore not a solid sample like the clay. However, water contents were still taken on the rubber gathered from around the hole. Water contents were taken in 1” increments, providing 10-12 water contents per plug. After taking the three plug samples, the rubber was removed from the top to approximate how much the clay had swelled during the saturation period. In rest periods, the top of the box was covered with a damp paper towel to maintain moisture.

Figure 17. Box with Compacted Soil and Crumb Rubber After Testing

Figure 18. Taking Soil Plug

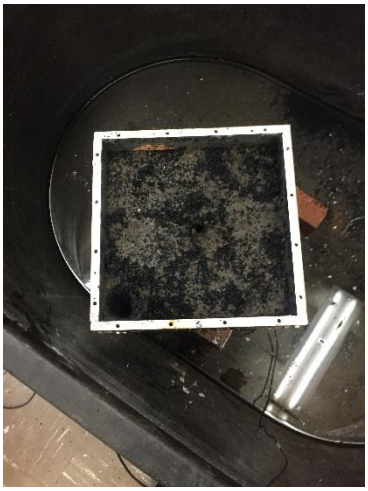

Figure 19. Box with no Crumb Rubber and Compacted Soil After Testing

Figure 20. Soil Plug

3.6.2 Box Test Two – No Backfill, 90% Compaction

During preparation of the soil for the second box test, some minor changes were made to the preparation procedures. During preparation for the second test, the soil was not redried and sieved down to pass a No. 4. Instead, the soil was taken directly from the box and broken apart while maintaining the final moisture content. The soil was then split into 4 trays, and the moisture regiment was completed to achieve the optimum moisture content of 24.2%. However, rather than taking three water contents per tray, five water contents were taken per tray.

Similar to the first box test, the box was assembled without the top plate and placed into the poly stock tank prior to compaction. The box was kept elevated off of the floor of the tub so that there was no interference with the swelling on the bottom plate and so that the pressure sensor wiring was not bent. The sides of the box were wrapped with plastic wrap to maintain moisture inside of the box once compaction began. However, during the compaction of the second box test, a moist paper towel was placed between the box walls

and the outside plastic wrap so that the paper towel was not in contact with the soil but better maintained the moisture content through the holes on the walls. The top plate was wrapped in plastic wrap separately with no moist paper towel. The bottom plate was not wrapped, but did not have any significant inlets for air.

The clay was compacted in ten 1" lifts, for a total of 12". However, it was determined that using fifteen 2/3" lifts, as done in Box Test 1, resulted in a more uniform compaction, and therefore the soil was compacted in the smaller lifts for subsequent tests. Rather than using a modified proctor hammer, an 8" by 8" tamping plate was used to compact each lift. Between the compaction of each lift, a moist paper towel was laid over the top of the box, making sure that it did not come in contact with the soil itself, and was then covered by the plastic wrapped top plate to hold in moisture. The trays with the moistest soil were compacted first so that any moisture that was lost would not significantly change the results.

For this and subsequent tests, the sampling rate was set at 1 sample every 10 seconds (or 0.1 samples/sec). After 21 days of soaking, the box was removed from the water bath because there was no more appreciable swelling. Water contents were taken every inch as described under Box Test 1, but were taken for all four corners during breakdown of the soil. Center samples were attempted prior to breakdown using a tubular soil sampler, but were not successful for the top 8 inches. Rather, the soil would push around the sampler and out of the open top. Therefore, it was determined that taking samples along

the edges of the box after removing the plates would produce the most accurate water contents.

Though 95% compaction is typically required, there were two main reasons that 90% was chosen. First, 90% compaction was chosen to serve as a baseline for comparison between tests. Because the first test was at 80%, a 90% compaction would give a reasonable value between compaction of 80% and 100%, with 100% compaction being ideal in real world applications. Second, compaction greater than approximately 90% resulted in the aluminum plates bowing outward, creating problems in putting the top plate on the box and starting the test.

3.6.3 Box Test Three – 2 Inch Backfill, 90% Compaction

For the third test, 2 inches of backfill and 10 inches of clay were compacted at 90% max dry density. These values were chosen for two main purposes. One, the 90% compaction was done previously with no crumb rubber, and therefore provided a baseline value for the expected swell pressures. Second, by running tests at different compaction percentages with the same amount of backfill, it was possible to find a potential correlation between compaction percentage and a reduction in swell pressure.

As done in the previous test, the soil was kept at the final water content while being broken down and prepared for the third test. After this was completed, the water regiment was completed until each of the 5 trays were within +/- 0.5% of the optimum water content. The crumb rubber was placed at 550 kg/m^3, as done in the first test.

Prior to compaction, the box was once again wrapped in plastic wrap to help maintain moisture. During compaction, an 8” by 8” tamping plate was used, and the soil was placed in fifteen 2/3” lifts. Between lifts, a damp paper towel was placed over the top of the open box to maintain the moisture content as much as possible.

After soaking for approximately 25 days, the box was removed from the water bath, final water contents were taken, and the soil was broken down. Unlike the second test, water contents were taken from the center during breakdown, but were done so approximately an hour after the box had been removed from the water bath. Water contents were not taken in the first two inches where the crumb rubber was present.

3.6.4 Box Test Four – 2 Inch Backfill, 89% Compaction

For the fourth and final test, it was determined that the third test would be repeated but with some retrofitting to the box that is explained in more detail in section 3.6.4.1 Box Retrofitting. The water content regiment was completed as done in the third test. The soil was broken down while maintaining the final water content and the soil was rewetted or dried out, as appropriate.

The soil was compacted as in previous tests in fifteen 2/3” lifts using an 8” x 8” tamping plate, with the final relative compaction being closer to 89% than 90%, allowing for accurate comparisons to Box Test 3 while still being able to differentiate the tests more effectively. After compacting the soil, a small auger drill bit was used to remove the soil at four points near the box center for the entire 10” depth. Images of this process can be

seen below in Figure 21 and Figure 22. The pipes were then pushed into the holes and the crumb rubber was compacted around the pipes for the final 2”. The box top was then bolted on and the setup was submerged in the tub.

Figure 21. Auger Drilling

Figure 22. Drilled Holes for Pipes

3.6.4.1 Box Retrofitting

For the fourth test, the box was retrofitted to allow for faster wetting. Because the final water contents in previous tests showed a lack of water getting to the center where the sensors were located, it was decided that four pipes with holes drilled in them would be

installed around the center to allow for water to penetrate the soil faster. Each pipe was approximately 15” long, with alternating holes drilled along the entire length of the pipe. No modifications were made to any part of the box except for the lid, which was only modified with the four additional pipe holes. The pipes were installed after soil compaction, after which the rubber were compacted around the pipes. Images of the pipes before and after installation can be seen below.

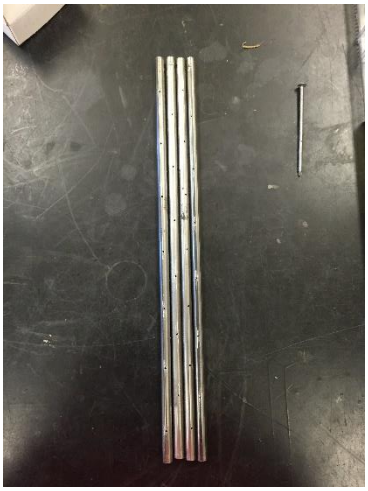

Figure 23. Drilled Pipes

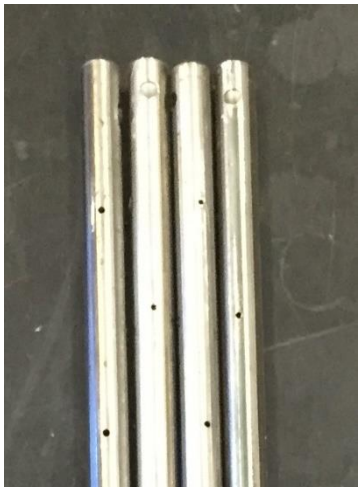

Figure 24. Close-up of Drilled Pipes

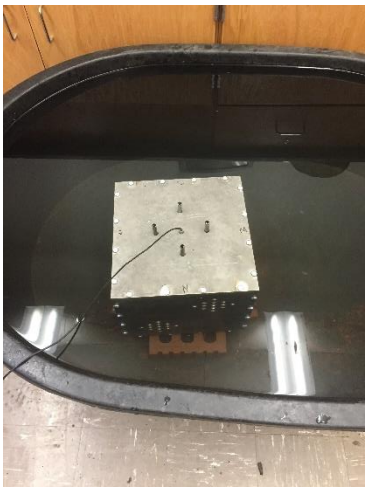

Figure 25. Installed Pipes

3.7 Finite Difference Modeling

The final stage of this project involved modeling the test box in FLAC 2D (a Finite Difference program), version 8.00. Modeling started with the simplest setup, Box Test 2 that included only soil, and was modified for the other testing setups with the crumb rubber, and eventually the retrofitted box. Simulations were run using the 'Swell' constitutive model, which is a plastic model based on the Mohr-Coulomb constitutive model and is designed specifically for geotechnical applications in expansive soil. The model was run using the units of feet, slugs, and seconds.

The crumb rubber was modeled 'elastic' for each analysis, and was placed in a single 2" lift, as done in the actual tests. The soil was modeled in lifts to simulate the actual compaction process. However, due to the limited allowable amount of zones, Box Tests 1, 3, and 4 were modeled as ten 1" lifts for the soil and one 2" lift for the rubber, compared to the actual fifteen 2/3" lifts for the soil and one 2" lift for the rubber. As each lift was modeled, the layers above were modeled as 'null' zones. After each lift, the system was

solved with a sensitivity value of f = 0.00001 pounds to make sure that the soil would come to equilibrium due to gravity and the boundary conditions. This was done until the entire box was filled, at which point a final analysis was run, once again solving with a tolerance of f = 0.0001 pounds. The swell parameters were then input to simulate what was happening inside the testing apparatus. In doing so, the model was calibrated for the Heiden clay. It should be noted that the 'Swell' model is based on triaxial test data. However, the parameters used in this model were taken from a 1-D swell test. Using 1-D swell test data, it was assumed that no swelling occurred in the x (or z, though this is not modeled in FLAC 2D) directions, and therefore the values for a3, c3, and m3 were assumed to be 0. A similar procedure was completed when predicting soil slope deformation due to wetting, in which a 1-D swell curve was used to find the swell parameters [41]. It should be noted that when calculating a1 and c1 using the swell curves, the vertical stress must be negative, so that the logarithmic term becomes positive, and that the strain in the y-direction must be in decimal form. Using these rules, the values presented in the above mentioned paper are able to be back-calculated accurately. Figures of the different modeling stages and analysis outputs can be seen in Appendix A: FLAC Modeling.

Chapter 4: Results

4.1 Characterizing Materials

4.1.1 Heiden Clay

As detailed in section 3.4.1 Heiden Clay, selected properties of the clay were obtained from prior research done by Lin [40]. As discussed previously, all of the clay used in experimentation was sieved down to pass a No. 4 standard sieve prior to the first box test, and three sieve analyses were run in accordance with ASTM D6913-04. The three sieve analyses were averaged to get an average gradation for the sample.

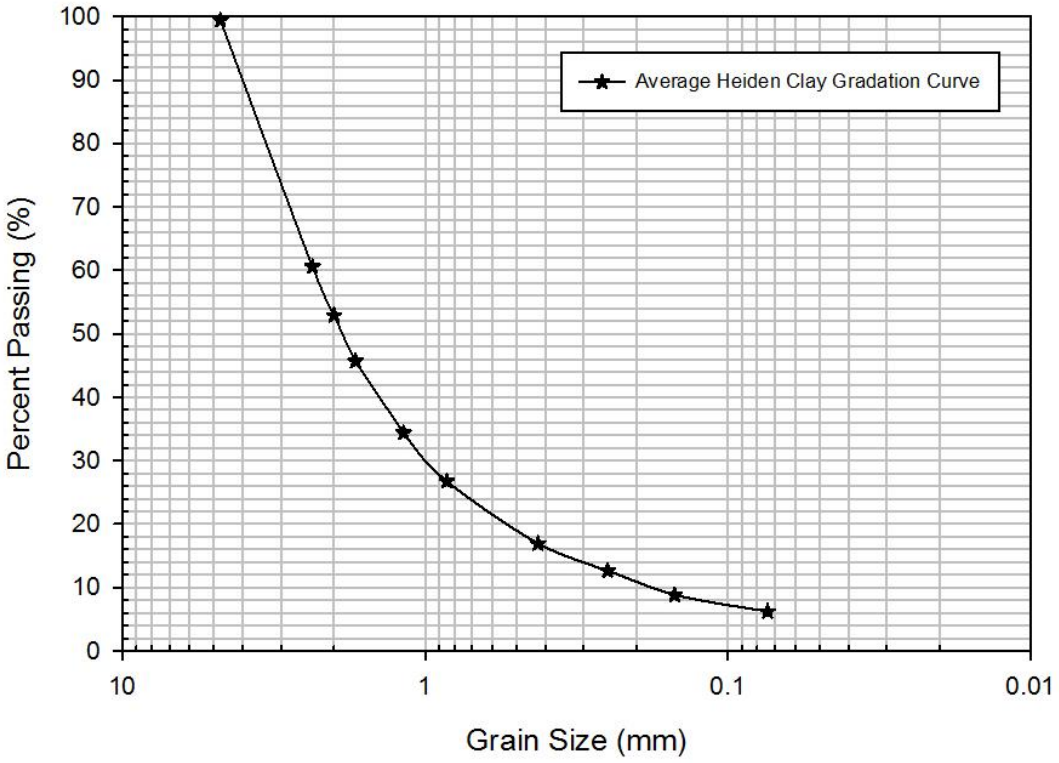

Figure 26. Heiden Clay Grain Size Distribution

Two hydrometer tests were performed on a sample sieved down to pass a No. 40 sieve. The soil was mixed with a dispersing agent and was allowed to sit for 24 hours, after which hydrometer readings were taken at predetermined intervals. Based on the hydrometer tests, it was determined that the soil was composed of 28% clay, 60% silt, and 12% sand. It should be noted that the soil had a much higher percentage sand and silt than originally anticipated.

Additional Atterberg limits were determined in accordance with ASTM D4318-10[1] as part of this study. Four Atterberg limit determinations were completed, and the calculated values were averaged. The average Atterberg limits were compared to those found previously, and can be seen below.

Table 4. Atterberg Limits for Heiden Clay

Property	Value Obtained by Lin	Value Obtained by Jacoby
LL	67	59
PL	23	31
PI	44	28

In addition to Atterberg limits, a one dimensional consolidation test was run on a remolded sample. The soil was compacted directly in the oedometer ring at 100% maximum dry density and -0.5% optimum water content. However, due to the highly disturbed nature, a good consolidation curve was not achieved. The end of increment stress-strain plot can be seen below in Figure 27.

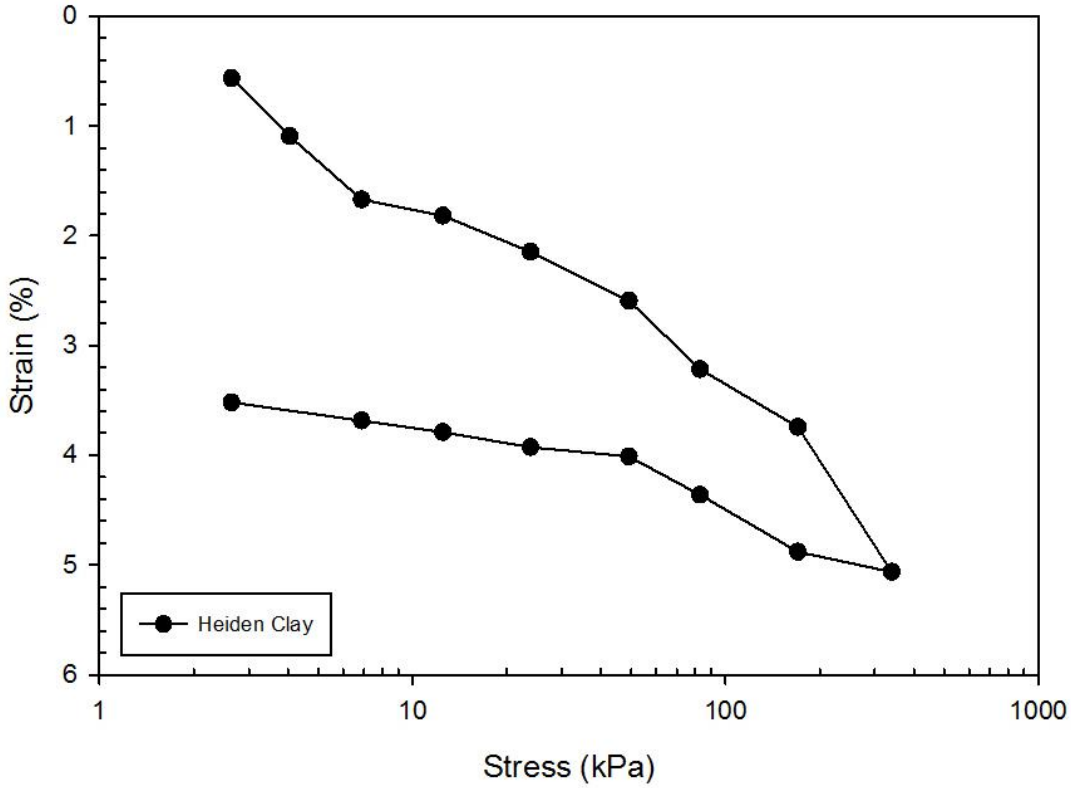

Figure 27. Stress-Strain Curve for Heiden Clay

Two supplementary free swell tests were run in accordance with ASTM D4546-14. To estimate the swell pressure, the clay was compacted at -0.2% optimum moisture content and 80% maximum dry density directly in the oedometer ring. A seating load of 1 kPa was applied to the specimen, which was then inundated with deionized water and allowed to swell until equilibrium was reached. After reaching equilibrium, incremental loads were placed on the sample until the original sample height was reached. The stress at which the strain is 0% is the swell pressure. As can be seen in Figure 28, the swell pressure of the clay at these conditions is approximately 155 kPa. The 'consolidation due to seating' is not pictured because the initial change in height was not recorded due to the small load placed on the sample.

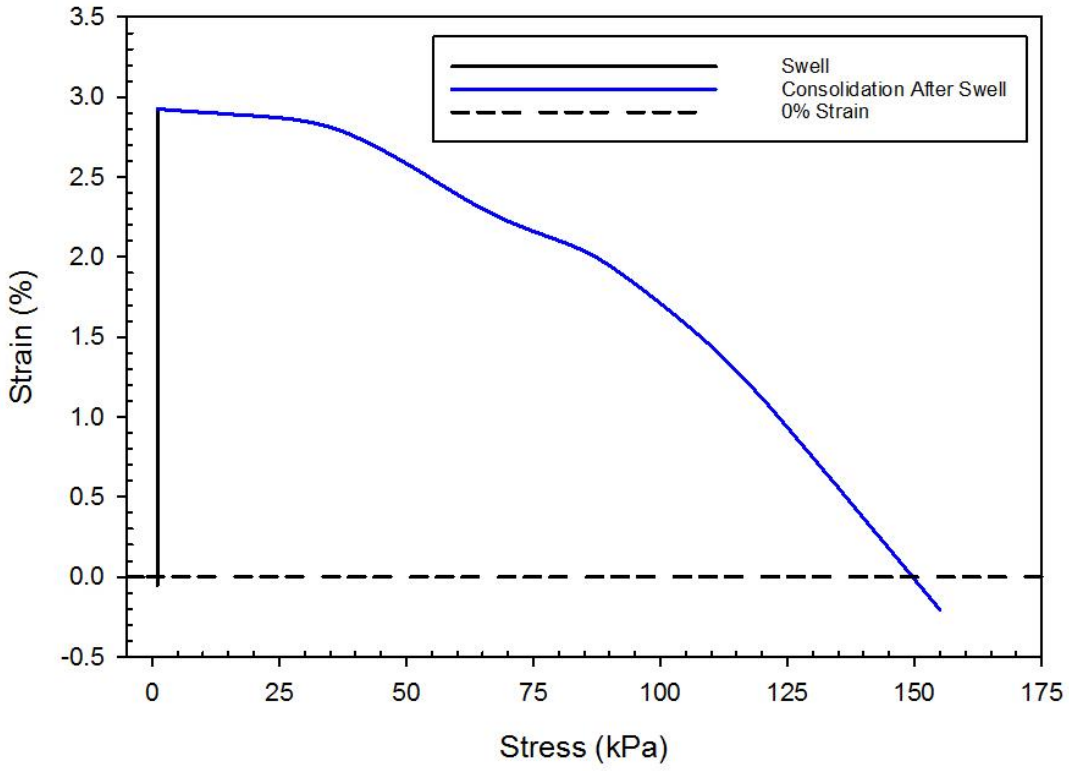

Figure 28. Free Swell Curve for Heiden Clay (80% Compaction, -0.2% Optimum Water Content)

An additional swell test was completed with the clay being compacted at maximum dry density and within -2% of the optimum water content. Using these parameters, the swell pressure is approximately 230 kPa, which agrees with Lin's (2012) value. This swell curve can be seen below in Figure 29. Note that the black line denoting "Seating" is the consolidation due to the 1 kPa seating load, and therefore is not very apparent on the curve.

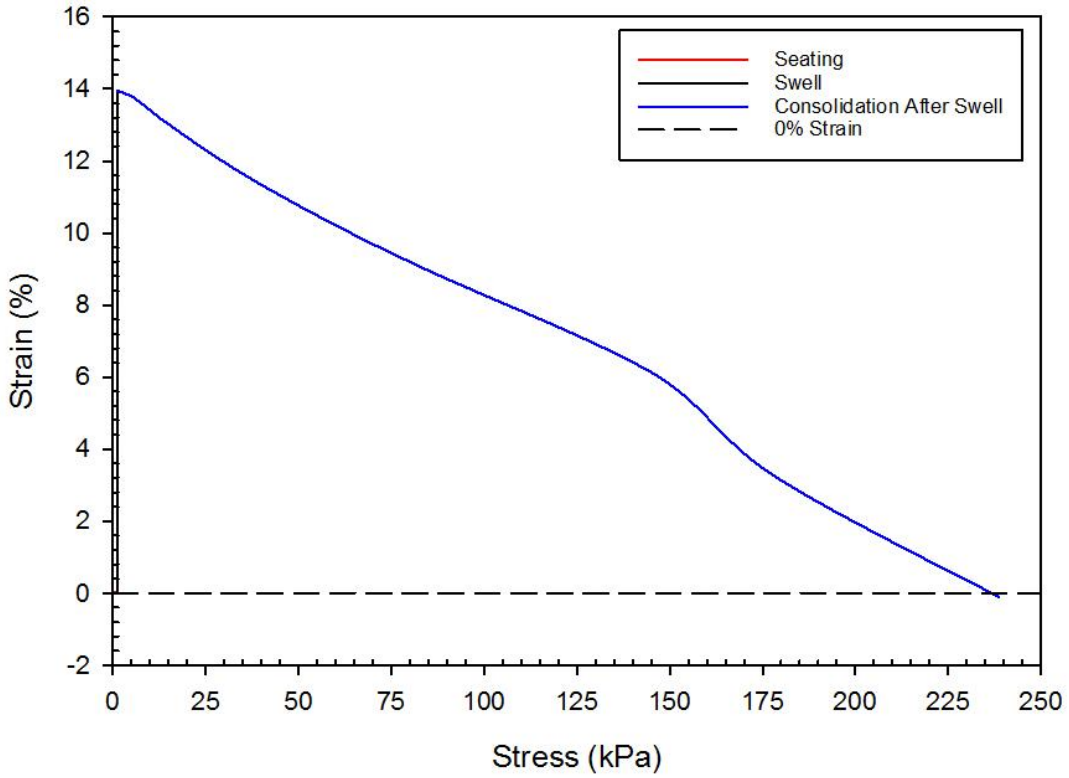

Figure 29. Free Swell Curve for Heiden Clay (100% Compaction, -2% Optimum Water Content)

Comparing the measured swell pressure to the correlations presented the literature review, the measured swell pressure is much greater than what would be expected based on the initial water content, dry density, and liquidity index. The following tables indicate the predicted swell pressure based on the previously mentioned values. As can be seen below, the predicted swell pressures are far below what was measured previously by Lin (230 kPa) or by what was determined as part of this study (155 kPa and 230 kPa).

Table 5. Predicted Swell Pressure of Heiden Clay Based on Initial Water Content[1]

Plasticity Index	Dry Density (g/cm^3)	Initial Water Content	Ps (kg/cm^2)	Ps (kPa)
30	1.58	0.242	0.27717	27.19
44	1.58	0.242	0.46060	45.18
50	1.58	0.242	0.53921	52.90

[1] Predictions determined by Erzin and Erol [4]

Table 6. Predicted Swell Pressure of Heiden Clay Based on Liquidity Index[2]

Plasticity Index	Dry Density (g/cm^3)	Liquidity Index	Ps (kg/cm^2)	Ps (kPa)
30	1.58	0.027	0.08620	8.46
44	1.58	0.027	0.15858	15.56
50	1.58	0.027	0.18960	18.60

[2] Predictions determined by Erzin and Erol [4]

The discrepancy in swell pressure predictions versus real swell pressure could be due to many reasons, including mineralogy, specific surface area, and cation exchange capacity. Because the correlations presented are only empirical correlations, they do not account for every possible difference in the soil, and therefore may be inaccurate when predicting the swell pressure. Also note, the values calculated use the old metric system. This means that the kilogram measurements are being presented as a force rather than a mass. Therefore, each of the values should be multiplied by approximately 100 to convert to kPa. These values can be seen in the far right columns, labeled "Ps (kPa)" in Table 5 and Table 6.

A flex wall permeability test was run to determine the permeability of the soil. This value was compared to the Web Soil Survey value, corresponding to the same clay type taken from the same general location. The soil survey provided a permeability of approximately 2.17e-5 cm/s, while the laboratory test produced an unreliable range of results. Therefore, the permeability was taken to equal 2.17e-5 cm/s.

Three unconfined compression tests were run to estimate the unconfined compression strength and undrained shear strength of the soil to be used in the finite difference modeling. The samples had a 2:1 (height to diameter) ratio. The results for the three tests

can be seen in Table 7. Comparing these values to Lin (2012), the values calculated were within 5% of Lin's. At optimum conditions, Lin calculated an unconfined compression strength of 313 kPa. Given that the water contents and percent compaction were lower in these tests, it is reasonable that the UCS is lower. The most comparable test, UCT 3, produces very similar results to Lin.

Table 7. Unconfined Compression Test Results

Test Number	Percent Compaction (%)	Water Content (%)	Strain Rate (in/min)	Unconfined Compressive Strength (kPa)	Undrained Shear Strength (kPa)
UCT 1	93	23.00	0.0305	253	126.5
UCT 2	93	23.42	0.0305	265	132.5
UCT 3	98	22.42	0.0305	301	150.5

A table comparing the soil characteristics to those of the soil used in similar studies can be found below. For this study, the swell pressure, liquid limit, plasticity index, permeability, and unconfined compression strength were tested for, while the optimum moisture content and maximum dry density were values obtained from previous work. Poisson's ratio and the elasticity modulus were calculated from test results in this study.

Table 8. Comparison of All Clay Properties

Soil	Property	Value	
Heiden Clay	Swell Pressure (kPa)	230[1]	230[2]
	Liquid Limit (%)	67[1]	59[2]
	Plasticity Index (%)	44[1]	27[2]
	Percent Clay/Silt/Sand		28/60/12[2]
	Optimum Moisture Content (%)		24.2[1]
	Maximum Dry Density (kN/m^3)		15.5[1]
	Unconfined Compressive Strength (kPa)		301[3]
	Permeability (cm/s)		2.17E-5[4]
	Poisson's Ratio		0.45[4]
	Elasticity Modulus (MPa)		225[5]
Black Cotton Soil (BCS)	Swell Pressure (kPa)		221[6]
	Liquid Limit (%)		71.40[6]
	Plasticity Index (%)		29.40[6]
	Optimum Moisture Content (%)		29.00[6]
	Maximum Dry Density (kN/m^3)		14.32[6]
	Permeability (cm/s)		1E-7[6]
Siran-2 Clay and Bentonite Mixture	Lateral Swell Pressure (kPa)		250[7]
	Vertical Swell Pressure (kPa)		278[7]
	Liquid Limit (%)		284.5[7]
	Plasticity Index (%)		228.9[7]
	Optimum Moisture Content (%)		11.60[7]
	Maximum Dry Density (kN/m^3)		8.63[7]
	Permeability (cm/s)		1.78E-7[7]

[1] Values determined by Lin [40].
[2] Values determined as part of this study.
[3] At 98% compaction, -2% optimum water content.
[4] Values determined by outside literature.
[5] Values based on empirical correlations. Correlation based on undrained shear strength and correlation factor (based on OCR and PI, with an OCR of 5 assumed)
[6] Values determined by Katti [9].
[7] Values determined by Ikizler [11].

4.1.2 Backfill Materials

4.1.2.1 Sieve Analyses

To fully characterize all of the backfill materials, three sieve analyses were done for each material. The three sieve analyses were then compiled to determine an average curve for each material. The individual average curve can be seen for each material in Figure 30,

Figure 31, and Figure 32. Figure 33 gives a comparison of the grain size distribution of each material.

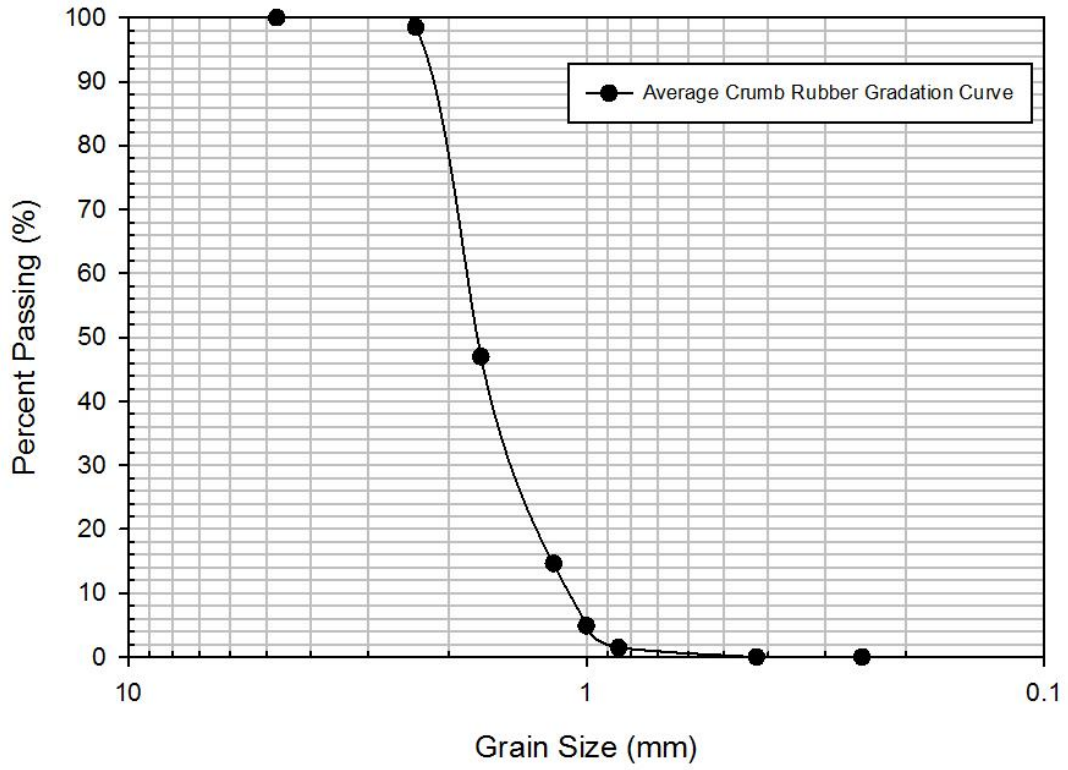

Figure 30. Crumb Rubber Grain Size Distribution

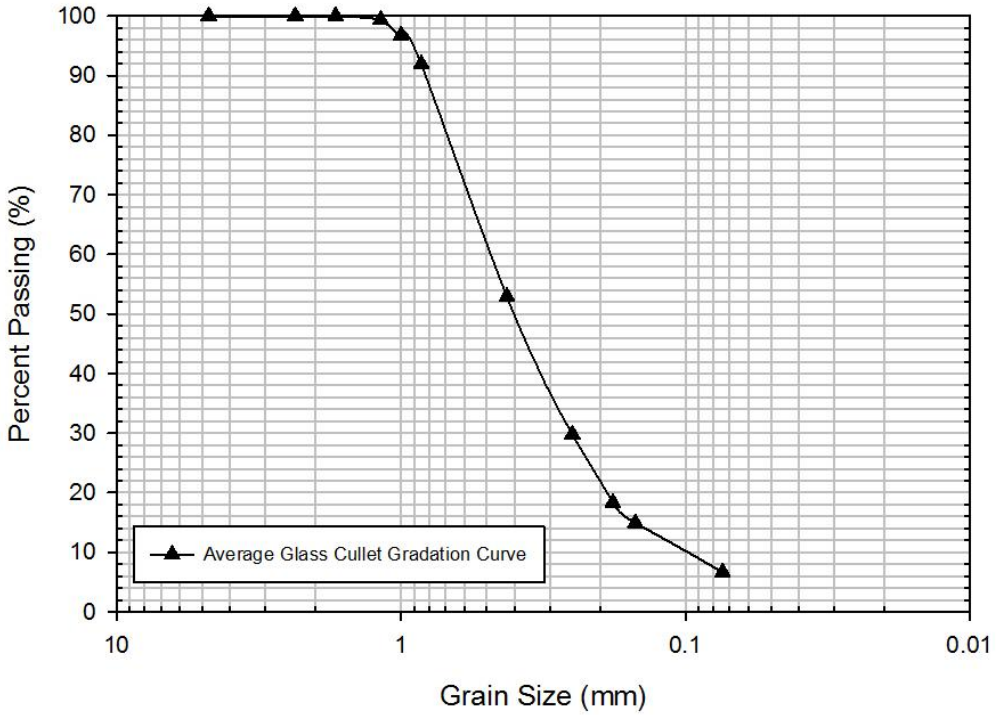

Figure 31. Glass Cullet Grain Size Distribution

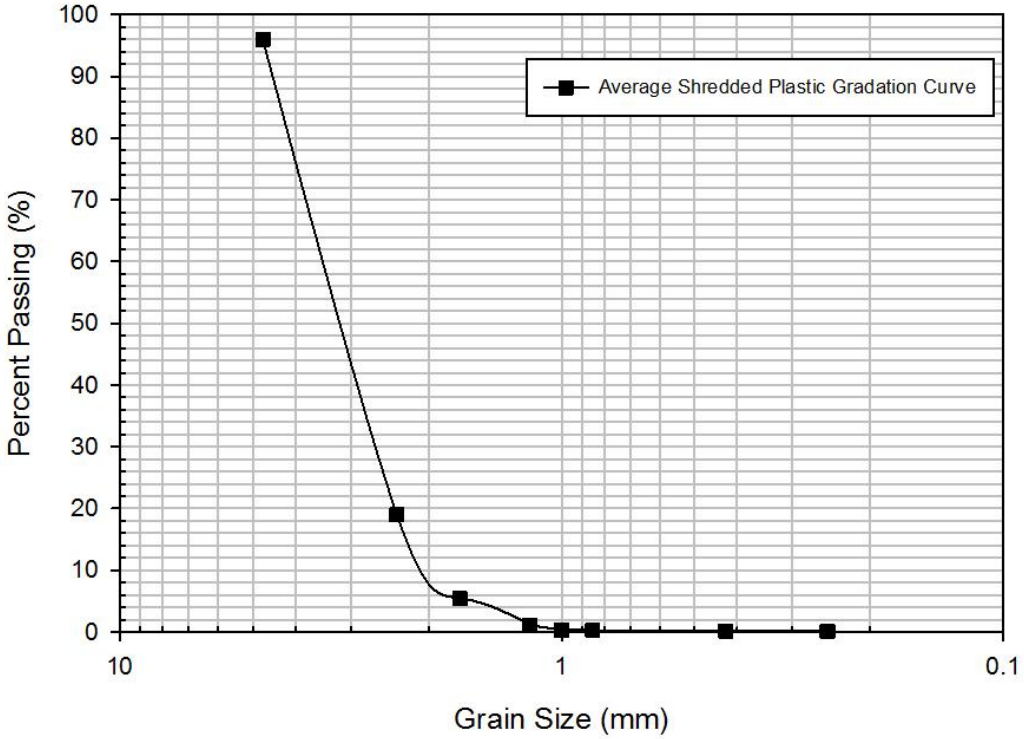

Figure 32. Shredded Plastic Grain Size Distribution

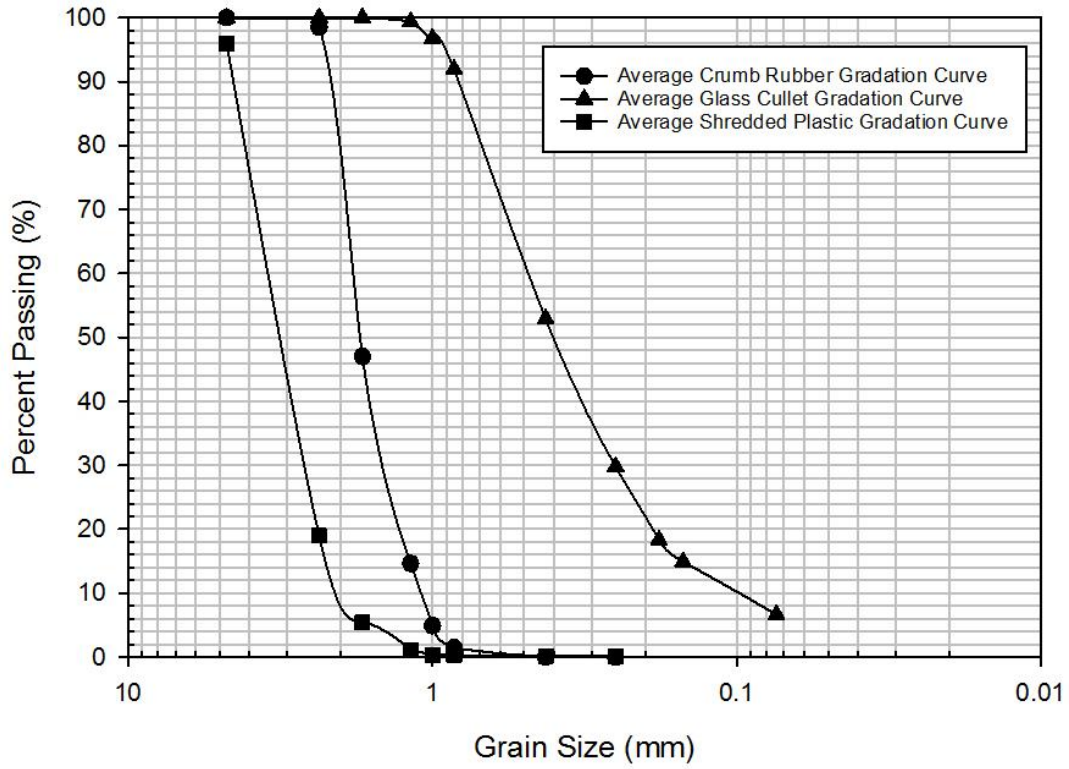

Figure 33. Compiled Grain Size Distributions

It should be noted that for all of the materials, the sieve was performed on the material as purchased and no further modification to the material was made. However, this may result in a skewed grain size distribution for certain materials. For example, though the plastic particles were previously shredded, they were not of a uniform shape. Some of the particles, as can be seen in Figure 7, were long and thin, while others were short and thick, which may change the results of the analysis. For instance, if a long, thin piece was turned vertically during shaking, it could fit through a No. 10 or No. 12 sieve, but would not do so horizontally.

4.1.2.2 Compressibility Tests

Compressibility tests were run on the crumb rubber, glass cullet, and shredded plastic. As discussed earlier, three compressibility tests were completed for the crumb rubber. Figure 34 shows all three of these curves. Tests 1 and 2 were run with similar loading schedules, but Test 2 had longer increment durations. Test 3 had increment durations similar to Test 1, but had a different loading schedule and was tested to a higher stress. As can be seen below, the duration and loading schedule did not make a significant difference on the compressibility.

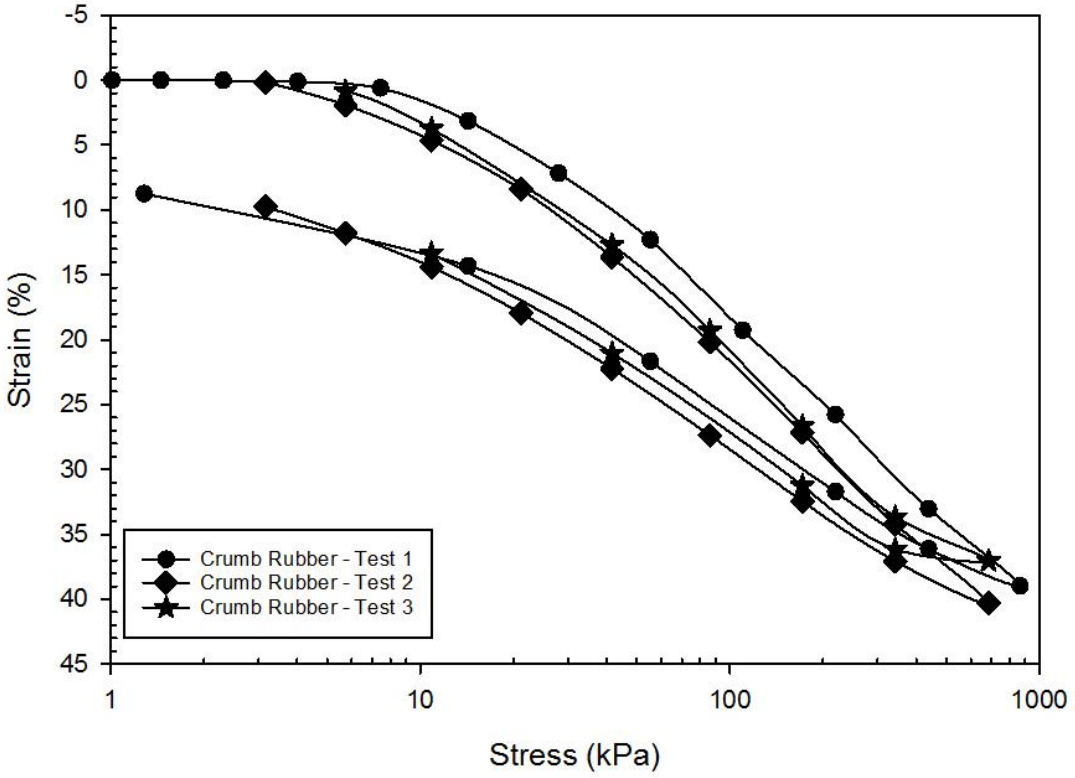

Figure 34. Combined Compressibility Curve for Crumb Rubber

Because the third test was tested at the highest stress, this one was compared to the plastic and glass compressibility curves. The compressibility curves for all three materials can

be seen below in Figure 35 through Figure 37, with Figure 38 having a side-by-side comparison of all three.

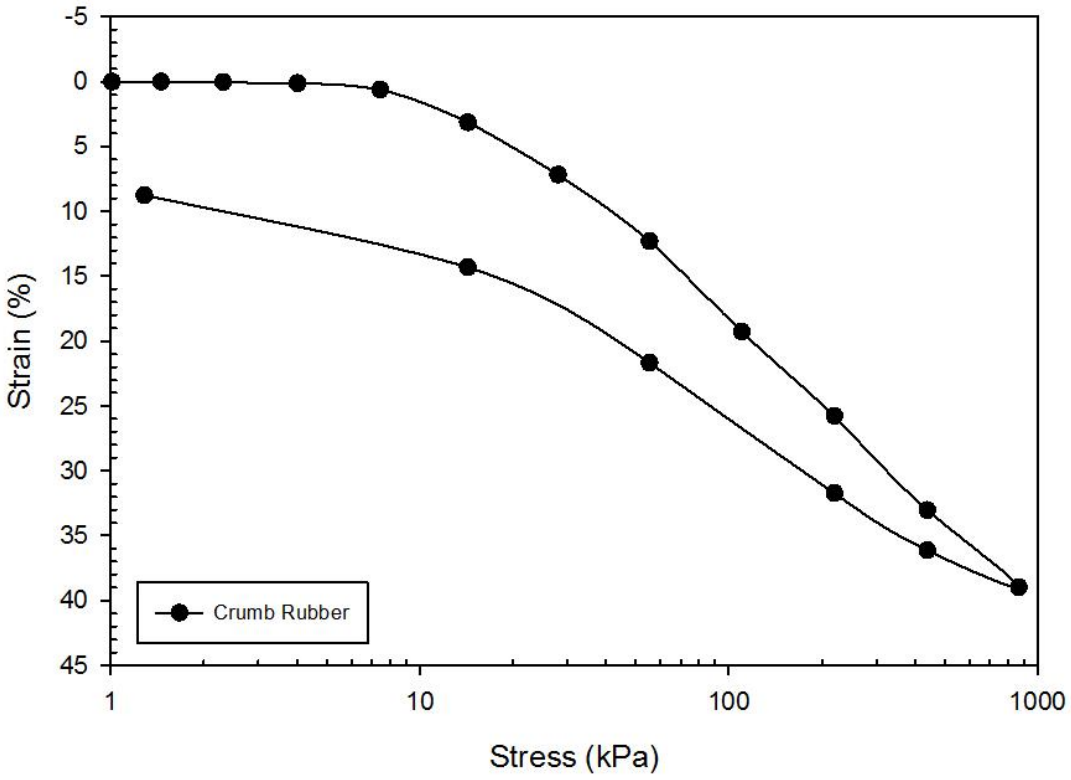

Figure 35. Compressibility Curve for Crumb Rubber

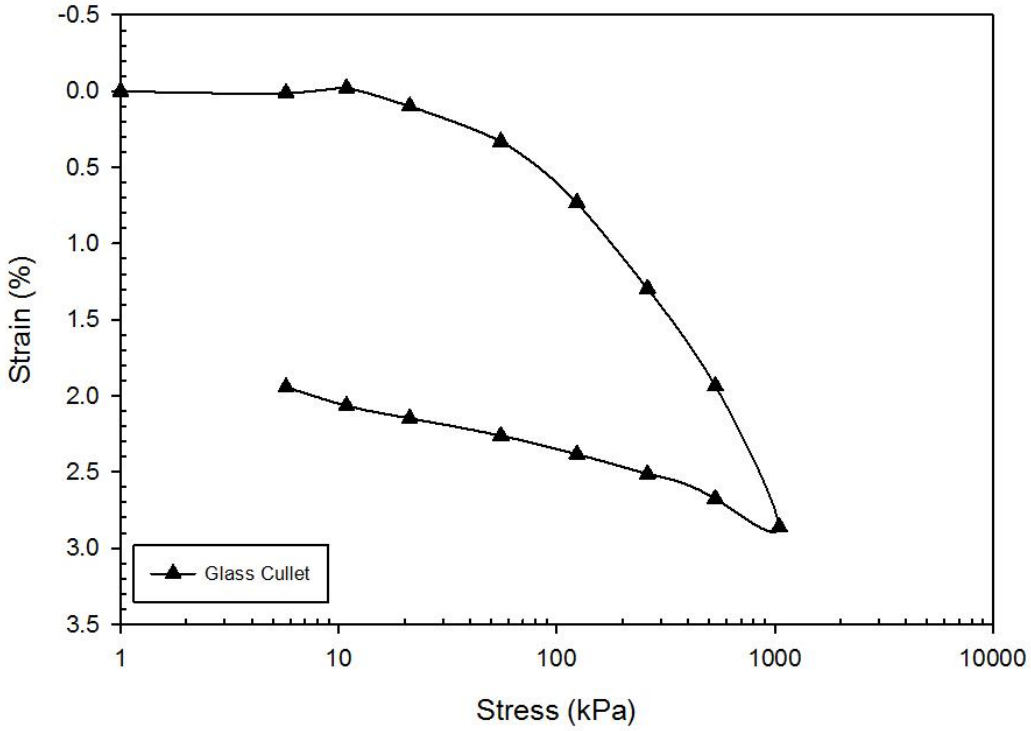

Figure 36. Compressibility Curve for Glass Cullet

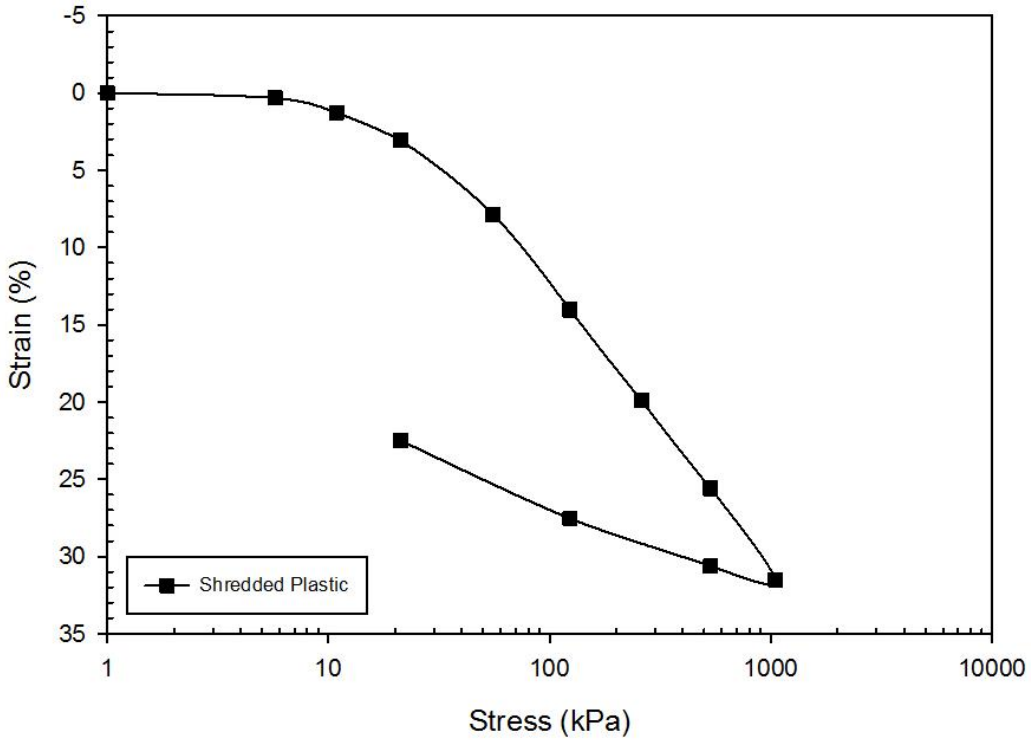

Figure 37. Compressibility Curve for Shredded Plastic

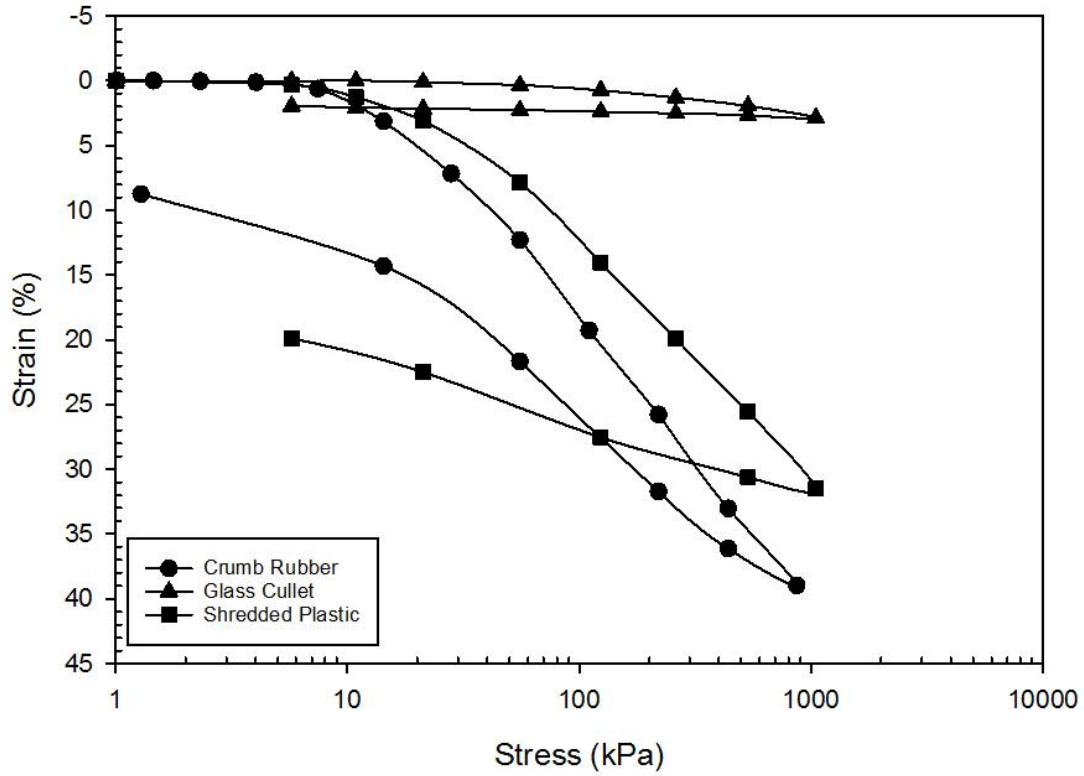

Figure 38. Combined Compressibility Curve for All Recycled Materials

Though the materials are all coarse grained materials that do not retain water, it should be noted that for the crumb rubber and plastic, consolidation curves were hard to define given their deformation characteristics. These materials are highly elastic, and rebound quickly to their original height, with the crumb rubber being more elastic than the plastic. Furthermore, because of their high compressibility, it is hard to define when consolidation for a specified loading increment is complete, resulting in some approximate curves. The compression and recompression indices were defined for each of the recycled materials, which can be seen in Table 9.

Table 9. Recompression and Compression Indices for Recycled Materials

Material	Recompression Index	Compression Index
Crumb Rubber	0.011073	0.211893
Glass Cullet	0.000769	0.021279
Shredded Plastic	0.013899	0.168921

The stress-strain curve for the crumb rubber was also compared to the stress-strain curve of geofoam at different densities. These combined curves can be seen below in Figure 39. Though the rubber curve does not reach the same stress as the geofoam at 10% strain, it is comparable in value. Furthermore, while the geofoam curve increases quickly and then begins to plateau, the rubber curve continues to increase, and increases at a faster pace. Extrapolating to higher strain rates, the rubber will be able to withstand a higher stress value at the same strain than the low density geofoam.

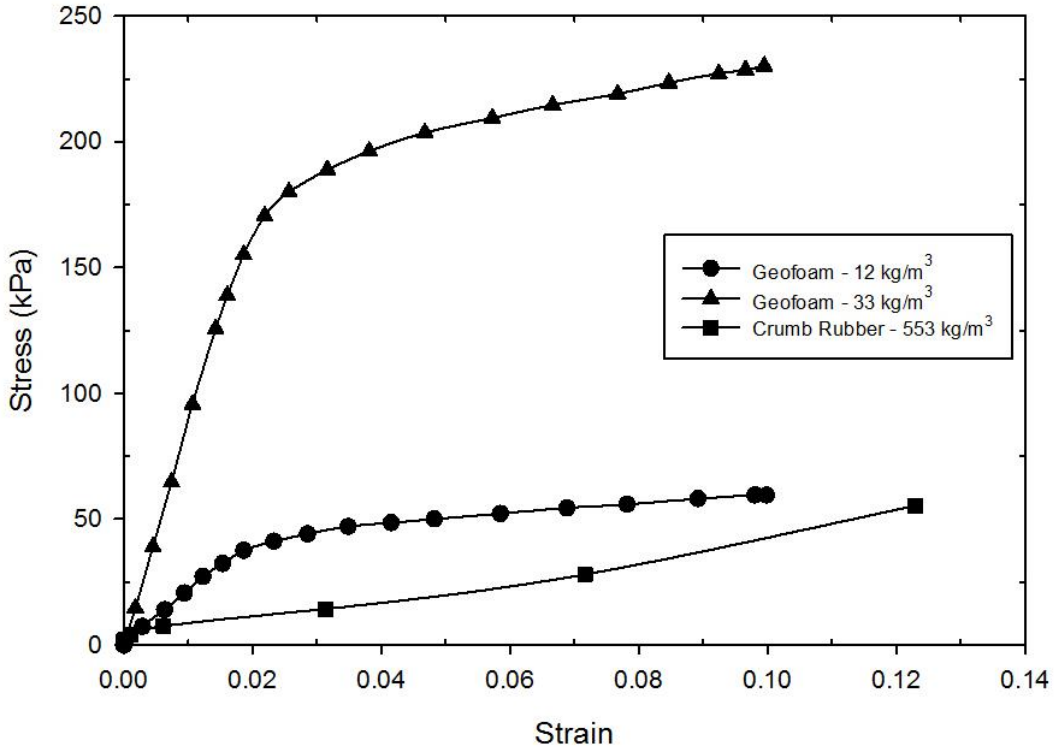

Figure 39. Comparison of Stress-Strain Curves for Crumb Rubber and Geofoam (Elragi 2000)

4.2 Box Tests

4.2.1 Box Test One – 2 Inch Backfill, 80% Compaction

The first box test began on December 15, 2015 and continued through February 15, 2016. The soil continuously swelled for the duration of the test, though the swelling pressures were significantly less than what was anticipated. The maximum swell pressure read by Sensor T was 22 kPa and the maximum swell pressure read by Sensor B was 62 kPa, accounting for the original pressure of the soil. As discussed previously, the box was compacted within +/- 0.5% of the optimum water content (24.2%), with the 100% saturation water content being approximately 43.0%. Note that the water content for this test is higher due to the lower compaction percentage. The final water contents ranged from approximately 24% to 36%, with the middle water contents generally being the lowest of the three soil plugs. However, because water content samples were not taken in each of the corners, water content contour plots were not able to be plotted, as was done in subsequent tests.

During removal, it was noted that the soil had swelled approximately ½" over the 60 day period. However, it was determined post testing that the soil density in the box was much lower than originally intended, at approximately 80%. Because of this, the swelling was significantly reduced from what would be expected.

Figure 40. Soil Swell After Testing

Overall, there does appear to be a reduction in swell pressure through the use of the crumb rubber. Accounting for the original pressure of the moist soil applied on the bottom sensor, there is a 66% reduction in swelling pressure between Sensor T and Sensor 2T (Sensor T of Box Test 2) and 31% reduction between Sensor B and Sensor 2B (Sensor B of Box Test 2). This is how all subsequent "percent reduction in swelling pressure" comparisons will be made. A comparison of the swelling curves can be seen in Figure 41.

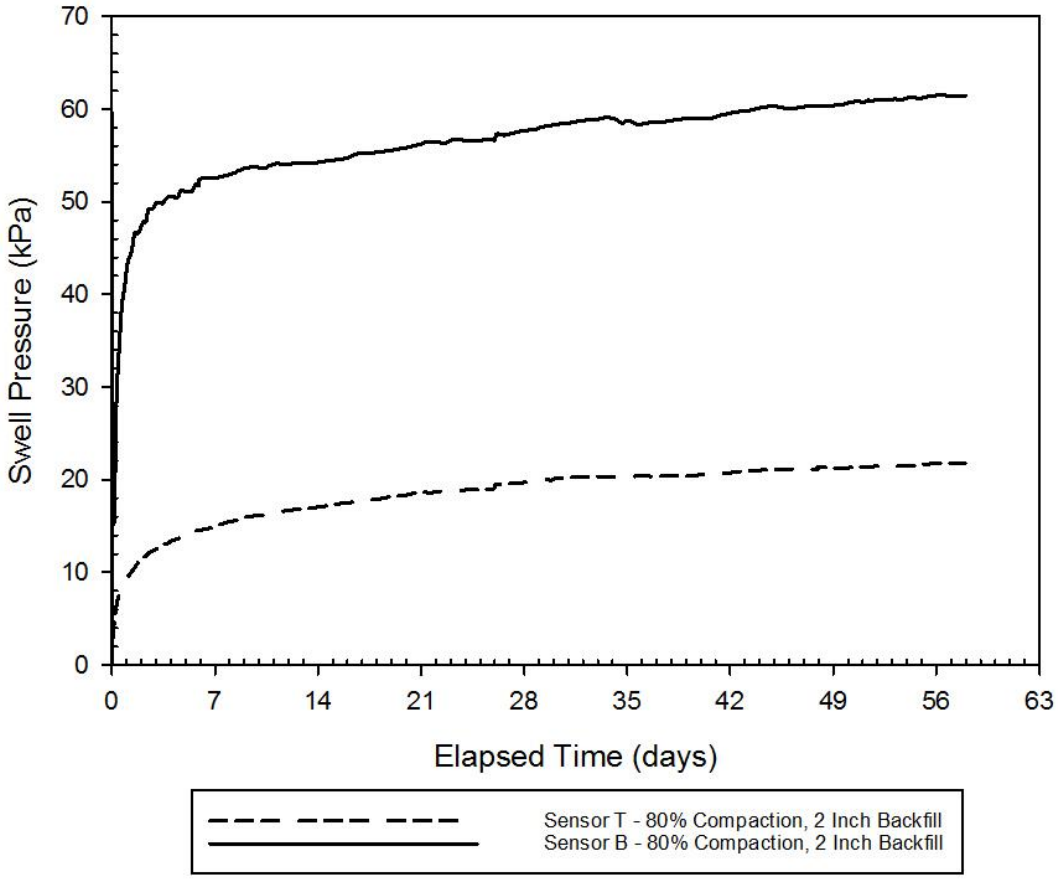

Figure 41. Swell Pressure vs. Elapsed Time for Box Test 1 (80% Compaction, 2 Inch Backfill)

4.2.2 Box Test Two – No Backfill, 90% Compaction

The second box test began on March 25, 2016 and continued through April 15, 2016, for a total soak time of 21 days. Though it was anticipated that the test would soak for a total of 60 days, there was no significant change in the swelling pressure after the first seven days, and therefore it was removed from the water bath early. The maximum swelling pressure read by Sensor T was 90 kPa and 64 kPa by Sensor B, accounting for the original pressure exerted on Sensor B due to the soil. However, the pressures had an approximately 25 kPa difference. Though there was no crumb rubber, there is still a rather significant difference in the swelling pressures measured. This can be attributed to two factors. One, because of the aspect ratio of the box, there is a large amount of side friction.

This would significantly reduce the swelling pressure in the vertical direction. Two, the soil on the bottom is in direct contact with the bottom plate and sensor due to compaction. However, though care was taken to make the top of the soil flush with the edge of the walls, the top of the soil may have had a small gap between the sensor and soil, allowing for some swelling to occur before registering the swell pressure. The swelling curves for both sensors can be seen in Figure 42.

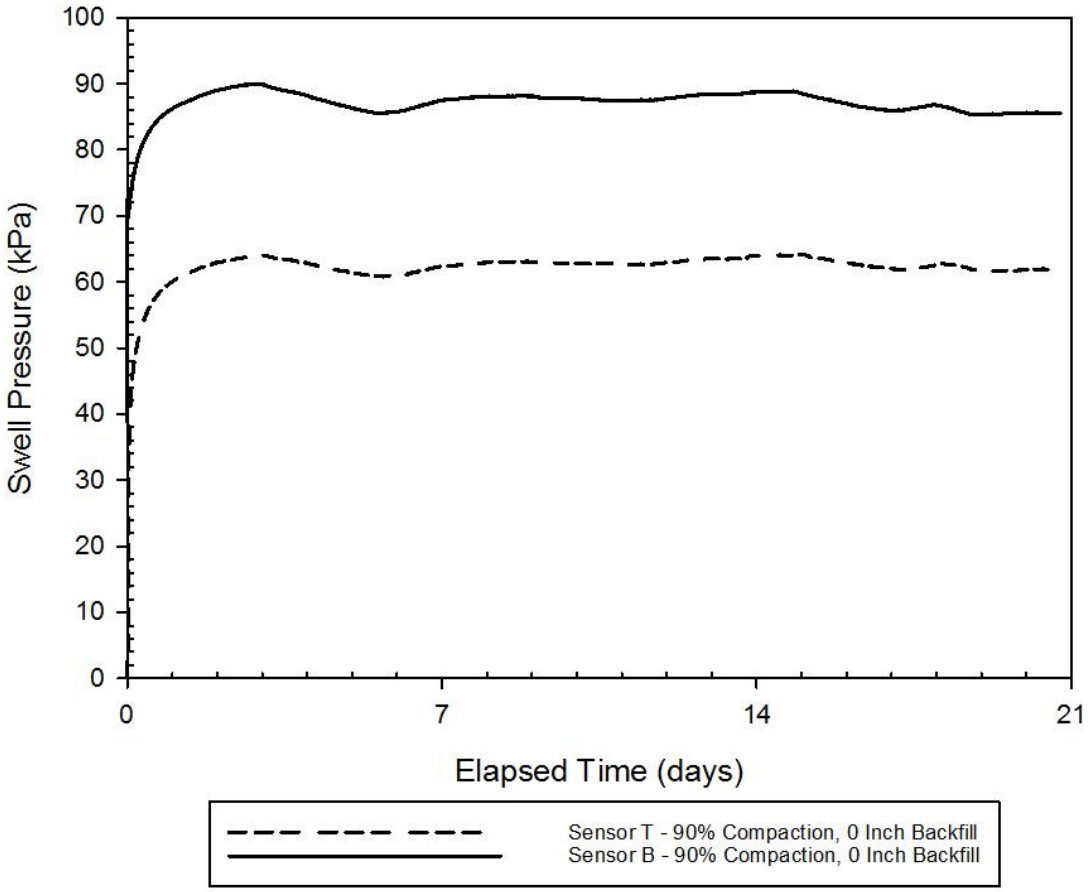

Figure 42. Swell Pressure vs. Elapsed Time for Box Test 2 (90% Compaction, 0 Inch Backfill)

After the test was completed, water contents were taken on all four corners of the box. The final water contents ranged from approximately 26% to 35%, with 100% saturation occurring at a water content of 34.2%. However, it should be noted that no water contents

were taken from the center of the box as the soil was not stiff enough to collect. Attempts were made to get water contents from the center, but because there was no confining pressure on the top, the soil sampler was unable to get a full soil sample from the center. The water content profiles can be seen in the following figures. Each plot depicts a plan view of the box, with the distances along the x and y axis being the distance from the southwest corner of the box. Each plot is averaged for a two inch deep section (i.e. 0-2 inches, 2-4 inches, etc.). Recall that the soil was compacted within +/- 0.5% of the optimum moisture content, and that 100% saturation is achieved when the water content is approximately 34.2%.

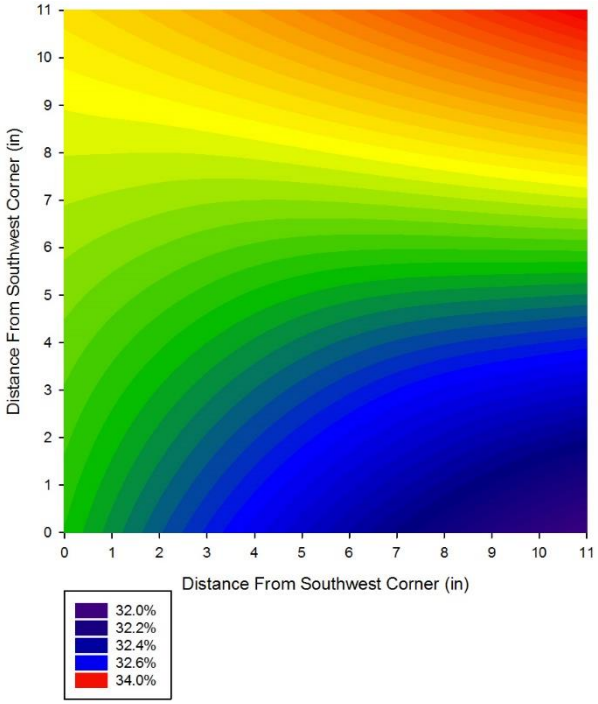

Figure 43. Average Final Water Content Profile, Box Test 2, 0-2 Inch Depth

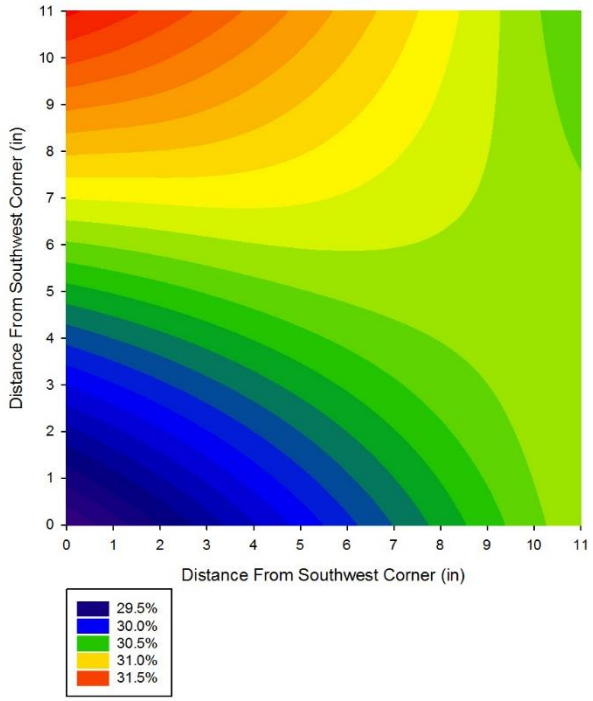

Figure 44. Average Final Water Content Profile, Box Test 2, 2-4 Inch Depth

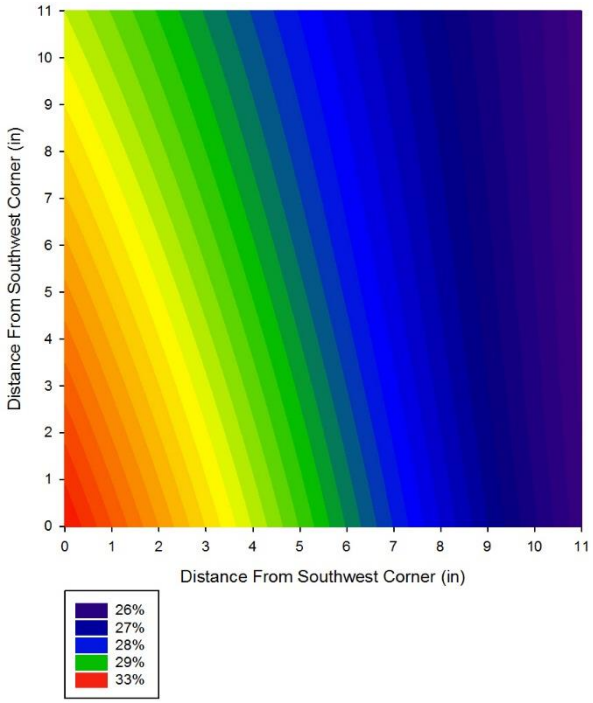

Figure 45. Average Final Water Content Profile, Box Test 2, 4-6 Inch Depth

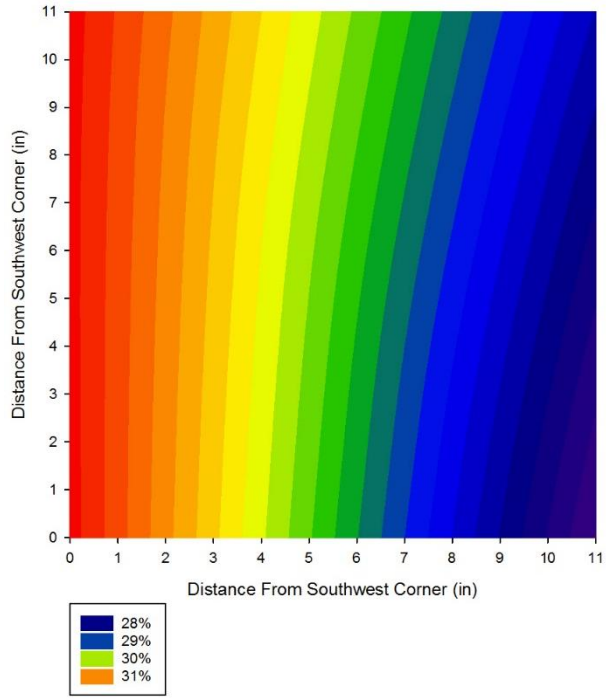

Figure 46. Average Final Water Content Profile, Box Test 2, 6-8 Inch Depth

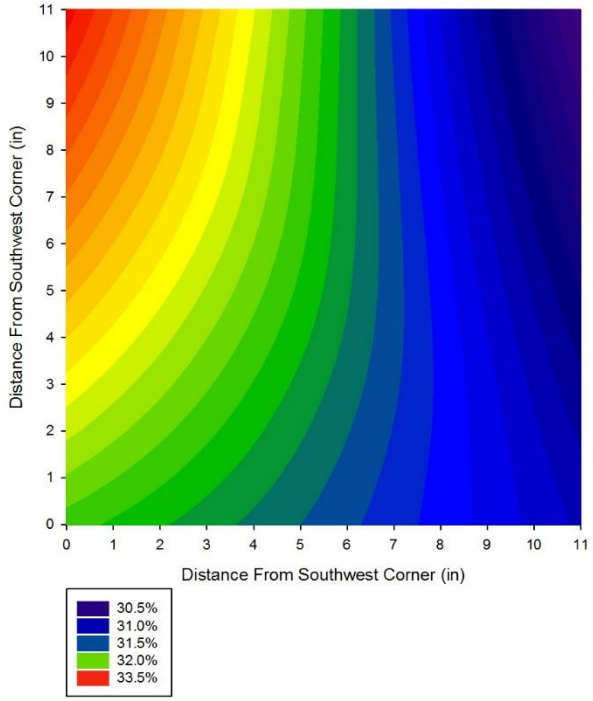

Figure 47. Average Final Water Content Profile, Box Test 2, 8-10 Inch Depth

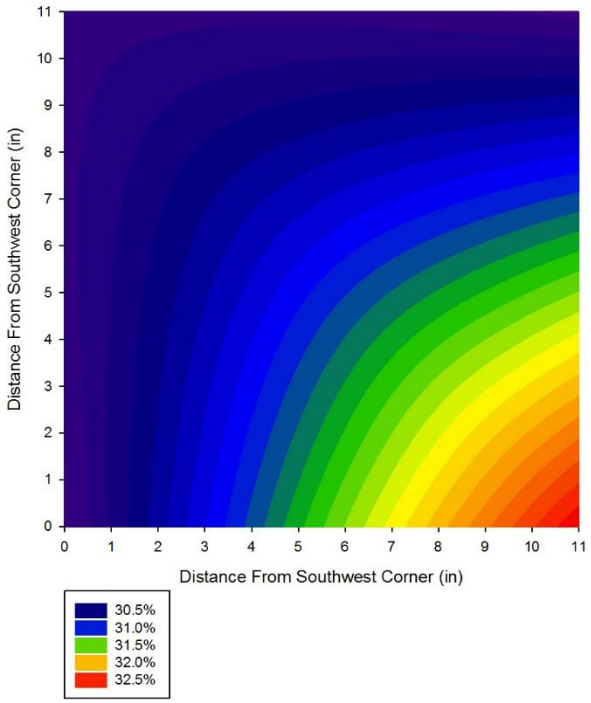

Figure 48. Average Final Water Content Profile, Box Test 2, 10-12 Inch Depth

As can be seen in the preceding figures, the water contents are not uniform throughout the box, even after being completely submerged for 60 days. For example, in the 0-2 inch depth, the highest water contents are along the west side of the box, specifically in the southwest corner. However, in the 10-12 inch depth profile, the highest water contents have alternated to the southeast side. This is due to the placement of the porous stones. When looking at the box plan view, the porous stones are placed in the upper left and lower right corners (see Figure 49). This typically results in higher water contents towards the west side in the upper half of the box, and higher water contents in the lower half of the box. This will be a common pattern throughout the final water content profiles, and can account for the heterogeneity in the plots.

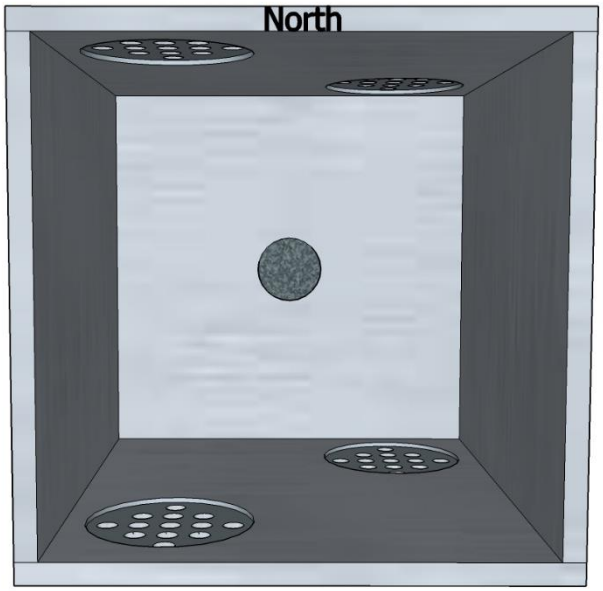

Figure 49. Porous Stone Layout

4.2.3 Box Test Three – 2 Inch Backfill, 90% Compaction

The third box test began May 2, 2016 and ended May 25, 2016, for a total of 23 days. However, during testing, Sensor T became disconnected from the DAQ system, resulting in inaccurate data between the ninth and twenty-third day. Therefore, the results presented are only for the first nine days for Sensor T. In the first nine days, the maximum swell pressure measured by Sensor T was 47 kPa and 68 kPa by Sensor B, excluding the first 24 hour period, as explained below Figure 50. Accounting for the original pressure exerted on Sensor B, there was approximately 27% reduction in swell pressure for Sensor T and approximately 24% reduction for Sensor B. The swelling curve for both sensors can be seen in Figure 50.

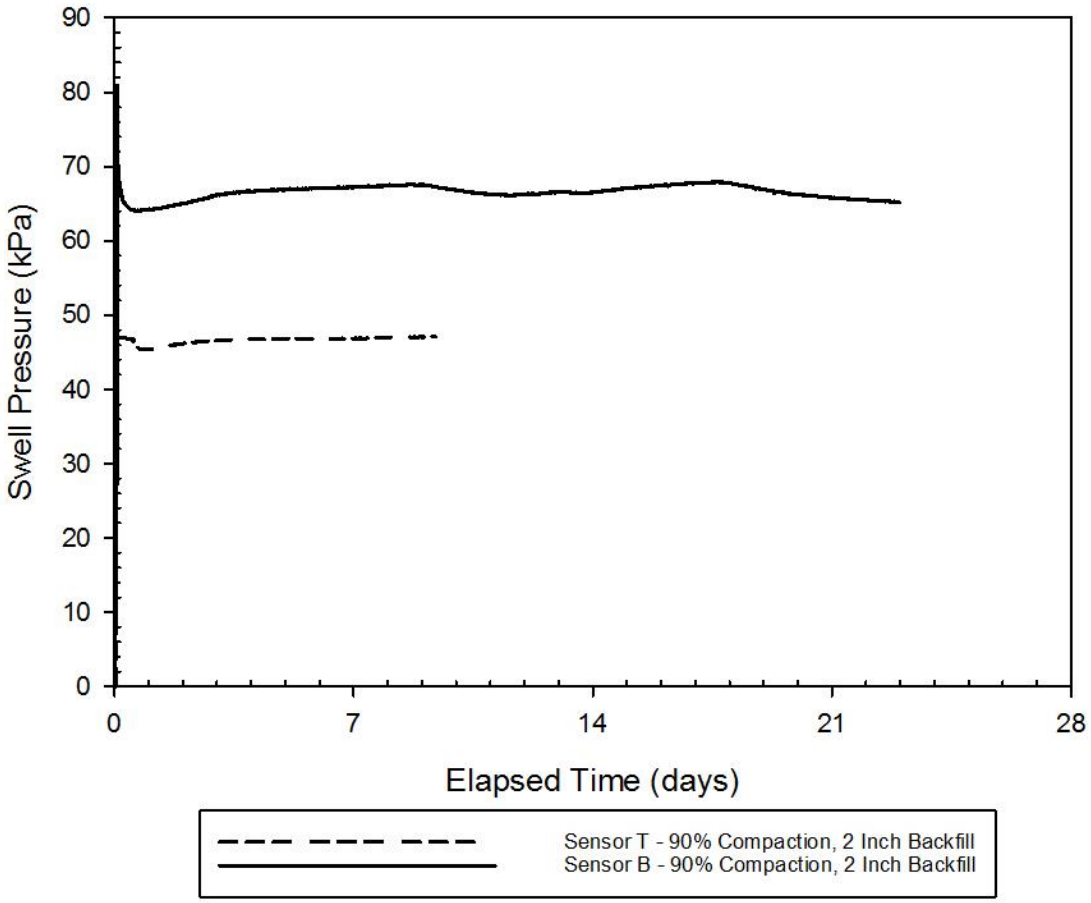

Figure 50. Swell Pressure vs. Elapsed Time for Box Test 3 (90% Compaction, 2 Inch Backfill)

It should be noted that the bump in the curve in the first 24 hours is most likely due to compaction, as the sensors take some time to come to equilibrium once a load is placed on or removed from them. For example, when applying a 5 kg test load and removing it a couple of hours later, the sensors may read the test load for a couple of hours before zeroing out. Larger loads take additional time. If large loads were placed on the sensors from compaction efforts, it would take some time for the sensors to come to equilibrium and read the correct load. The bump in Sensor T is the same concept, except that instead of being from compaction efforts, is most likely due to force applied to the top during

attachment, as the rubber would not be perfectly flush with the top of the box before attaching the top.

Once again, after the test was completed, water content samples were taken from each corner. No water contents were taken for the crumb rubber. However, as discussed previously, water content samples were taken from the center portion of the box during breakdown of the soil. The final water contents ranged from approximately 27% to 35%. Note that these values may be less than the actual value as the center samples were not able to be retrieved immediately after removing the box from the water bath. The final water content contour plots can be seen in the following figures. Once again, the contour plots are a plan view of the box, and are averaged over each two inch section. Saturation is achieved at a water content of approximately 34.2%.

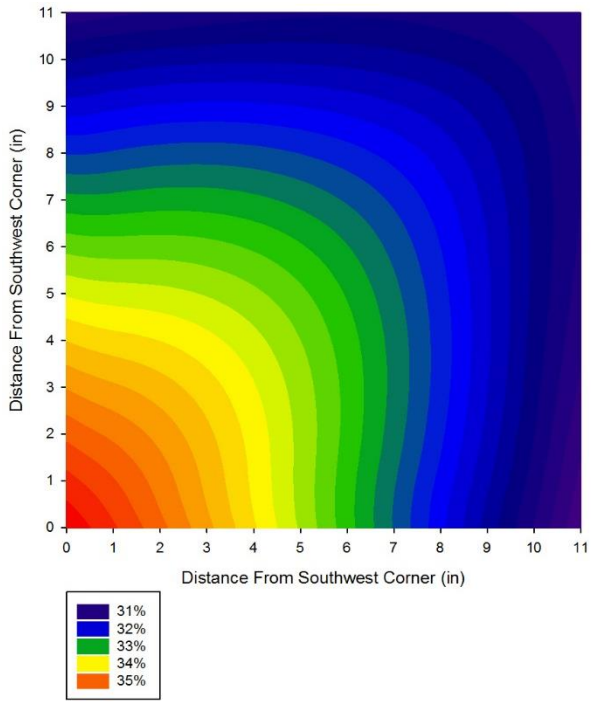

Figure 51. Average Final Water Content Profile, Box Test 3, 2-4 Inch Depth

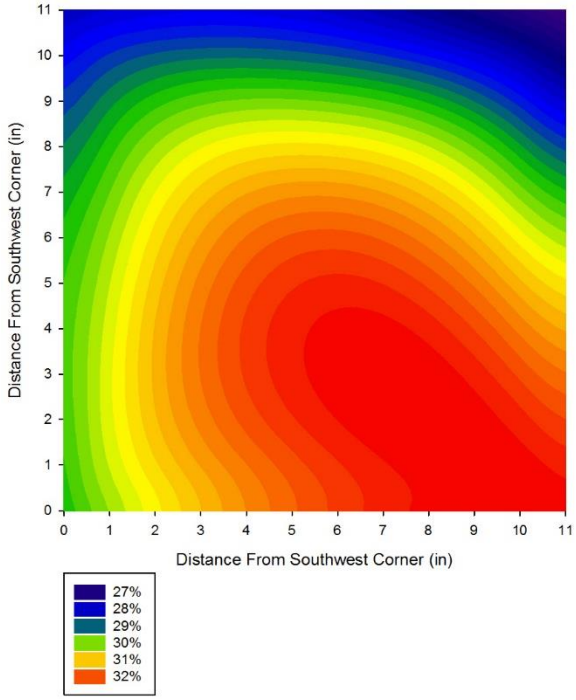

Figure 52. Average Final Water Content Profile, Box Test 3, 4-6 Inch Depth

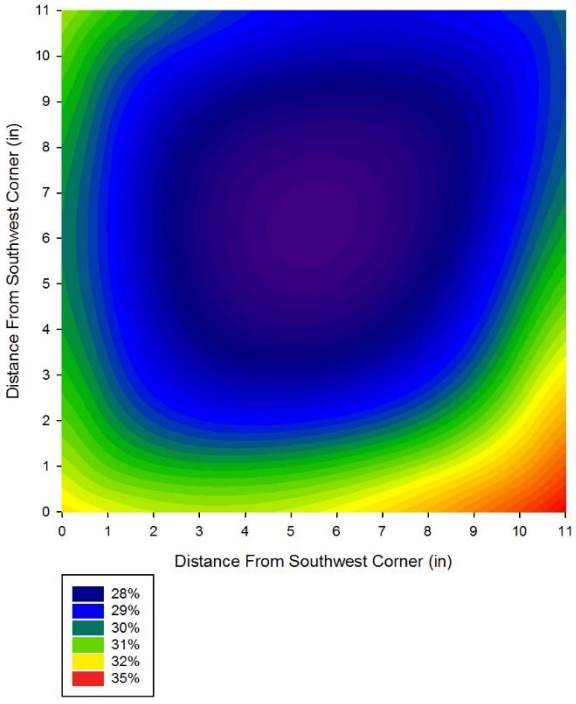

Figure 53. Average Final Water Content Profile, Box Test 3, 6-8 Inch Depth

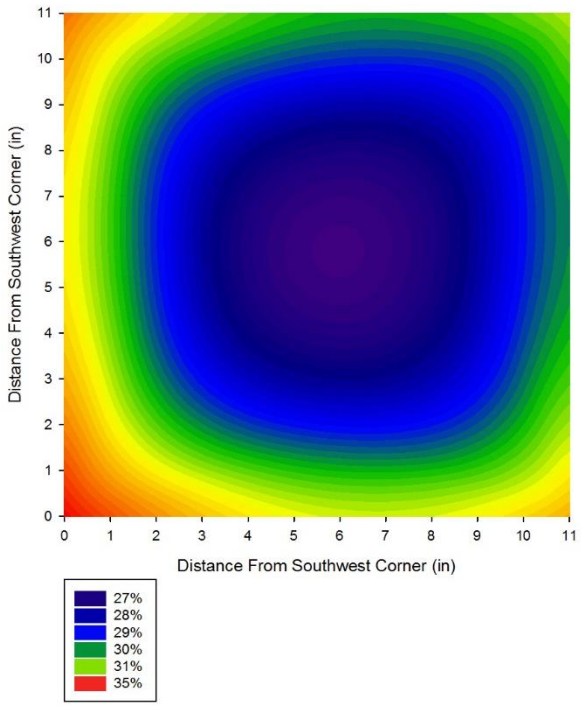

Figure 54. Average Final Water Content Profile, Box Test 3, 8-10 Inch Depth

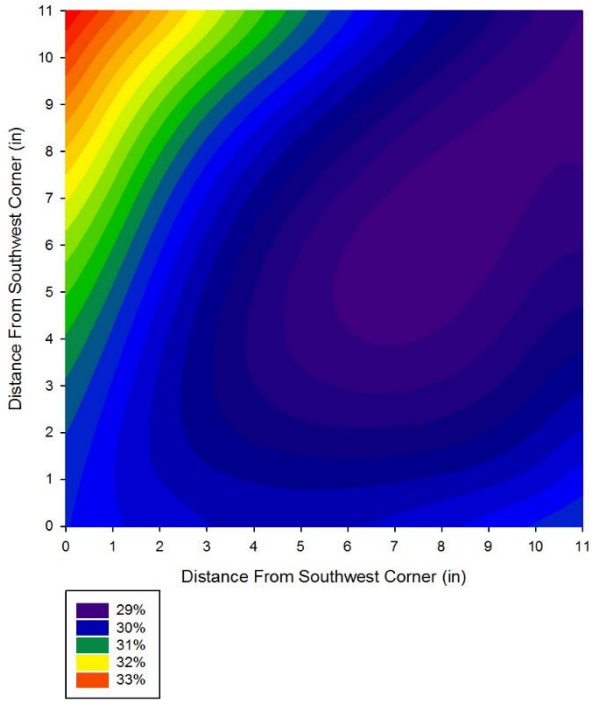

Figure 55. Average Final Water Content Profile, Box Test 3, 10-12 Inch Depth

As discussed in the preceding section, the water content profiles generally have higher values on the west side for the top 6 inches of the box, and higher values on the east side for the bottom 6 inches of the box. However, the middle 4 inches have more homogenous water contents, which is consistent with what would be expected, as water would be traveling from both the top and bottom at equal distances. Additionally, because of the rubber's high permeability, water could travel more easily through the rubber and to the soil, explaining the overall higher water contents in the 2-4 inch water content profile.

4.2.4 Box Test Four – 2 Inch Backfill, 89% Compaction

The final box test began June 8, 2016 and continued through July 18, 2016. The soil stopped swelling at approximately three days, with maximum swelling pressures reaching 47 kPa for Sensor T and 62 kPa for Sensor B. These values exclude the first 24 hours where the sensors may have been affected by compaction. Accounting for the original soil pressure exerted on Sensor B, the percent reduction is approximately 27% for Sensor T and 31% for Sensor B. The swelling curve for the final box test can be seen below.

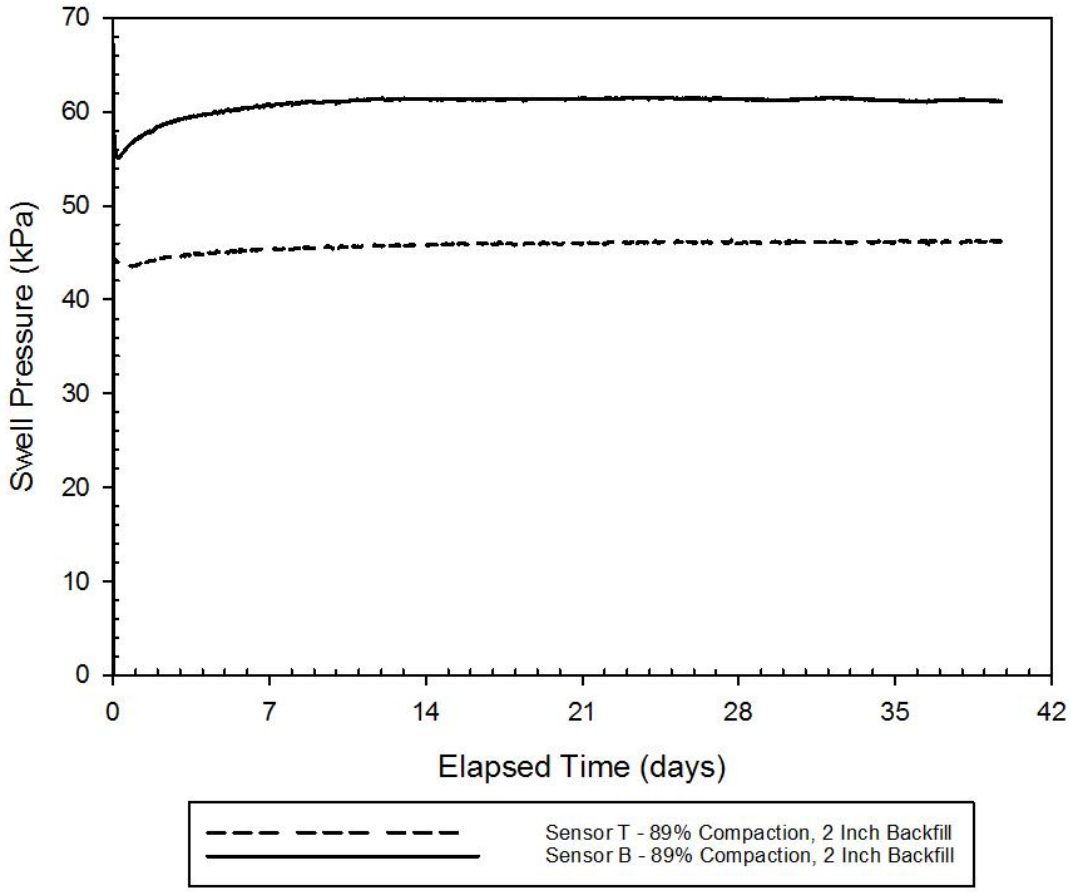

Figure 56. Swell Pressure vs. Elapsed Time for Box Test 4 (89% Compaction, 2 Inch Backfill)

After the test was removed from the water bath, water contents were taken using a soil sampler in the four corners and the center. For this final test, a sample for the rubber was taken in the five sampling locations. However, it should be noted that the rubber dried very quickly, and therefore the water contents may not be representative of the true water content. The final water contents for the soil ranged from approximately 27% to 36%, with some portions of the box reaching 100% saturation. The water content profiles were then plotted and can be seen below. Also note that these water content contour plots were completed after the box retrofit, and therefore differ from the previous water content patterns. Recall that saturation is attained at a water content of approximately 34.2%.

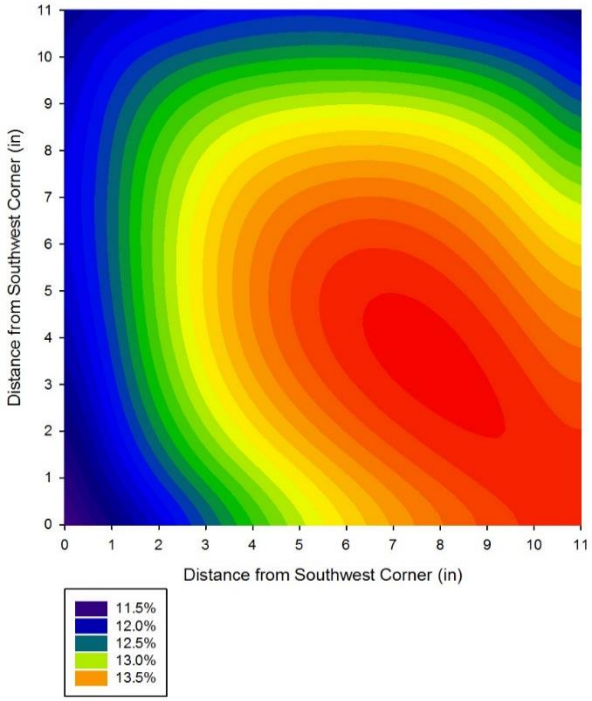

Figure 57. Average Final Water Content Profile, Box Test 4, 0-2 Inch Depth

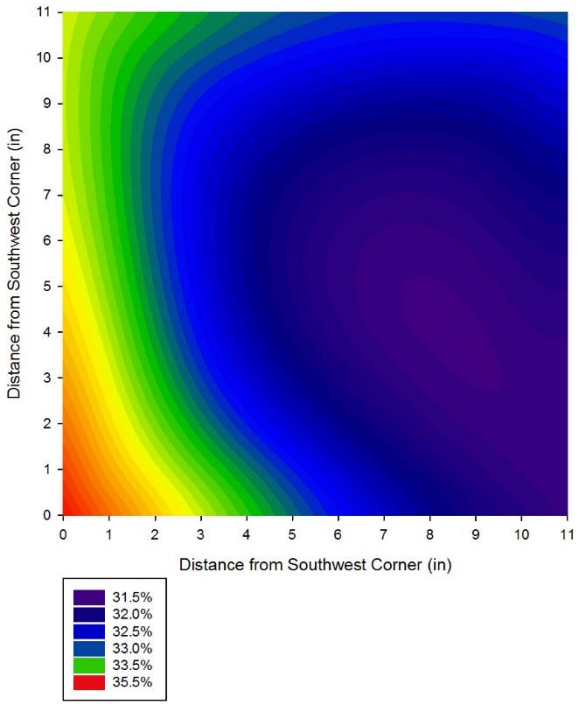

Figure 58. Average Final Water Content Profile, Box Test 4, 2-4 Inch Depth

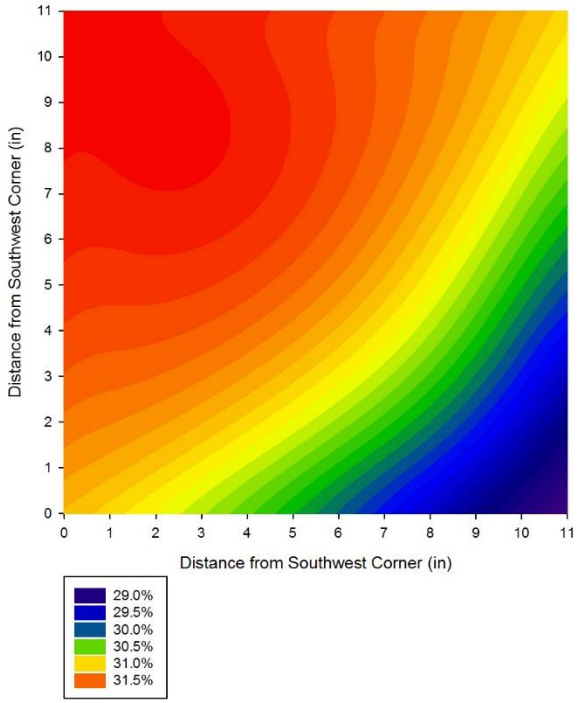

Figure 59. Average Final Water Content Profile, Box Test 4, 4-6 Inch Depth

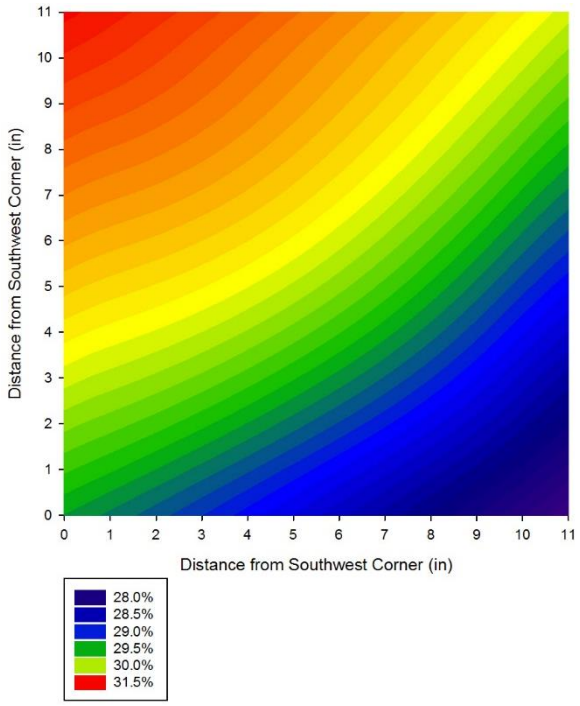

Figure 60. Average Final Water Content Profile, Box Test 4, 6-8 Inch Depth

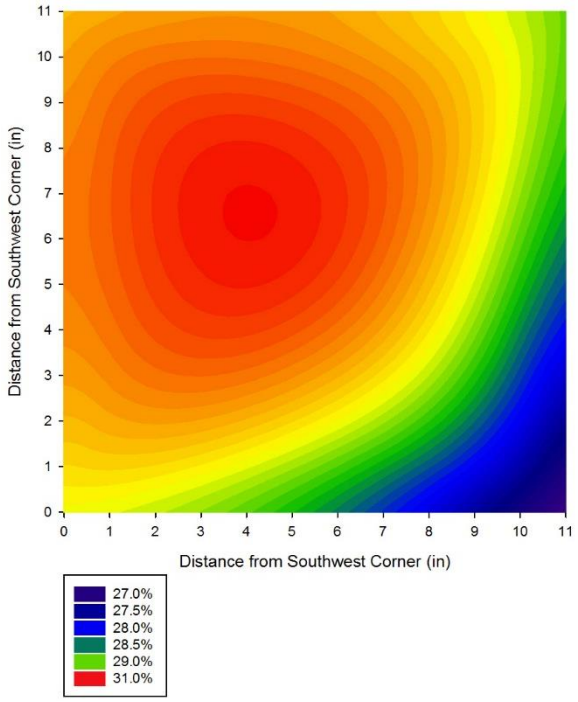

Figure 61. Average Final Water Content Profile, Box Test 4, 8-10 Inch Depth

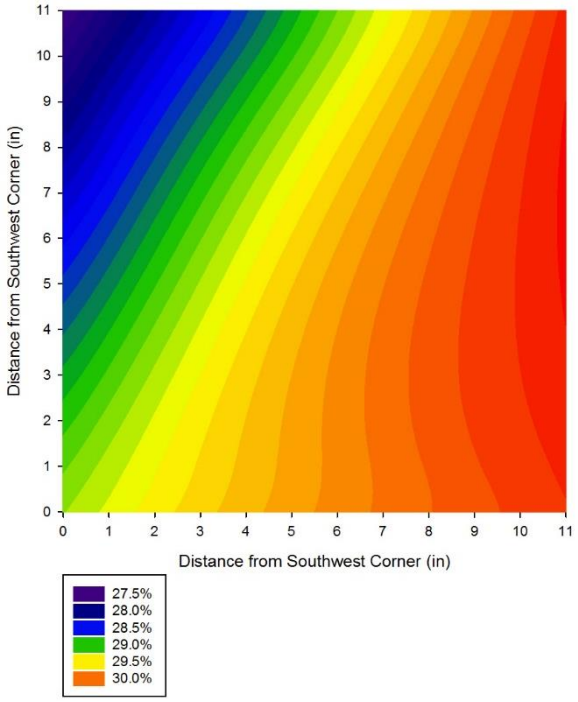

Figure 62. Average Final Water Content Profile, Box Test 4, 10-12 Inch Depth

With the addition of the pipes, the water contents were greater towards the center of the box, but were approximately the same in the four corners. This can also be seen in the swelling of the clay. The center portion of the box swelled more than the outer edges, resulting in a sort of dome shape. This may be attributed to additional water towards the center of the box, as well as friction between the wall and soil. However, the soil simply may have not reached equilibrium, and therefore, the water contents were not homogenous. This could be due to the high plasticity and low permeability of the clay. Though the pipes did result in a more homogenous water content distribution, a longer soaking period may have resulted in a more even distribution. Once again, the 2-4 inch profile has generally higher water contents compared to the lower 8 inches. This is most likely due to the crumb rubber serving as a quick path for water to travel.

4.2.5 Test Comparisons

The following figures compare each of the swell curves for the four completed tests. Figure 63 compares the swell curves for Sensor T for all four tests, Figure 64 compares the swell curves for Sensor B for all four tests, and Figure 65 compares both sensors for all four tests.

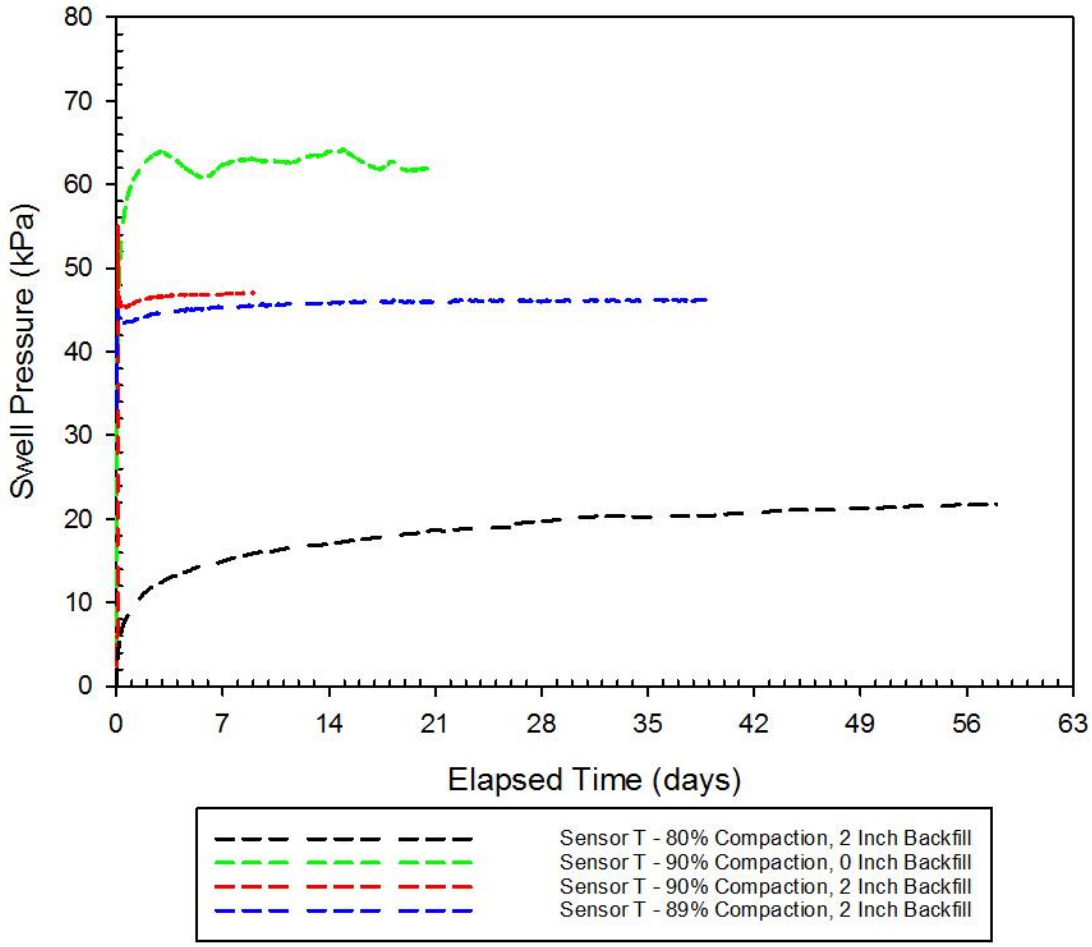

Figure 63. Swell Pressure vs. Elapsed Time for Sensor T for Box Tests 1-4

It can be seen that the top sensor for Box Test 2 swelled much more than the other tests, which is to be expected given that there was no crumb rubber present, and therefore the clay was in direct contact with the pressure sensor. Box Test 3 and 4 showed similar swell pressure values, with Box Test 4 showing slightly less swell. Again, this was predicted given that Box Test 3 and 4 had the same amount of rubber present, with very similar densities. Box Test 1 showed very low swell pressures at the top sensor, due to the low compaction percentage. The low compaction would also explain the gradual swelling pattern compared to the more immediate swell and plateau pattern exhibited in Box Tests

2, 3, and 4, given that there were more voids to fill within the box before expanding outward.

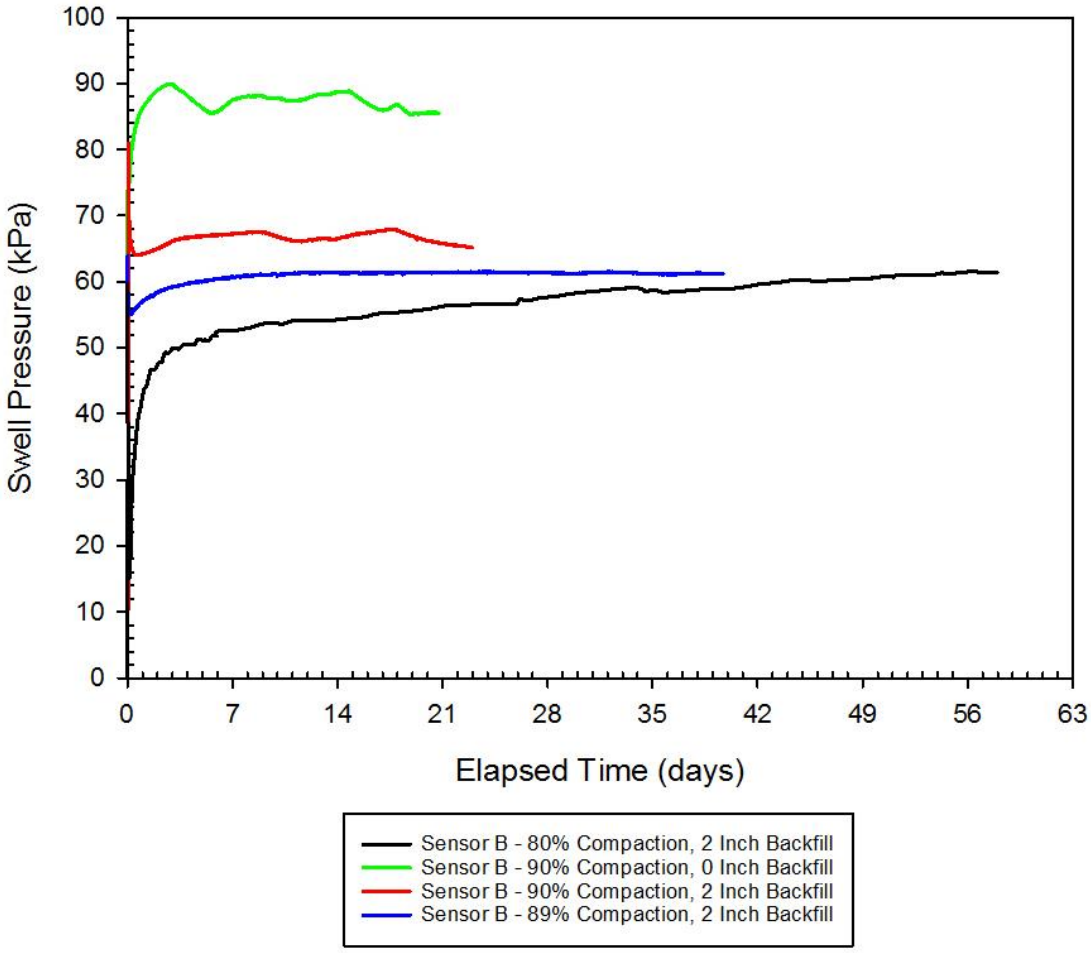

Figure 64. Swell Pressure vs. Elapsed Time for Sensor B for Box Tests 1-4

The bottom sensors in each test showed basically the same trends as the top sensors, with Box Test 2 having the highest swell, Box Test 3 and 4 showing similar swell pressures and then Box Test 1 having the lowest swell pressures. The bottom sensors recorded higher swell pressures than the top sensors in each Box Test, most likely because of the combined effects of gravity and the weight of the entire soil sample on top of the sensor. In all of the tests performed at 90% compaction (Box Tests 2, 3, and 4), there was a

relatively consistent difference between the top and bottom sensors. These differences can be seen in the following figure and table, Figure 65 and Table 10. For each of the tests with 90% compaction, there was approximately 25% to 30% reduction in swell pressure, despite the disparity in actual swelling pressures. However, the large disparity between the top and bottom sensor pressures in all of the tests can be attributed to side friction effects. Because of the 1:1 aspect ratio, friction along the wall most likely resulted in smaller swelling pressures in the center of the box (where the sensors were located), producing lower swell pressures than anticipated. This is further confirmed when looking at the swelling of the soil itself upon removal of the crumb rubber after the saturation period, where the soil tended to bulge in the middle of the box, creating a sort of domed shape. This was most noticed after Box Test 4, where the center portion of the box received more water than in previous tests.

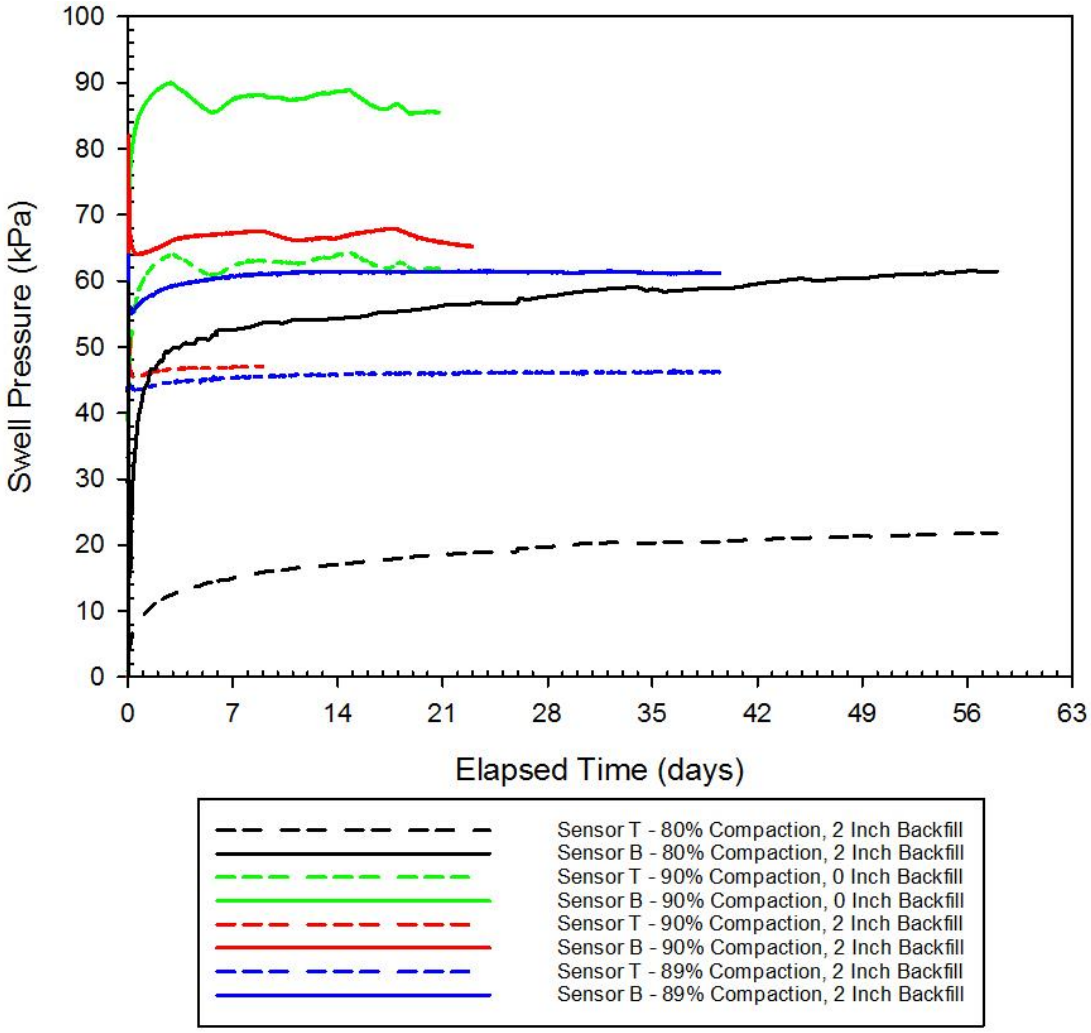

Figure 65. Swell Pressure vs. Elapsed Time for Sensors T and B for Box Tests 1-4

Table 10. Box Test Comparisons

Test Description	Backfill Thickness to Total Height Ratio	Maximum Swelling Pressure, Sensor T (kPa)	Maximum Swelling Pressure, Sensor B (kPa)	Percent Reduction, Sensor T vs. Sensor 2T	Percent Reduction, Sensor B vs. Sensor 2B
Box Test 1: 80% Comp., 2 Inch Backfill	1:6	22	62[1]	66	31
Box Test 2: 90% Comp., 0 Inch Backfill	0:12	64	90[1]	0	0
Box Test 3: 90% Comp., 2 Inch Backfill	1:6	47	68[1]	27	24
Box Test 4: 89% Comp., 2 Inch Backfill	1:6	47	62[1]	27	31

[1]These values have been corrected to include the original pressure of the soil.

Please note, in the preceding table, the percent reduction for Sensor T vs. Sensor 2T is comparing that individual test's Sensor T value to the Sensor T value of Box Test 2. For example, to find the percent reduction for Box Test 1, the maximum swelling pressure for Sensor T for Test 1 would be subtracted from the maximum swelling pressure for Sensor T for Test 2, and then divided by the maximum swelling pressure for Sensor T for Test 2 (so, (64-22)/64, resulting in 66% reduction). This same concept can be applied to Sensor B.

4.2.6 Comparison to Previous Work

After all of the box tests were completed, a comparison was made to Katti and Ikizler's previous work. The gray highlighted cells in Table 11 are tests with similar backfill thickness to total height ratios swelling in comparable directions for a more accurate

comparison. Though Katti and Ikizler measured lateral swell in the majority of their testing, the non-swelling material was placed in the lateral direction and therefore has comparable results (swelling direction perpendicular to non-swelling material). More specifically, the tests with the most comparable results are Katti's 'BCS with 0 CNS on Top' and Ikizler's 'Siran - 2 Clay and Bentonite Mixture - Lateral Swell' test results. Comparing the box test results to those of Katti and Ikizler, it can be concluded that the box tests with approximately 90% compaction (tests three and four) reduce the swelling pressure much less than either Katti's non-swelling cohesive soil or Ikizler's geofoam. However, it is very important to note that in Katti's study, there was no confinement on the top of the test setup. By allowing vertical movement, the lateral swelling can be significantly altered. Because of this, Katti's results may not be analogous.

The blue highlighted cells in Table 11 are tests with similar backfill thickness to total height ratios where the pressure being measured is not in direct contact with the non-swelling material. Looking at the vertical swell measured in Ikizler's experiments (where geofoam was only present between a vertical wall and soil) and the vertical swell on the bottom sensor in each of the box test experiments, the percent reduction in the crumb rubber tests is still significantly less than those in the geofoam study. While these results are not perfectly comparable (i.e. the non-swelling material and swelling are not in the same placement or direction) and it is typically assumed that vertical swelling (swelling in direction of compaction) is greater than lateral swelling, it can still be concluded that the crumb rubber did not reduce the swelling pressures as effectively as the geofoam.

Table 11. Box Test Results Compared to Previous Work

Soil	Backfill Thickness (cm)	Backfill Thickness to Total Height Ratio		Percent Reduction in Swell Pressure (%)
Heiden Clay - Vertical Swell, Top Sensor	5[1]	1:6	0.17	66[α]
	5[3]	1:6	0.17	27[α]
	5[4]	1:6	0.17	27[α]
Heiden Clay - Vertical Swell, Bottom Sensor	5[1]	1:6	0.17	31*
	5[3]	1:6	0.17	24*
	5[4]	1:6	0.17	31*
Black Cotton Soil (BCS) with 0 CNS on Top - Lateral Swell	20	1:16	0.06	48.0
	40	1:8	0.13	81.67
	60	3:16	0.19	86.26
	100	5:16	0.31	90.0
Black Cotton Soil (BCS) with 100 CNS on Top - Lateral Swell	20	1:15	0.07	38.88
	60	1:5	0.20	72.98
	100	1:3	0.33	87.92
Siran - 2 Clay and Bentonite Mixture - Lateral Swell	0.9	0.9:25	0.04	52
	2.5	1:10	0.10	64
	5	1:5	0.20	76
Siran - 2 Clay and Bentonite Mixture - Vertical Swell	0.9	0.9:25	0.04	25
	2.5	1:10	0.10	26
	5	1:5	0.20	50

[1] Indicates Box Test 1.
[3] Indicates Box Test 3.
[4] Indicates Box Test 4.
[α] For each test, the swell pressure for Sensor T is being compared to Sensor T in Test 2.
* For each test, the swell pressure for Sensor B is being compared to Sensor B in Test 2.

In the above table, the values noted with an α are calculated as described in Table 10, where Sensor T for an individual test is compared to Sensor T of Box Test 2. Likewise, the values noted with an * are compared to the swelling pressure of Sensor B of Test 2. Therefore, for each comparison, the calculation is the maximum swelling pressure for Sensor T or B for Test 2, subtracting the maximum swelling pressure for Sensor T or B for that specific test, and then dividing by the maximum swelling pressure for Sensor T or B for Test 2 (for example, (90-62)/90, resulting in 31% swell pressure reduction of Sensor B in Test 2). Comparing these results in graphical form, it is clear that the percent

reduction using crumb rubber is much less than when using non-swelling cohesive backfill or geofoam, though the graph only depicts the values for Sensor T for the box tests. As stated previously, the most accurate comparisons are by grouping Tests 3 and 4 with BCS with 0 CNS on top and Siran - 2 clay with lateral swell. Looking at these values on the graph (depicted with an x, hexagon, circle, and square, respectively and highlighted in red), it is apparent that the box test reduction values are less than half of what the non-swelling cohesive backfill and geofoam reduction values are.

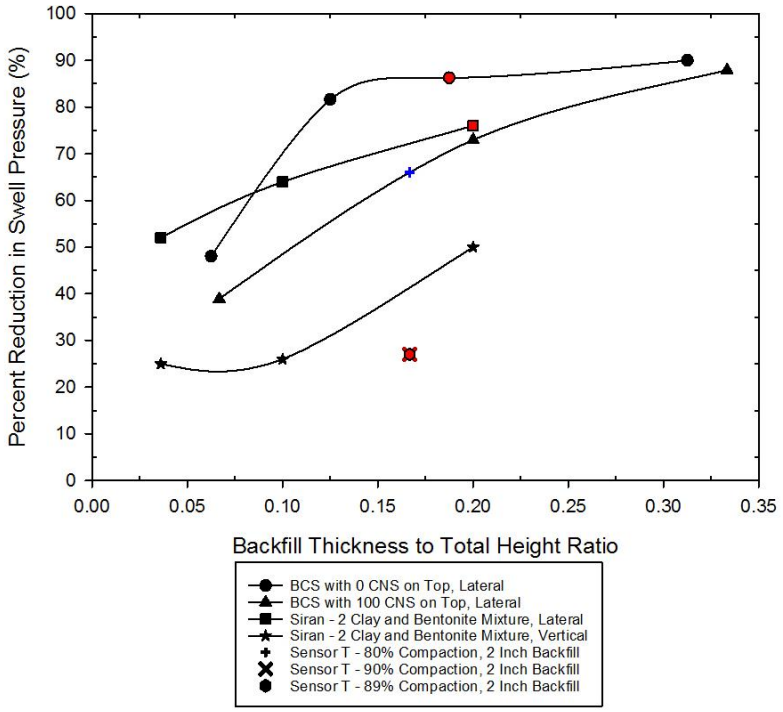

Figure 66. Backfill Thickness to Total Height Ratio vs. Percent Reduction in Swell Pressure

As can be seen in the preceding figure, Box Test 1 (80% compaction with 2 inch backfill, highlighted in blue) agrees very well with the curve for Katti's tests with 100cm CNS on top. Though Box Test 1 did not reach the same amount of total percent reduction in swell pressure, it did achieve approximately 65% reduction in the swelling pressure. The key

difference between these two test comparisons is Katti's experiments have non-swelling material on both the vertical and horizontal faces of the test setup, whereas the box tests completed in this study only have non-swelling material in the horizontal direction.

4.3 Percent Reduction vs. Compaction Percentage Correlations

Comparing the compaction percentages to the percent reduction in swelling pressure for Sensor T, there does appear to be a very strong correlation between the two. Using the percent reduction for the tests with 80%, 89%, and 90% compaction and 2 inches of backfill, the trendline is almost perfectly linear with a coefficient of determination (R^2) of 0.9918. This correlation can be seen below in Figure 67. Using this trendline, the percent reduction values can be extrapolated for 95% and 100% compaction. However, to keep the same R^2 value, the rubber would be required to reduce the percent reduction by -11% with 100% compaction. Since this is not possible, it is assumed that at 100% compaction, the percent reduction is 0%. Using this 0% reduction at 100% compaction, we get a percent reduction of 12% at 95% compaction and an R^2 value of 0.9723. This correlation can be seen in Figure 68.

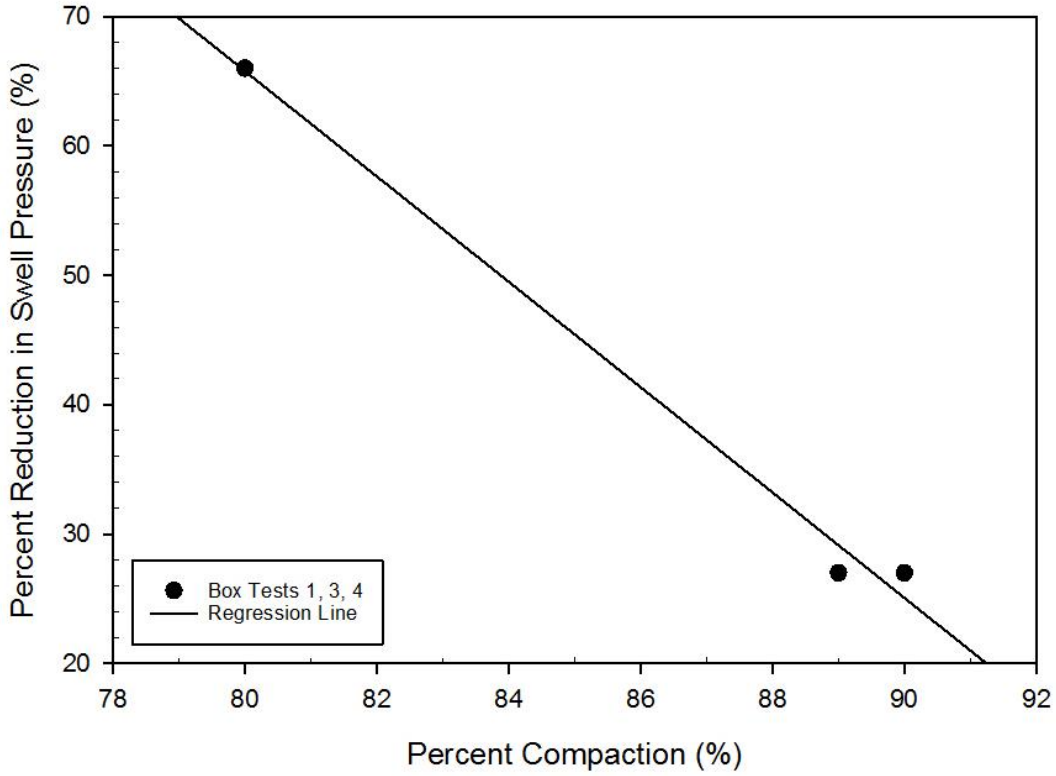

Figure 67. Compaction Percentage vs. Percent Reduction in Swell Pressure

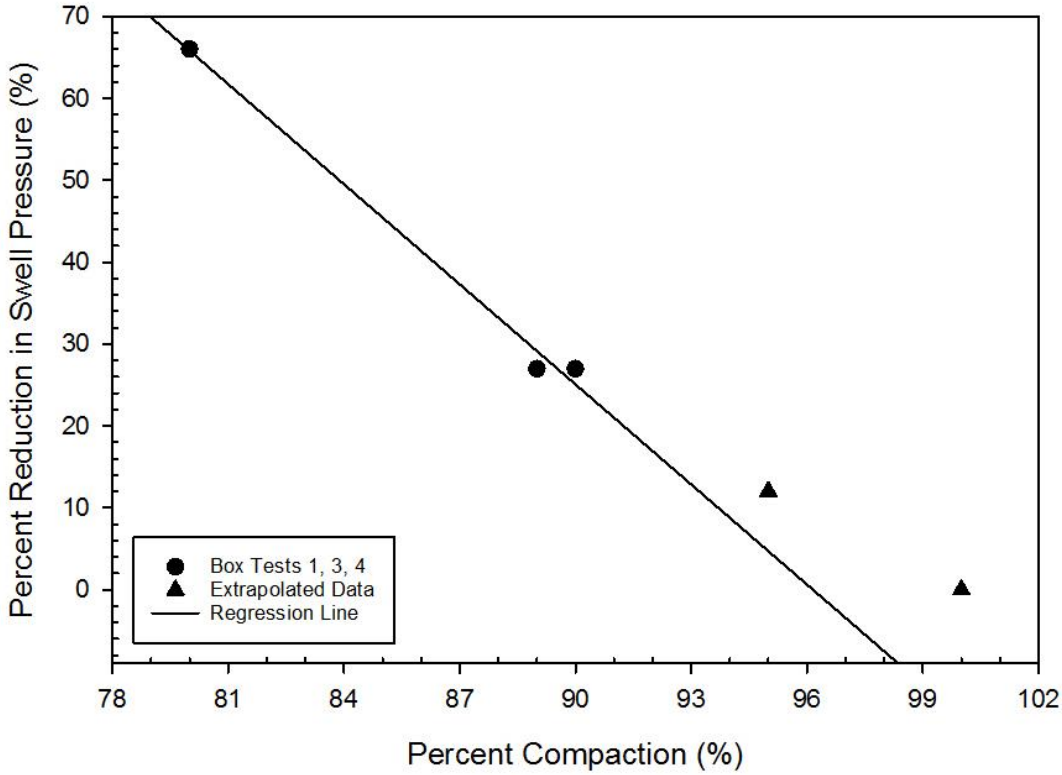

Figure 68. Compaction Percentage vs. Percent Reduction in Swell Pressure with Extrapolation

4.4 Finite Difference Modeling

As discussed in section 3.7 Finite Difference Modeling, the box test was modeled in compaction layers, with the layers above modeled as null and ‘placed’ after the compaction of each individual layer. Figure 69 shows the first compaction layer modeled in FLAC, where the lifts above it are modeled as null. Note that the lines running across the model denoted with multiple black lopsided ‘x’ are not physical boundaries, but layer boundaries marking each compaction lift. The aluminum walls were modeled as beams, with each square along the outer boundaries being a node, with one beam segment between two nodes. These segments were given properties consistent with the aluminum used in the physical tests. The left and right boundaries are fixed in the x direction, whereas the top and bottom boundaries are fixed in both the x and y direction. Interfaces were applied between the soil and walls on all sides of the box, so that the walls were not treated as frictionless surfaces in the analysis, and are modeled as a black ‘x’ at each node.

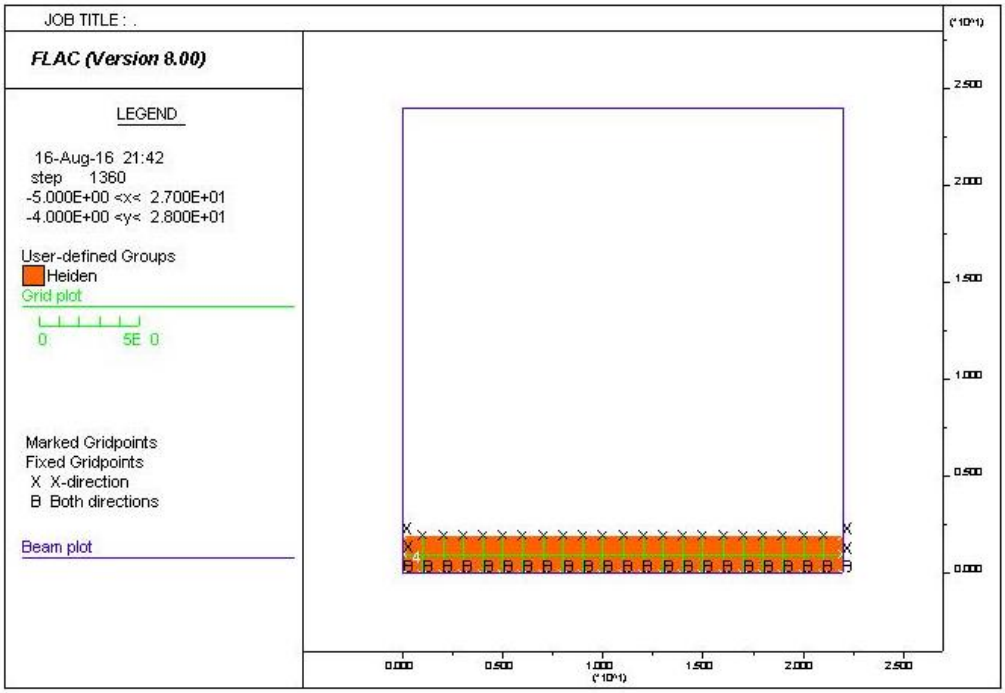

Figure 69. First Compaction Layer

Figure 70 shows the box after all of the layers have been 'placed,' and there are no null zones left. Between each layer, the unbalanced force was solved with a tolerance of 0.00001 pounds. After the box was fully filled with soil (or soil and rubber in subsequent analyses), a final unbalanced force calculation was completed.

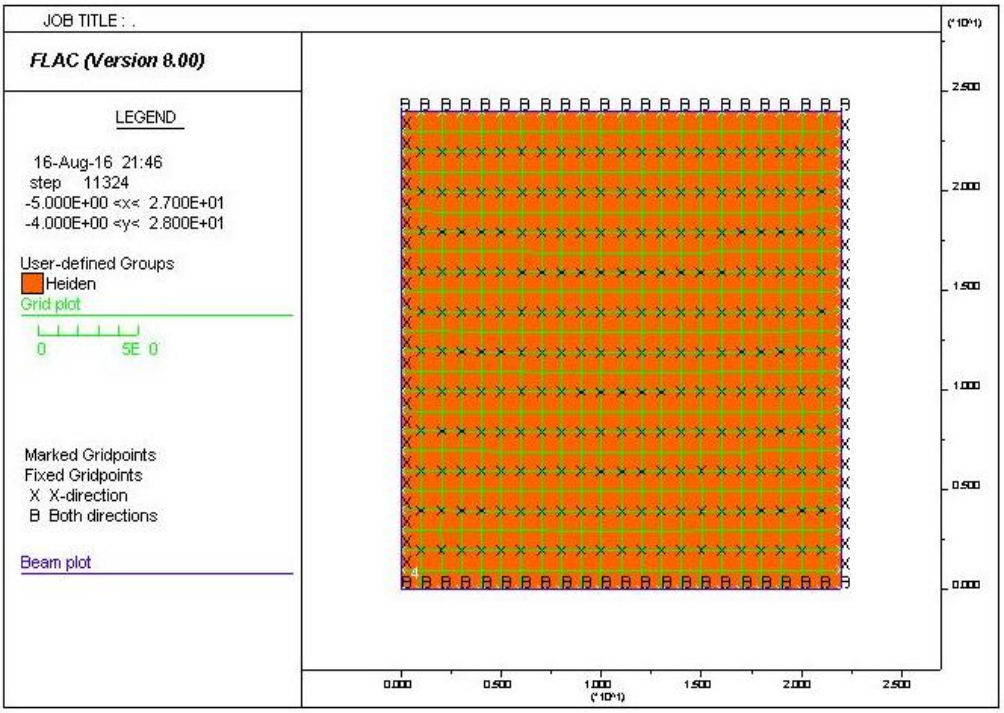

Figure 70. Final Compaction Layer

The pipes installed during the retrofit were implemented within the existing models with crumb rubber. However, in the analysis, there was no change in the existing density or initial pressure, as it was assumed that any change would be negligible. The pipes were modeled as cylindrical ‘beams’ with a radius of 3/8” and having the same properties as the aluminum walls. A schematic of this model can be seen in Figure 71.

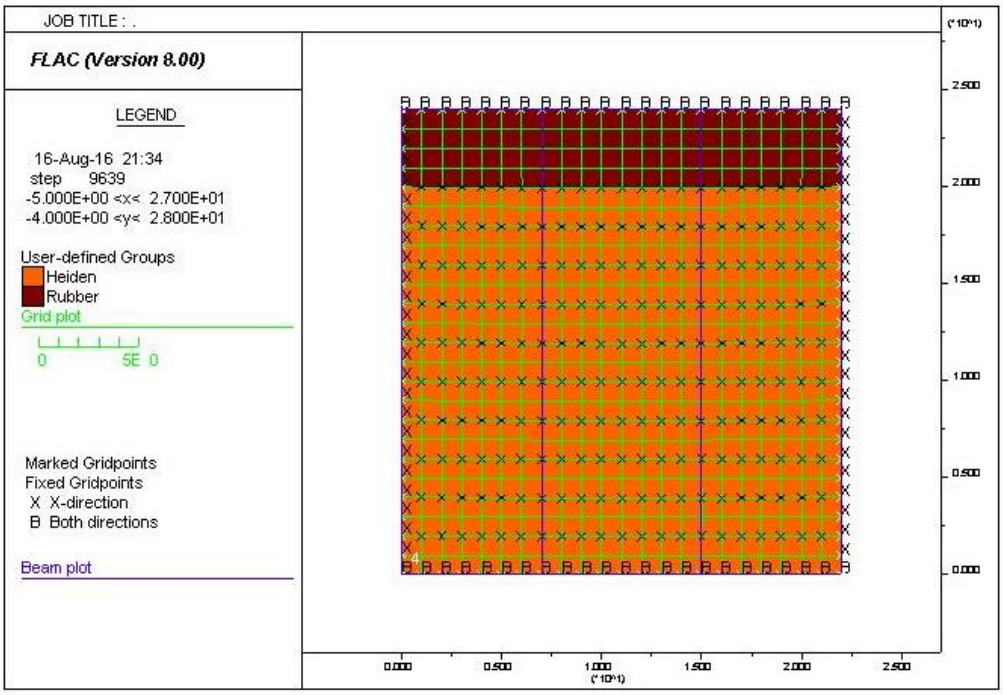

Figure 71. Box Test 4 Before Swell

After filling the box and solving for the unbalanced force, the swell parameters were put into the code to simulate the swelling of the soil after submersion. Using the method discussed in section 3.7 Finite Difference Modeling, the swell parameters were back-calculated from a 1-D swell curve. This resulted in values of 45 for a1, -3.35 for c1, and 0.06245 for m1. Note that this is based on a logarithmic swell curve, and that there is not one particular solution, but multiple possible solutions. It was assumed that a3, c3, and m3 were all zero, as there was no swelling in the x direction. After inputting these parameters, a final unbalanced force analysis was run, and the results were plotted in FLAC. The plots for y-stress contours with displacement vectors, x-stress contours with displacement vectors, y-displacement contours with displacement vectors, reaction forces, accumulated volumetric strain, displacement vectors, and magnified grid

distortion can be seen in Appendix A: FLAC Modeling. Note that negative values are not actually negative, but signify compressive forces.

The general patterns of the model are consistent with what would be expected, with the crumb rubber compressing as the clay swells and the greatest forces being exerted in the center of the box, particularly at the bottom of the box. However, the values measured are larger than what was actually measured in the box tests. For example, in the model of Box Test 2 (soil only), the maximum stress in the y-direction is -3.6e4 psf, which is equal to approximately 1720 kPa. This is far greater than what was measured in the actual tests. This could be due to inaccurate soil properties, such as bulk modulus or shear modulus, or, more likely, inaccurate interface properties. Models were run with their assigned friction and cohesion interface values, as well as with friction or cohesion values of zero, and the analyses concluded that the interface friction or cohesion values did not alter the results. However, if a structural element (in this case, a beam) is modeled without an interface, the model will treat the structural element as frictionless. It was also determined that changing the clay friction angle or cohesion to zero could significantly change the results. Furthermore, the pipes do not appear to affect the swelling behavior or resulting swell pressures. It should also be noted that the similarities between Box Tests 1-3 and Box Test 4, where Box Test 4 is modeled after retrofitting, is most likely due to how the swell model is defined. Because the swell model is based on a swell curve calculated from separate laboratory tests starting at an unsaturated state and ending in a saturated state, it does not take into account the changes in water content as they occur in the box.

Therefore, a two-phase flow model may provide different results because the changes in water content is modeled as saturation occurs.

4.5 Feasibility

Part of this study is to determine the feasibility of using crumb rubber as an alternative fill material. To do so, the amount of crumb rubber needed for fill in an average size house was compared to the amount of sand that would be needed for a house of the same size. The average single-family house size was found through the United States Census Bureau from August 2015 [42]. Using this data, the average size home is approximately 2,467 ft^2. Assuming the average size house is single story and that the basement is the same footprint of the superstructure, the outside dimensions would be approximately 50 ft x 50 ft. For this analysis, it is assumed that 3 feet of soil would typically be excavated away from the perimeter of the foundation. It is also assumed that the basement walls extend 10 feet below the ground surface. A schematic can be seen below in Figure 72.

Figure 72. Full Scale Basement Schematic

Using these dimensions would result in approximately 4500 ft^2 of wall area for the basement, and 9500 ft^3 of excavation area (not including the excavation for the basement itself). Using a 1:6 backfill to total height ratio, then approximately 5355 box footprints (with each footprint being 11" x 11") would be needed to cover the entire surface area of the basement walls. Therefore, approximately 2250 ft^3 of rubber would be needed to surround the foundation. Using this value and the density of 34 lb/ft^3 (550 kg/m^3), approximately 76500 pounds of rubber would be necessary. At the time of this analysis, the company from which the crumb rubber was initially purchased had gone out of business. Therefore, other companies selling the same or similar products were compared for pricing. The price averaged approximately $610 for a one ton bag. Neglecting shipping costs, 39 bags of crumb rubber would be needed. This would result in a cost of approximately $23330. However, it should be noted that to buy smaller bags, the price is

less per pound when comparing to the larger bag prices. If smaller bags were used, 1530 bags, each of 50 lb weight, would be needed. At a cost of $9/bag, it would cost approximately $13770 for the crumb rubber alone.

For this analysis, it is assumed that a sand backfill would have a maximum dry unit weight of 19 kN/m^3 with an optimum water content of 9% [43]. It is assumed that 90% compaction would be adequate, as in the crumb rubber analysis above. Using these values, the density would be approximately 1900 kg/m^3. Assuming 270 m^3 (9500 ft^3) would need to be excavated as explained above, approximately 513000 kg (1130970 lbs) would need to be placed. Comparing costs of three different companies in the Oklahoma City area, the average cost per ton of washed sand fill ranged from $4.75 per ton to $37.50 per ton, neglecting shipping costs. This would result in a range of $2690 to $21200 for the sand fill. Comparing these costs, using rubber is not an economical option.

Chapter 5: Conclusions

The following conclusions can be taken from this study:

1. Crumb rubber is not an adequate fill material at higher soil densities. Though the overall swell pressure is reduced using crumb rubber, at 90% compaction it is only reduced by 24% to 31%. At higher compaction percentages, it is not likely that the swelling pressure would be reduced enough to make it a suitable fill material.
2. There is a strong correlation between compaction percentage and percent reduction in swell pressure, with an R^2 value of 0.9918. Using this correlation and extrapolating to 95% compaction, the percent reduction in swell pressure would be approximately 12% using the same 1:6 backfill to total height ratio.
3. Comparing the crumb rubber to Katti's non-swelling cohesive backfill and Ikizler's geofoam, both the non-swelling cohesive material and geofoam reduce the swelling pressure more than the crumb rubber.
4. If crumb rubber was used as a backfill material with a 1:6 backfill to total height ratio and 90% compaction, a typical house in Norman, Oklahoma would require approximately 2250 cubic feet of crumb rubber for backfill.
5. Normalizing the cost of crumb rubber and sand for the amount needed as a fill material, crumb rubber costs approximately 1.1 to 8.7 times as much as sand, depending on the sand provider. If smaller bags of crumb rubber are used, rubber costs approximately 0.7 to 5.1 times as much as sand.

Chapter 6: Recommendations and Continuing Research

Additional laboratory testing should be done to better characterize the Heiden clay. In particular, constant volume swell tests may be more appropriate for estimating the swell pressures expected in the box tests. In future calibration for the pressure sensors, it is recommended that the sensors be tested in the box with an air bladder. This should be done with a small layer of soil placed on top of the sensor while in the box and inflating the air bladder to a known pressure and comparing this known pressure to what the sensor reads. This would indicate if there are any significant value differences between the sensor readings inside and outside of the box.

It is recommended that some additional retrofits be made to the box. First, additional porous stones should be added to allow for faster and more thorough permeation. If the wall strength is of concern, smaller stones could be used in lieu of the larger 4" stones. Secondly, the aspect ratio of the box should be altered to reduce the frictional effects. Rather than an approximately 1:1 (height to length or height to width) ratio, a 1:2 or 1:3 ratio may be more effective in reducing the friction effects of the walls and thus produce more reasonable swelling pressures. If the box dimensions are kept as is, it is recommended that a steel strap be used around the box during compaction so that higher compaction percentages can be tested to simulate more realistic field conditions. Additionally, greasing the walls or other friction reducing measures should be taken to reduce the frictional effects as much as possible.

It is not recommended that crumb rubber be used as an alternative backfill material. This is due to the following reasons. One, using the 1:6 ratio used in this study, the percent reduction for 95% compaction would only be about 12%. If potential structures are being built in a highly plastic clay, this amount of reduction will most likely not be adequate. Two, to achieve a higher reduction in swell pressure, the amount of crumb rubber would need to be increased and would no longer be economical. Three, normalized for the amount of material needed, crumb rubber is on average more expensive than a typical sand backfill and therefore is not economically feasible. For these reasons, it is recommended to not use crumb rubber as a fill material unless used in a clay with low plasticity, and thus lower swelling pressures. However, though crumb rubber may not be economical, tire chips may be a viable option using the same ratios presented in this study. In the bench scale tests, tire chips would have scale effects and therefore were not used, but in real world applications may be a cheaper alternative.

To continue the finite difference modeling, it is recommended that a two-phase flow model be completed and compared to the 'swell' model. Because the swell model is based on swell curves completed in separate laboratory tests and not the changes in water content, a two-phase flow model may provide a different perspective on how the soil undergoes changes as water is added to the system.

For this project, there are five main aspects of research that should be carried on to gain a better understanding of using recycled materials as a backfill material. The following are suggested facets of the research to improve on.

1. Test different thicknesses of crumb rubber with various compaction percentages. Additionally, crumb rubber could be placed in both the horizontal and vertical faces to see how the vertical fill affects the overall reduction.
2. Test different recycled materials in the box testing setup that may be suitable fill materials. Some possible recycled materials have been introduced as part of this research, but were unable to be tested in the box testing setup due to time constraints. Additional materials should be tested with different thicknesses, as well as different soil compaction percentages.
3. Test different clays with varying physical properties with crumb rubber as a fill material. Additionally, test different clays with other recycled materials.
4. Test the crumb rubber mixed with the soil to determine if the crumb rubber reduces the swelling pressure or swelling percentage of the soil.
5. Continue the finite difference modeling and calibrate the model with various recycled materials, fill thicknesses, compaction percentages, and constitutive models. Furthermore, the model should eventually be implemented in 3D modeling programs to compare the difference between 2D and 3D results.

References

[1] R. M. Brooks, "Soil Stabilization With Flyash and Rice Husk Ash," *International Journal of Research and Reviews in Applied Sciences,* vol. 1, no. 3, December 2009.

[2] O. Rendon-Herrero, "Special Issue on Construction on Expansive Soils," *Journal of Performance of Constructed Facilities,* vol. 25, no. 1, pp. 2-4, February 2011.

[3] D. Mockbee and J. Jones, "Engineer's Legal Exposure for Facilities Built on Expansive Soils," *Journal of Performance of Constructed Facilities,* vol. 25, no. 1, pp. 7-17, February 2011.

[4] Y. Erzin and O. Erol, "Correlations for Quick Prediction of Swell Pressures," *Electronic Journal of Geotechnical Engineering,* vol. 9, no. Bundle F, 2004.

[5] International Code Council, *2012 International Building Code*, Country Club Hills, 2012.

[6] A. Al-Rawas, A. Hago and H. Al-Sarmi, "Effect of lime, cement and Sarooj (artificial pozzolan) on the swelling potential of an expansive soil from Oman," *Building and Environment,* vol. 40, pp. 681-687, 2005.

[7] J. H. Beeghly, "Recent Experiences with Lime - Fly Ash Stabilization of Pavement Subgrade Soils, Base, and Recycled Asphalt," in *International Ash Utilization Symposium*, Lexington, 2003.

[8] E. Cokca, V. Yazici and V. Ozaydin, "Stabilization of Expansive Clays Using Granulated Black Furnace (GBFS) and GBFS-Cement," *Geotechnical and Geological Engineering,* vol. 27, no. 4, pp. 489-499, August 2009.

[9] R. K. Katti, E. S. Bhangale and K. K. Moza, "Lateral Pressure in Expansive Soil With and Without a Cohesive Non-Swelling Soil Layer - Application to Earth Pressures on Cross Drainage Structures in Canals and Key Walls in Dams," Central Board of Irrigation and Power, New Delhi, March 1983.

[10] A. F. Elragi, "Selected Engineering Properties and Applications of EPS Geofoam," State University of New York, Syracuse, December 2000.

[11] S. B. Ikizler, M. Aytekin and E. Nas, "Laboratory Study of Expanded Polystyrene (EPS) Geofoam Used With Expansive Soils," *Geotextiles and Geomembranes,* vol. 26, no. 2, pp. 189-195, 2008.

[12] M. Attom, T. Khedaywi and S. A. Mousa, "The Effect of Shredded Waste Tire on the Shear Strength, Swelling and Compressibility Properties of the Clayey Soil," *Journal of Solid Waste Technology and Management,* vol. 33, no. 4, pp. 219-227, 2007.

[13] L. C. Heyer, "Swell, Stiffness and Strength of Expansive Soil-Rubber (ESR) Mixtures at Various Scales: Effect of Specimen and Rubber Particle Sizes," Colorado State University, Fort Collins, 2012.

[14] A. J. Graettinger, P. W. Johnson, P. Sunkari, M. C. Duke and J. Effinger, "Recycling of plastic bottles for use as a lightweight geotechnical material," *Management of Environmental Quality: An International Journal,* vol. 16, no. 6, pp. 658-669, 2005.

[15] M. M. Disfani, A. Arulrajah, M. W. Bo and R. Hankour, "Recycled crushed glass in road work applications," *Waste Management,* vol. 31, no. 11, pp. 2341-2351, 2011.

[16] B. Sapaz, "Lateral Versus Vertical Swell Pressures in Expansive Soils," Middle East Technical University, Ankara, 2004.

[17] J. Powell, G. Siemens, W. Take and V. Remenda, "Characterizing the Swelling Potential of Bearpaw Clayshale," *Engineering Geology,* vol. 158, pp. 89-97, 2013.

[18] A. Rao, B. Phanikumar and R. Sharma, "Prediction of Swelling Characteristics of Remoulded and Compacted Expansive Soils Using Free Swell Index," *Quarterly Journal of Engineering Geology and Hydrogeology,* vol. 37, no. 3, pp. 217-226, 2004.

[19] J. S. C. Mbagwu, "Evaluation of Shrink-Swell Potential of Soils by Two Procedures," *Pedologie,* vol. 42, no. 1, pp. 69-82, 1992.

[20] C.-H. Tsai, "Correlations of swell potential of a clay with pre-test environments, soil suction and physical properties," University of Texas at Arlington, Arlington, 1993.

[21] A. L. Sargeant, "The Application of Post-Consumer Glass as a Cementing Agent in Mine Backfill," Queen's University, Kingston, 2008.

[22] J. Wartman, M. F. Natale and P. M. Strenk, "Immediate and time-dependent compression of tire derived aggregate," *Journal of Geotechnical and Geoenvironmental Engineering,* vol. 133, no. 3, pp. 245-256, 2007.

[23] A. Mladenovic, J. Turk, J. Kovac, A. Mauko and Z. Cotic, "Environmental evaluation of two scenarios for the selection of materials for asphalt wearing courses," *Journal of Cleaner Production,* vol. 87, pp. 683-691, 2015.

[24] S. Olsson, E. Karrman and J. P. Gustafsson, "Environmental systems analysis of the use of bottom ash from incineration of municipal waste for road construction," *Resources, Conservation and Recycling,* vol. 48, no. 1, pp. 26-40, 2006.

[25] C. J. Engelsen, G. Wibetoe, H. A. van der Sloot, W. Lund and G. Petkovic, "Field site leaching from recycled concrete aggregates applied as sub-base material in road construction," *Science of the Total Environment,* Vols. 427-428, pp. 86-97, 2012.

[26] M. A. Imteaz, M. Y. Ali and A. Arulrajah, "Possible environmental impacts of recycled glass used as a pavement base material," *Waste Management and Research,* vol. 30, no. 9, pp. 917-921, 2012.

[27] M. M. Disfani, A. Arulrajah, M. W. Bo and N. Sivakugan, "Environmental risks of using recycled crushed glass in road applications," *Journal of Cleaner Production,* vol. 20, no. 1, pp. 170-179, 2012.

[28] B. Ruffino, S. Fiore and M. C. Zanetti, "Environmental - sanitary risk analysis procedure applied to artificial turf sports field," *Environmental Science and Pollution Research Journal,* vol. 20, no. 7, pp. 4980-4992, 2013.

[29] R. K. Goswami and C. Mahanta, "Leaching characteristics of residual lateritic soils stabilised with fly ash and lime for geotechnical applications," *Waste Management,* vol. 27, no. 4, pp. 466-481, 2007.

[30] K. Komonweeraket, "Leaching from soil stabilized with fly ash: behavior and mechanisms," University of Wisconsin-Madison, Madison, 2010.

[31] S. K. Bhatia and R. M. Bakeer, "Use of the Finite Element Method in Modelling a Static Earth Pressure Problem," *International Journal for Numerical and Analytical Methods in Geomechanics,* vol. 13, no. 2, pp. 207-213, 1989.

[32] R. Karpurapu and R. J. Bathurst, "Behaviour of Geosynthetic Reinforced Soil Retaining Walls Using the Finite Element Method," *Computer and Geotechnics,* vol. 17, no. 3, pp. 279-299, 1995.

[33] D. Loukidis and R. Salgado, "Active pressure on gravity walls supporting purely frictional soils," *Canadian Geotechnical Journal,* vol. 49, no. 1, pp. 78-97, 2012.

[34] K.-H. Yang and C.-N. Liu, "Finite Element Analysis of Earth Pressures for Narrow Retaining Walls," *Journal of GeoEngineering,* vol. 2, no. 2, pp. 43-52, 2007.

[35] T. Pichler, T. Pucker, T. Hamann, S. Henke and G. Qiu, "High-Performance Abaqus Simulations in Soil Mechanics Reloaded - Chances and Frontiers," in *SIMULIA Community Conference*, Providence, 2012.

[36] U. Contreras, G. Li, C. D. Foster, A. A. Shabana, P. Jayakumar and M. D. Letherwood, "Review of Soil Models and Their Implementation in Multibody System Algorithms," University of Illinois at Chicago, Chicago, 2012.

[37] C. Phillips and Y. M. Hashash, "A simplified constitutive model to simultaneously match modulus reduction and damping soil curves for nonlinear site response analysis," in *Geotechnical Earthquake Engineering and Soil Dynamics IV*, Sacramento, 2008.

[38] R. J. Brinkgreve, "Selection of Soil Models and Parameters for Geotechnical Engineering Application," in *GeoFrontiers 2005,* Austin, 2005.

[39] K. S. Ti, B. B. Huat, J. Noorzaei, M. S. Jaafar and G. S. Sew, "A Review of Basic Soil Constitutive Models for Geotechnical Application," *Electronic Journal of Geotechnical Engineering*, vol. 14, no. Bundle J, pp. 1-18, 2009.

[40] B. Lin, "A Comprehensive Investigation on Microscale Properties and Macroscopic Behavior of Natural Expansive Soils," University of Oklahoma, Norman, 2012.

[41] I. Noorany, S. Frydman and C. Detournay, "Prediction of soil slope deformation due to wetting," in *FLAC and Numerical Modeling in Geomechanics*, Rotterdam, 1999.

[42] United States Census Bureau, "Characteristics of New Housing," 1 June 2016. [Online]. Available: https://www.census.gov/construction/chars/highlights.html. [Accessed 26 July 2016].

[43] J. P. Stewart, E. Taciroglu, J. W. Wallace, A. Lemnitzer, C. H. Hilson, A. Nojoumi, S. Keowen, R. L. Nigbor and A. Salamanca, "Nonlinear Load-Deflection Behavior of Abutment Backwalls with Varying Height and Soil Density," University of California, Los Angeles, Los Angeles, 2011.

Appendix A: FLAC Modeling

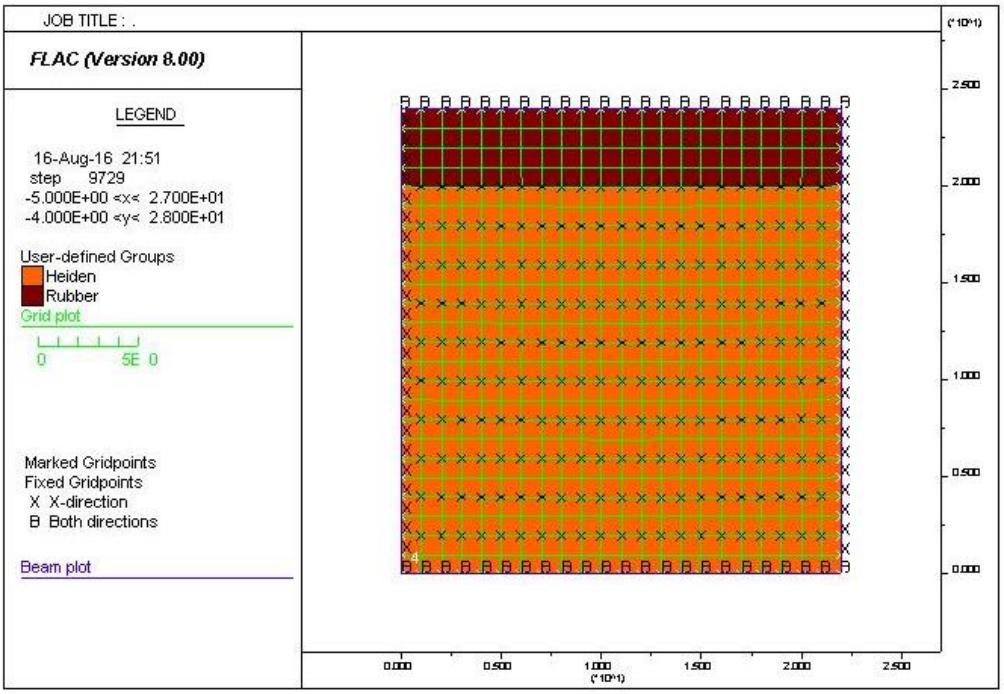

Figure 73. Box Test 1 – Initial Setup

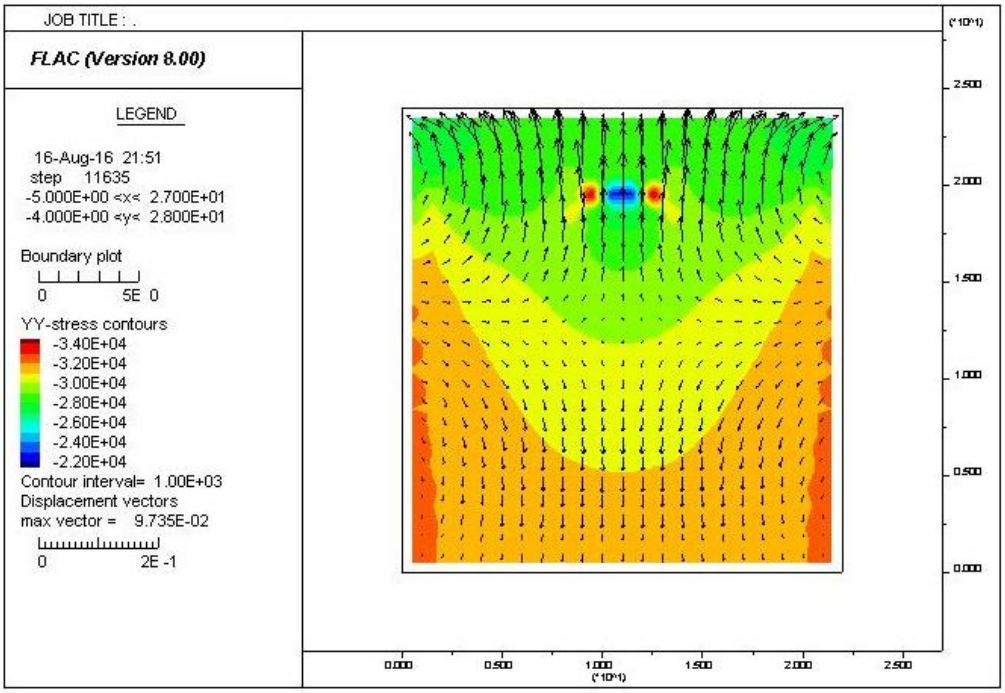

Figure 74. Box Test 1 – Y Stress Contours with Displacement Vectors

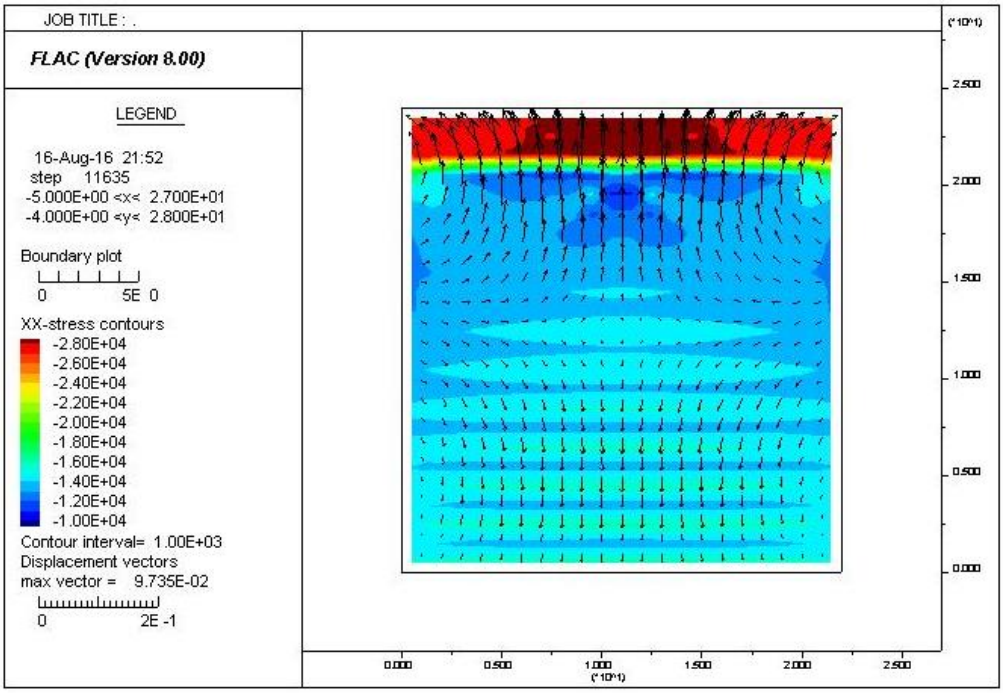

Figure 75. Box Test 1 – X Stress Contours with Displacement Vectors

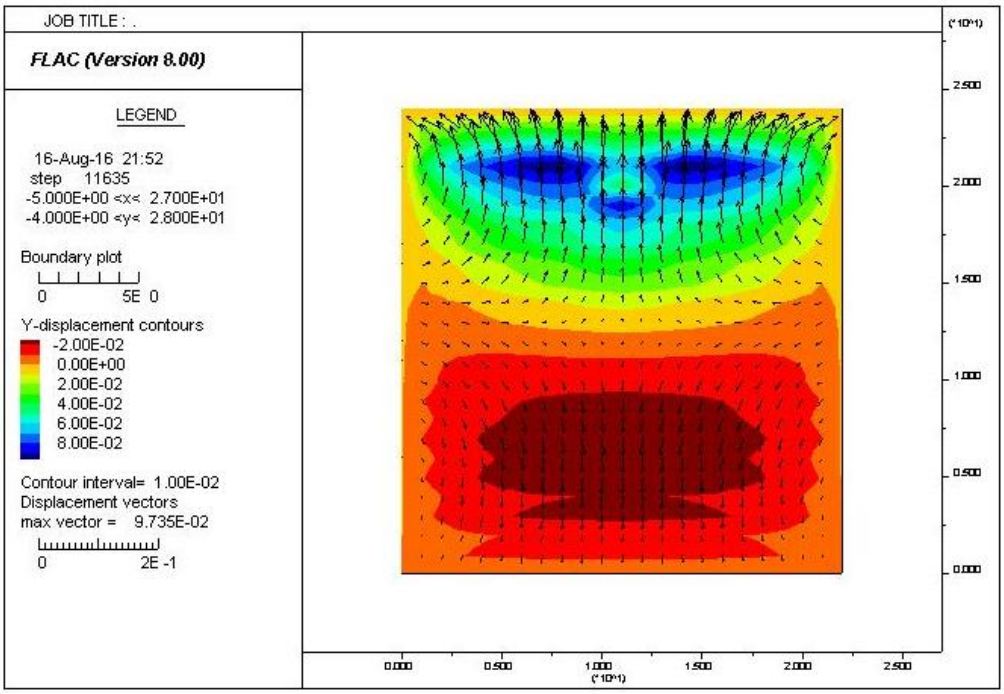

Figure 76. Box Test 1 – Y Displacement Contours with Displacement Vectors

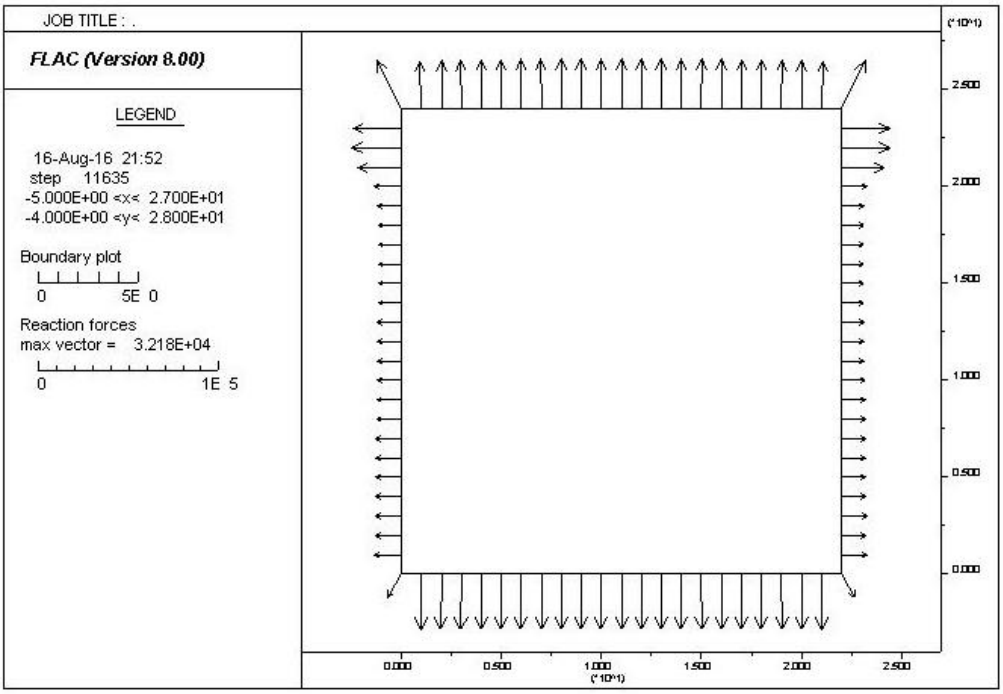

Figure 77. Box Test 1 – Reaction Forces

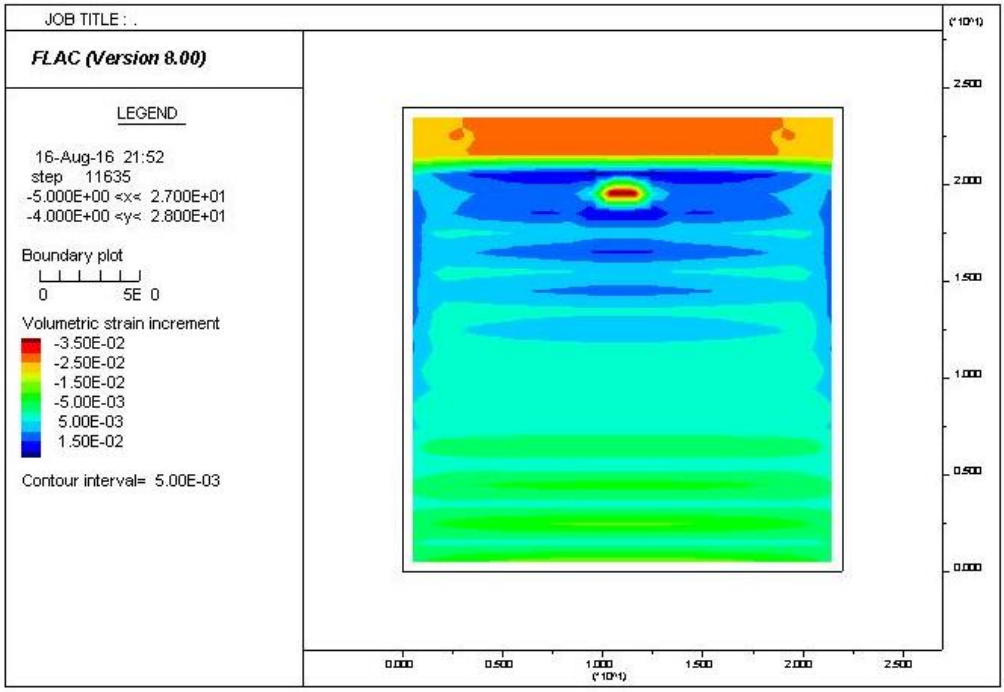

Figure 78. Box Test 1 – Accumulated Volumetric Strain

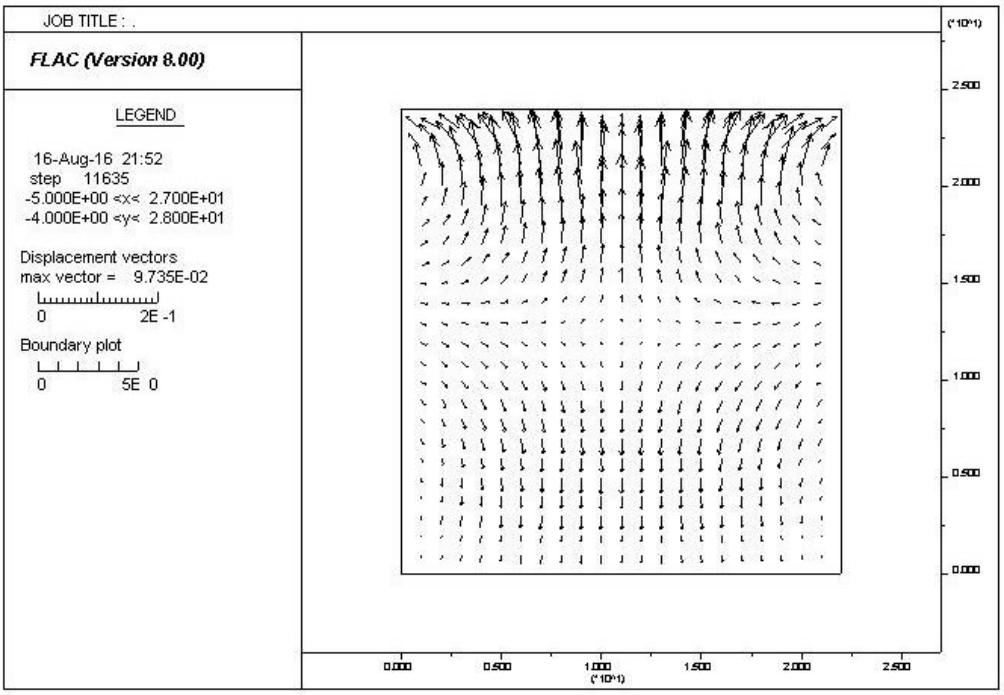

Figure 79. Box Test 1 – Displacement Vectors

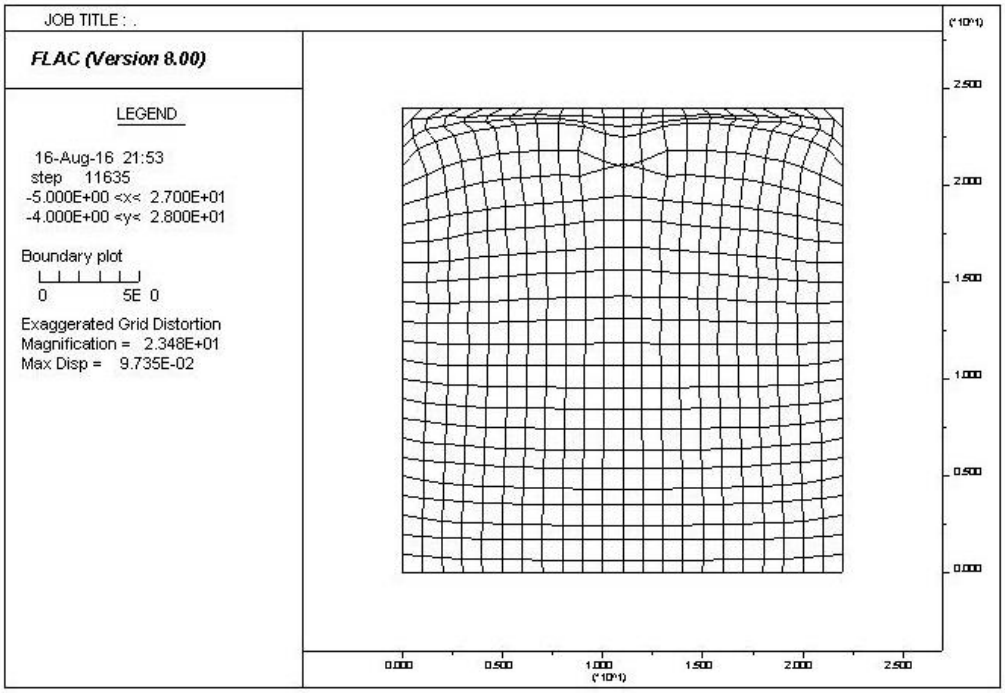

Figure 80. Box Test 1 – Magnified Grid Distortion

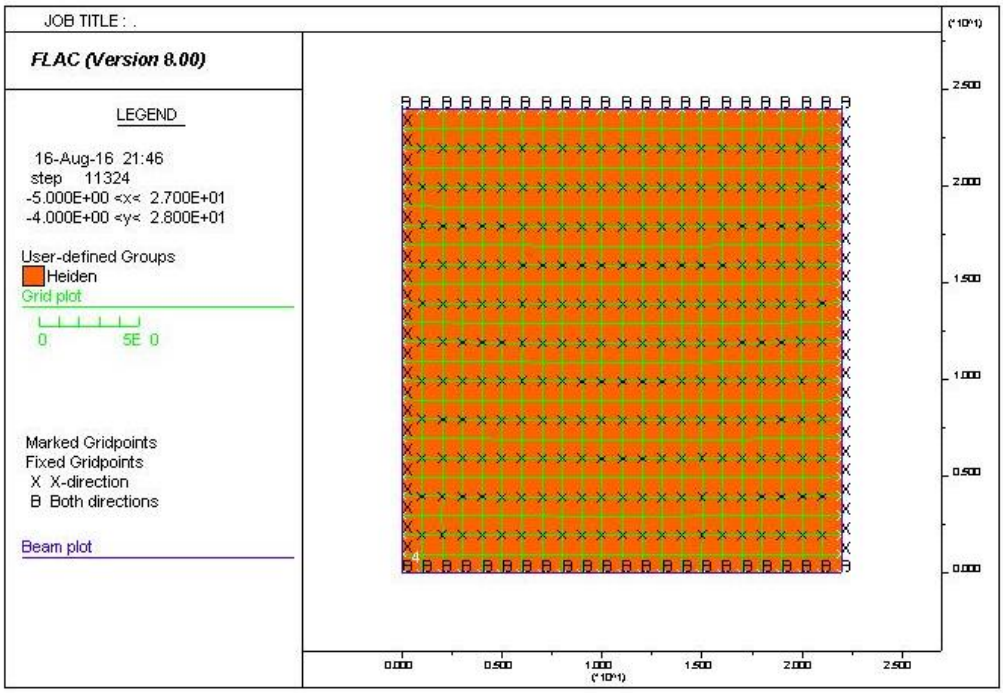

Figure 81. Box Test 2 – Initial Setup

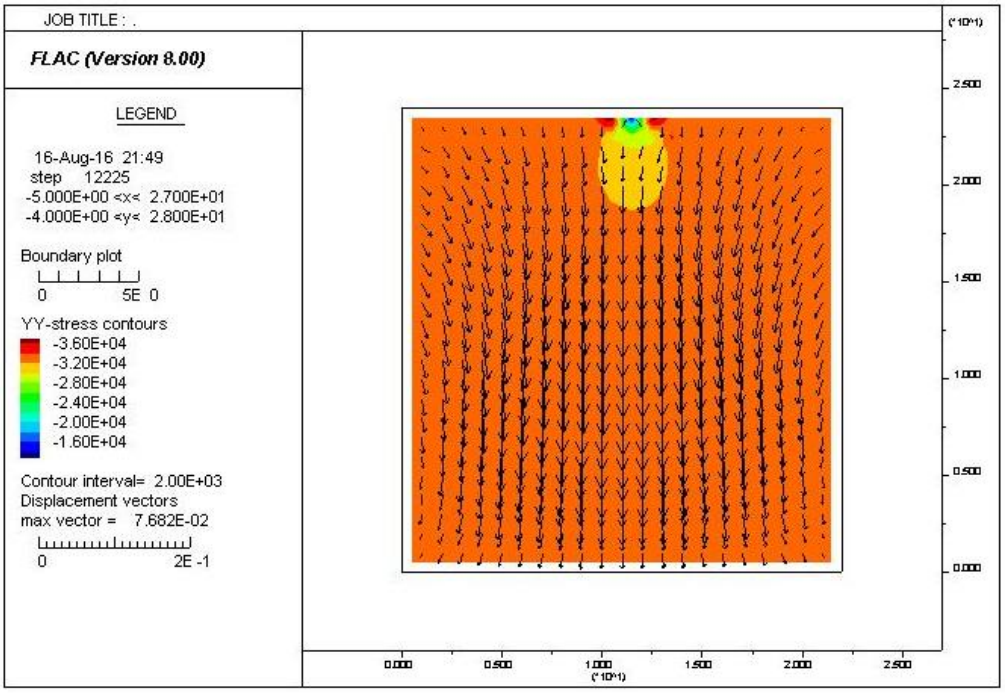

Figure 82. Box Test 2 – Y Stress Contours with Displacement Vectors

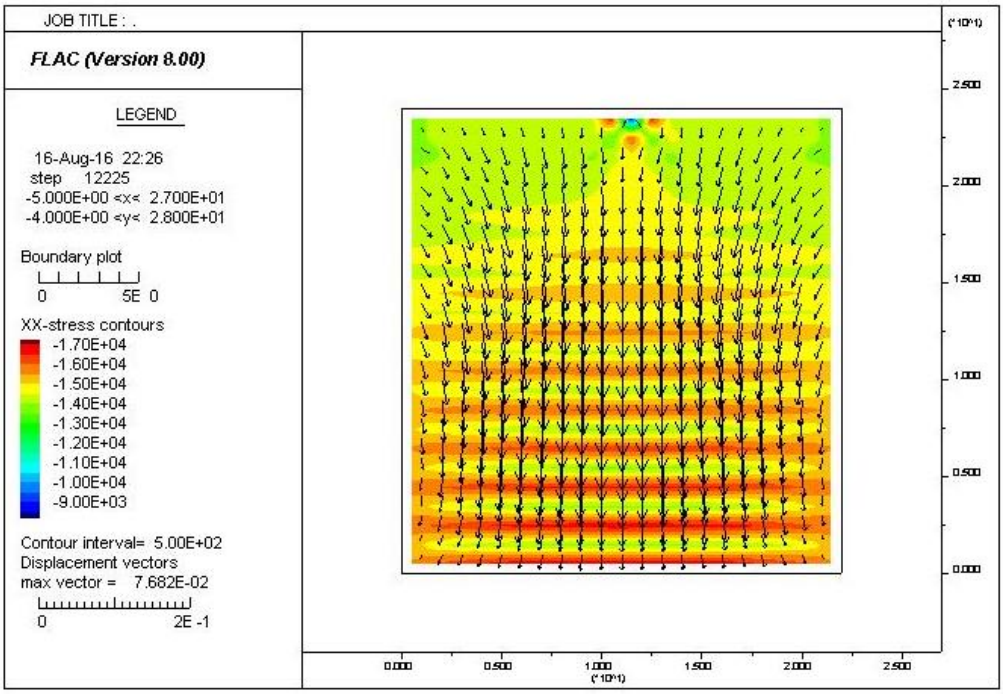

Figure 83. Box Test 2 – X Stress Contours with Displacement Vectors

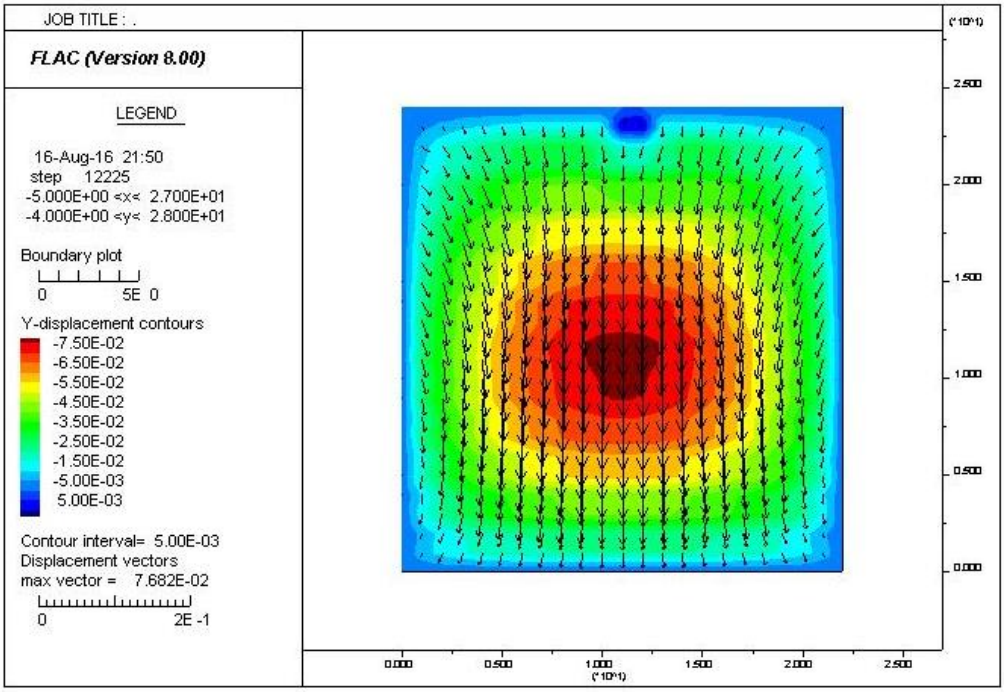

Figure 84. Box Test 2 – Y Displacement Contours with Displacement Vectors

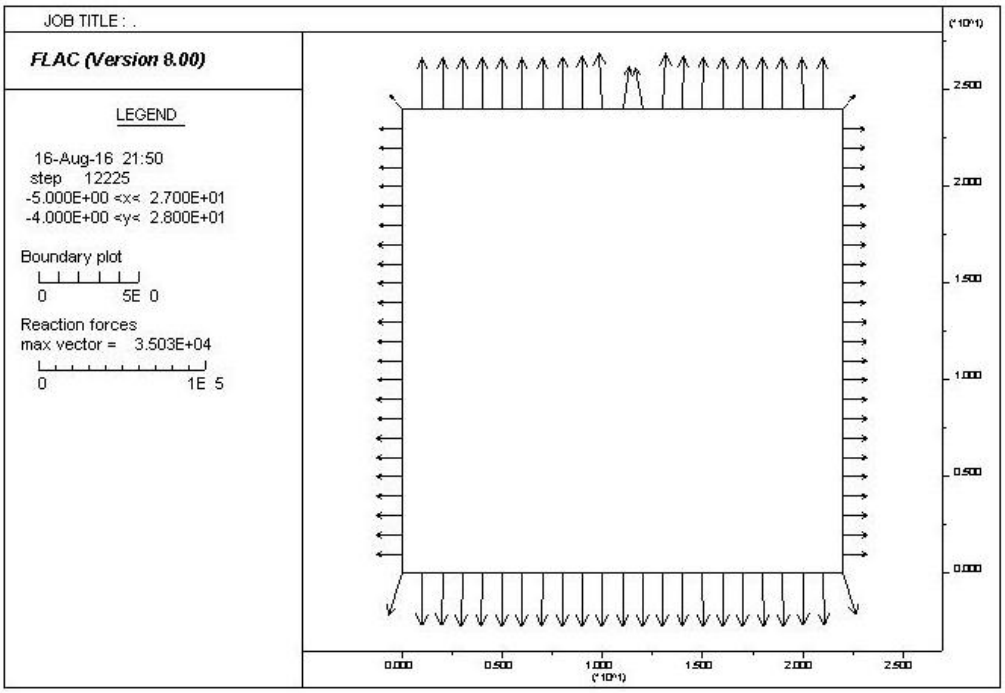

Figure 85. Box Test 2 – Reaction Forces

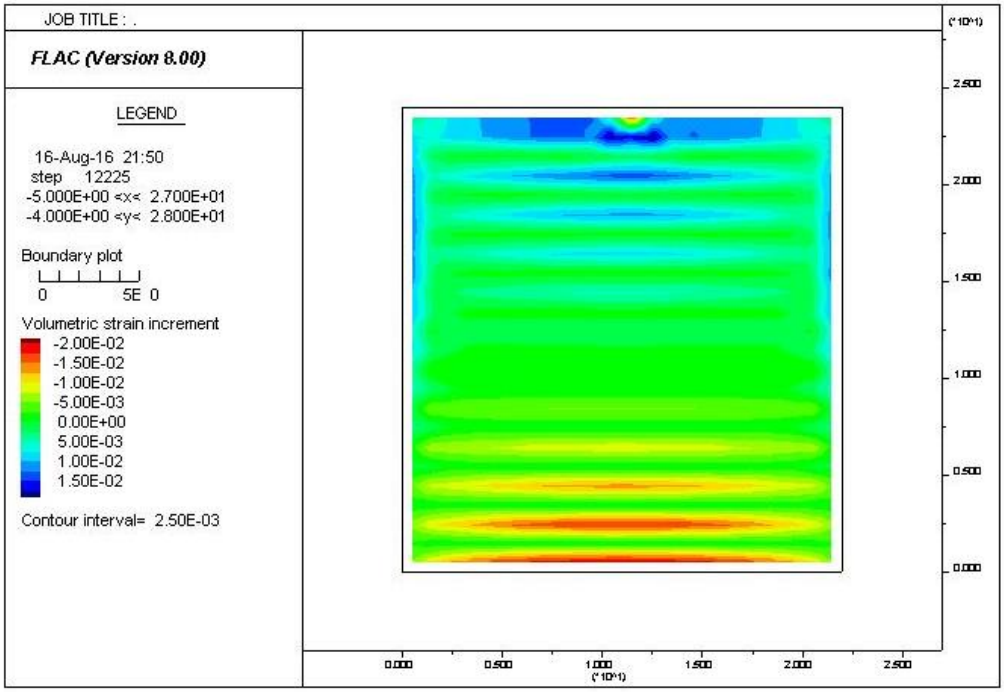

Figure 86. Box Test 2 – Accumulated Volumetric Strain

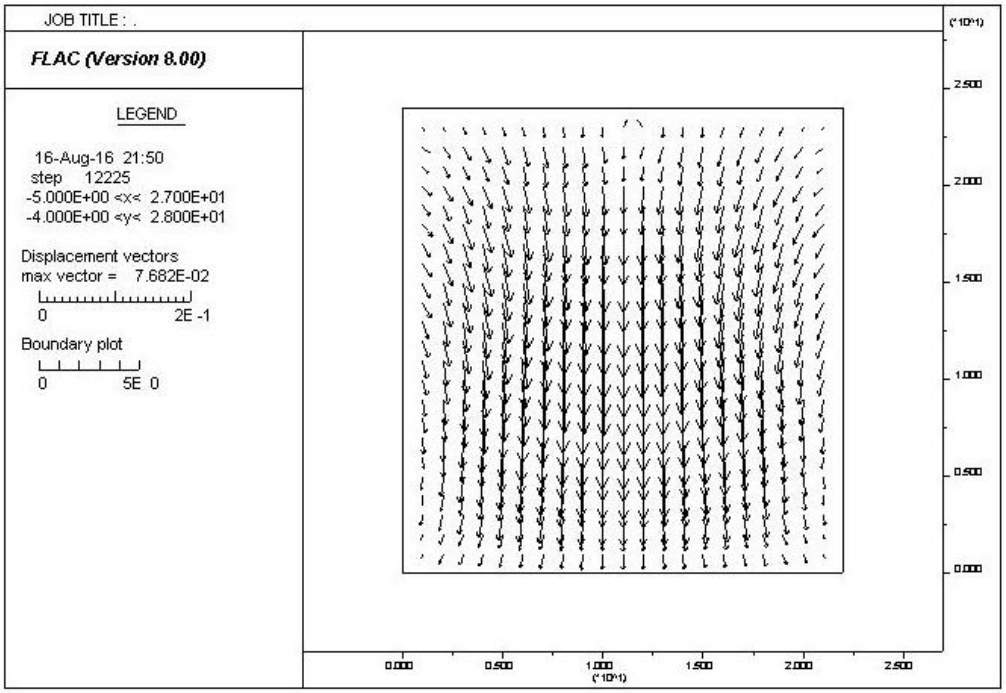

Figure 87. Box Test 2 – Displacement Vectors

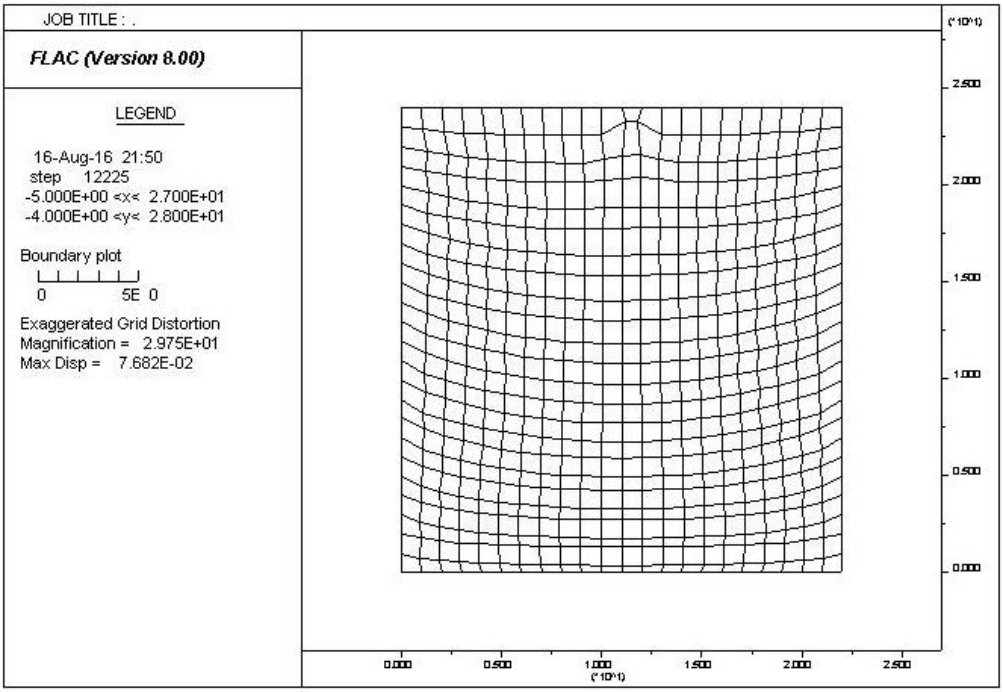

Figure 88. Box Test 2 – Magnified Grid Distortion

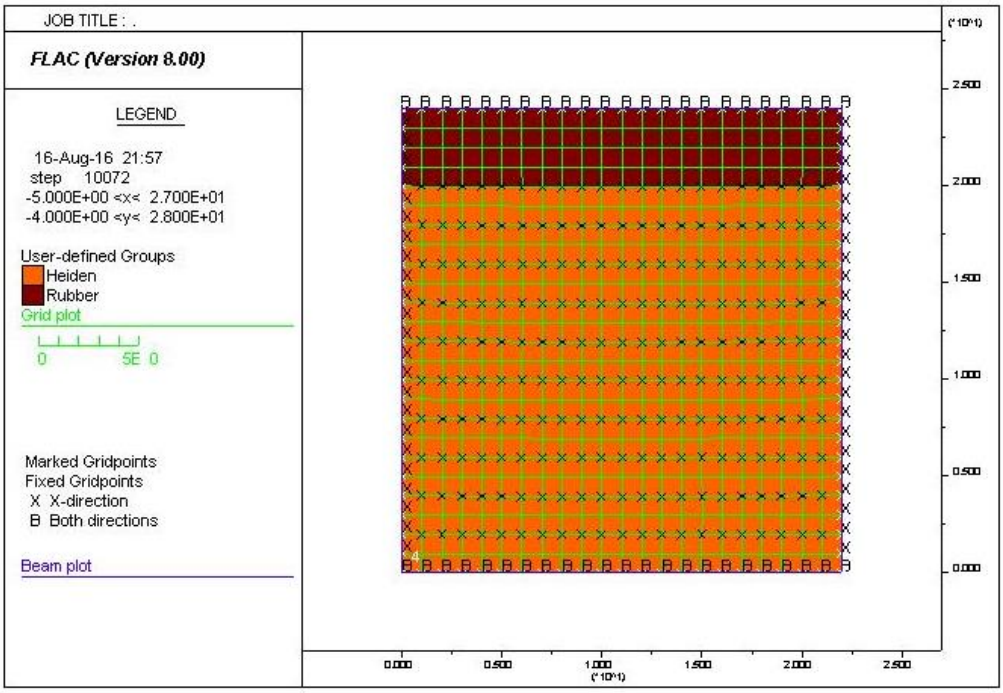

Figure 89. Box Test 3 – Initial Setup

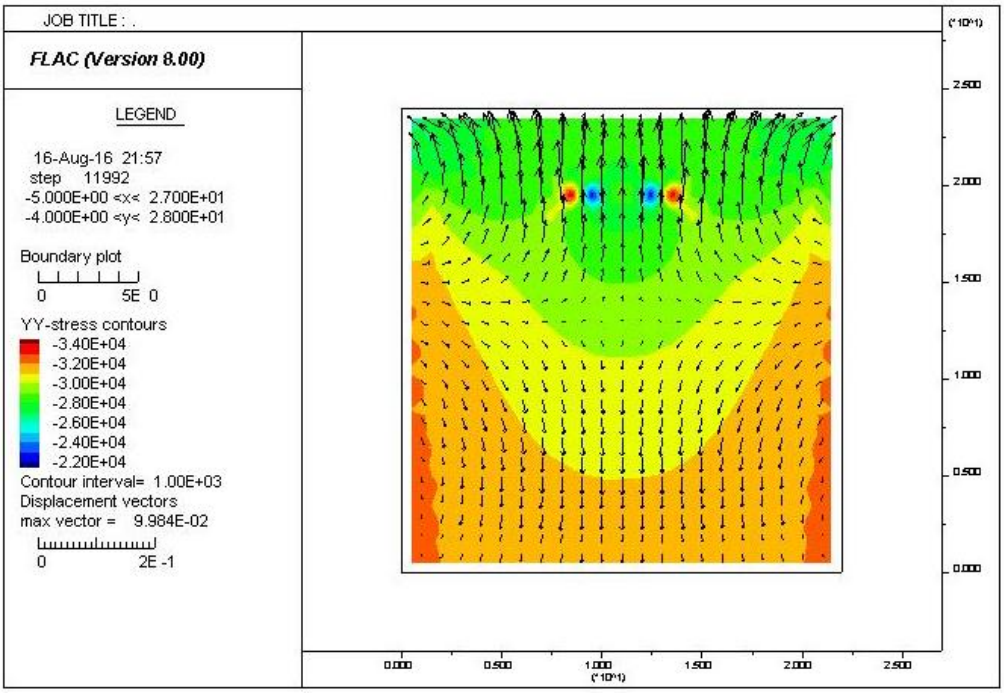

Figure 90. Box Test 3 – Y Stress Contours with Displacement Vectors

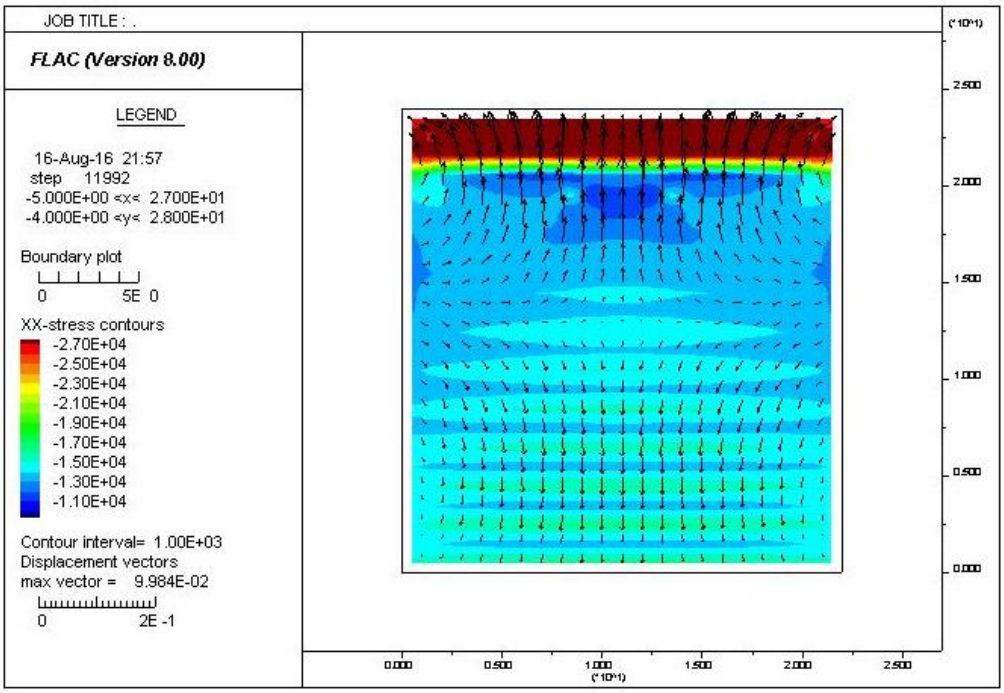

Figure 91. Box Test 3 – X Stress Contours with Displacement Vectors

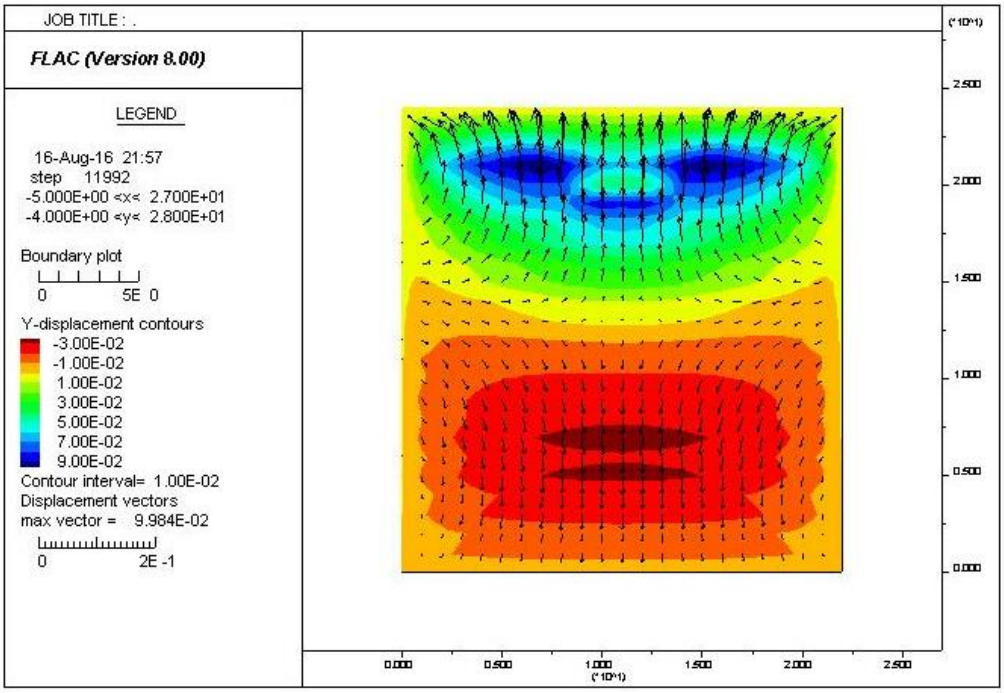

Figure 92. Box Test 3 – Y Displacement Contours with Displacement Vectors

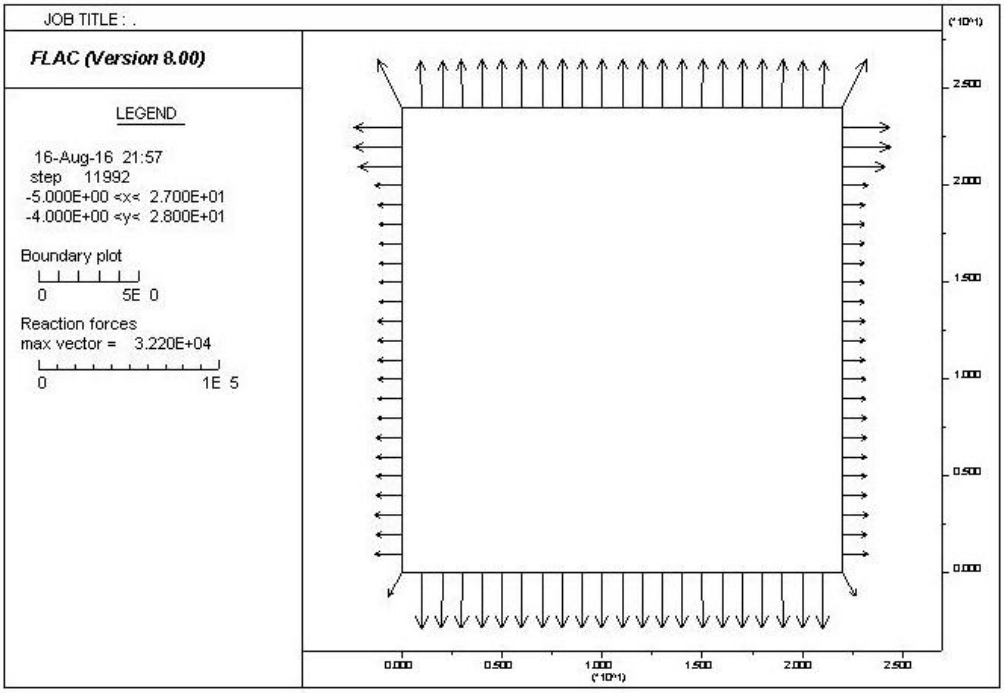

Figure 93. Box Test 3 – Reaction Forces

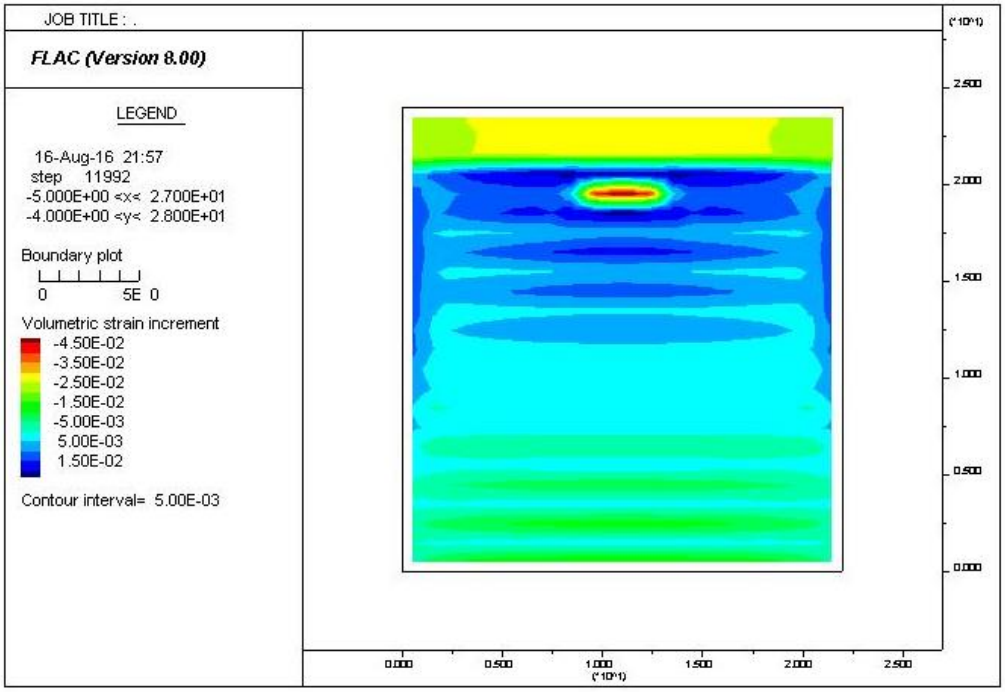

Figure 94. Box Test 3 – Accumulated Volumetric Strain

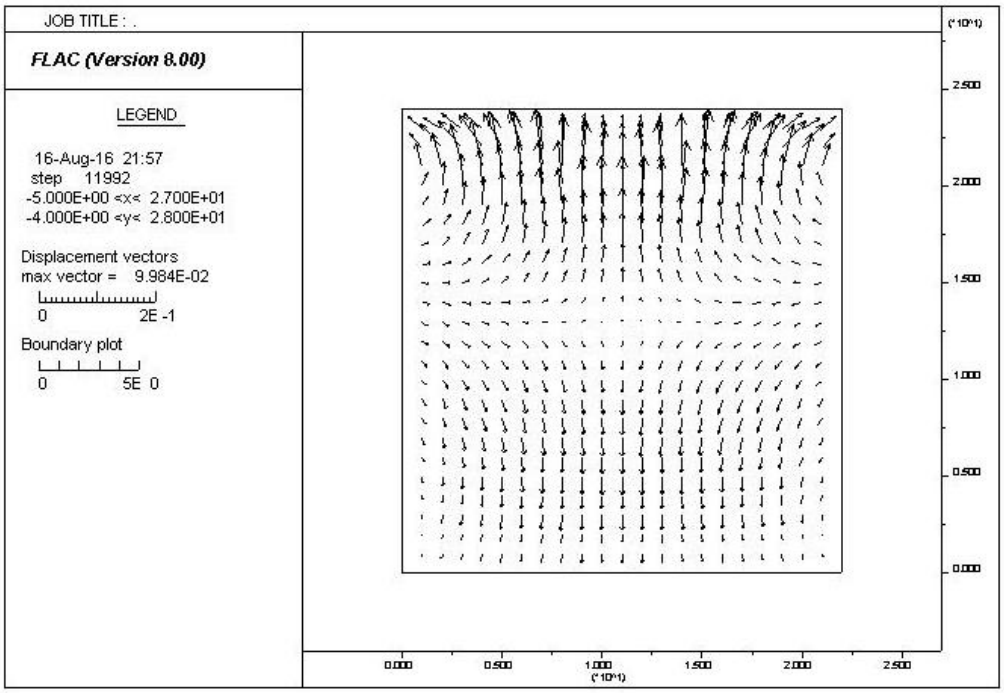

Figure 95. Box Test 3 – Displacement Vectors

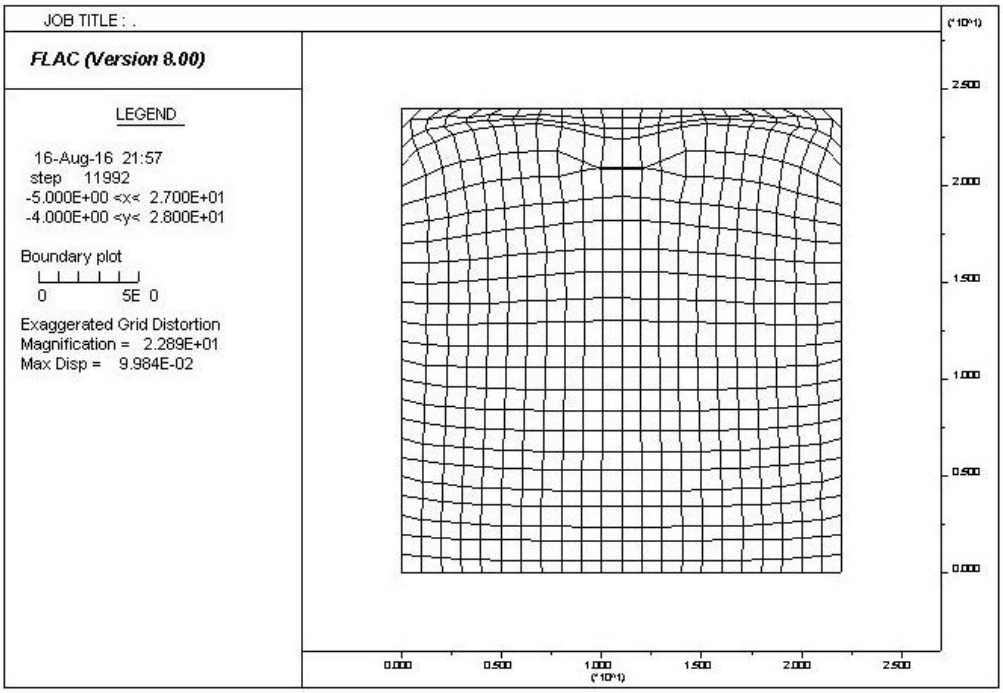

Figure 96. Box Test 3 – Magnified Grid Distortion

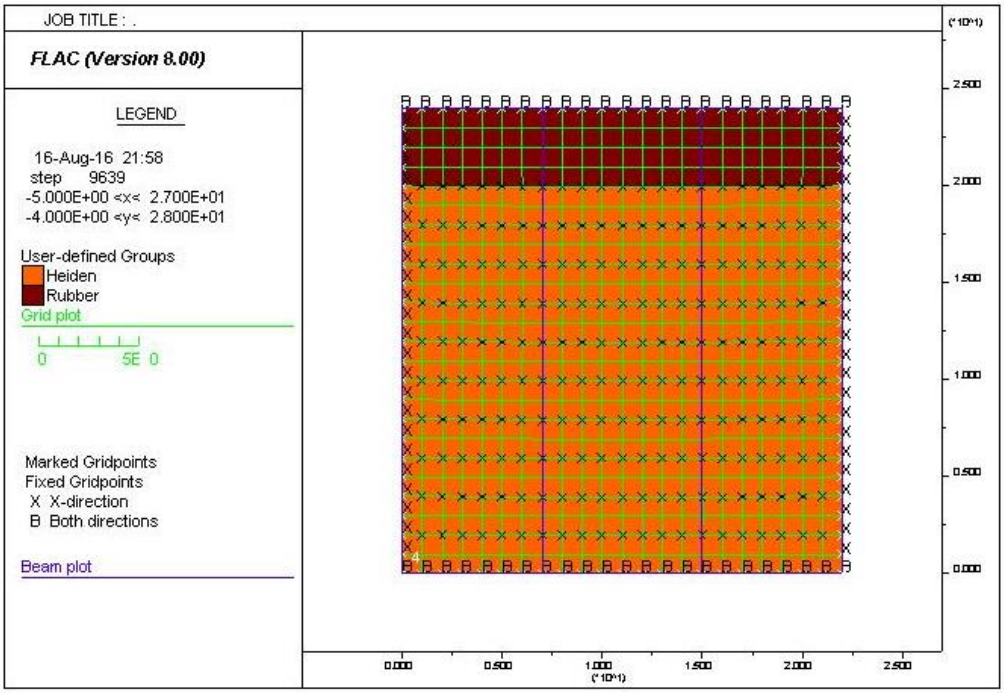

Figure 97. Box Test 4 – Initial Setup

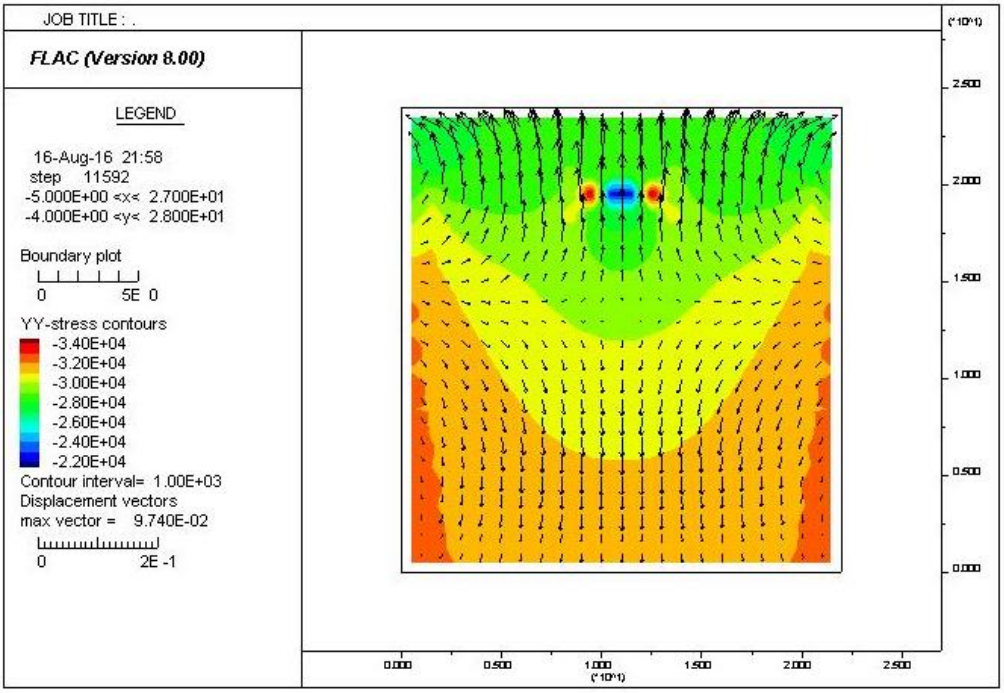

Figure 98. Box Test 4 – Y Stress Contours with Displacement Vectors

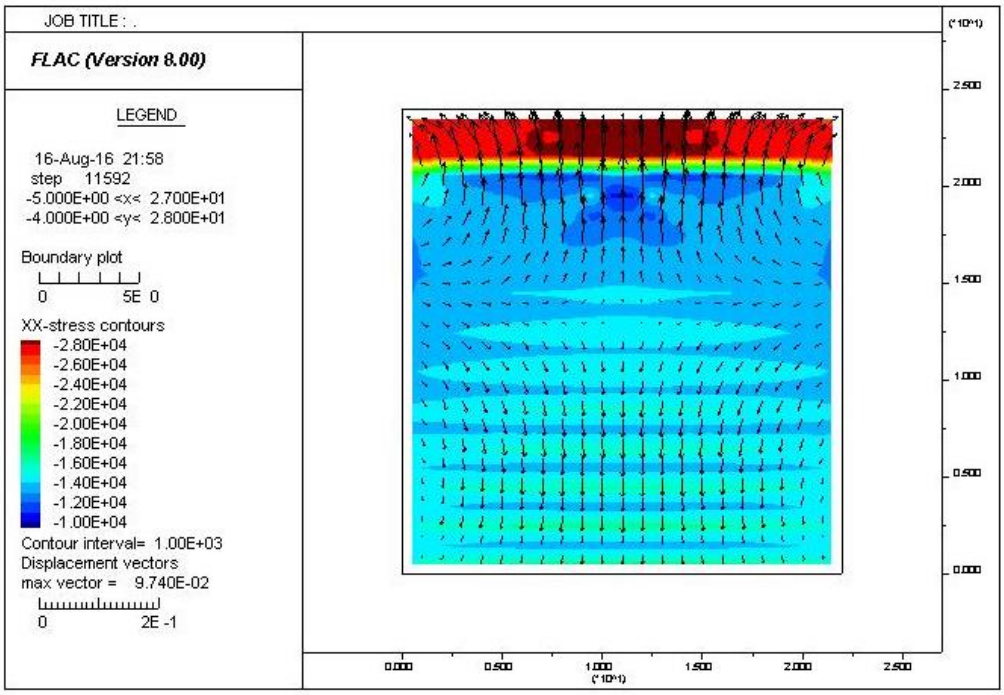

Figure 99. Box Test 4 – X Stress Contours with Displacement Vectors

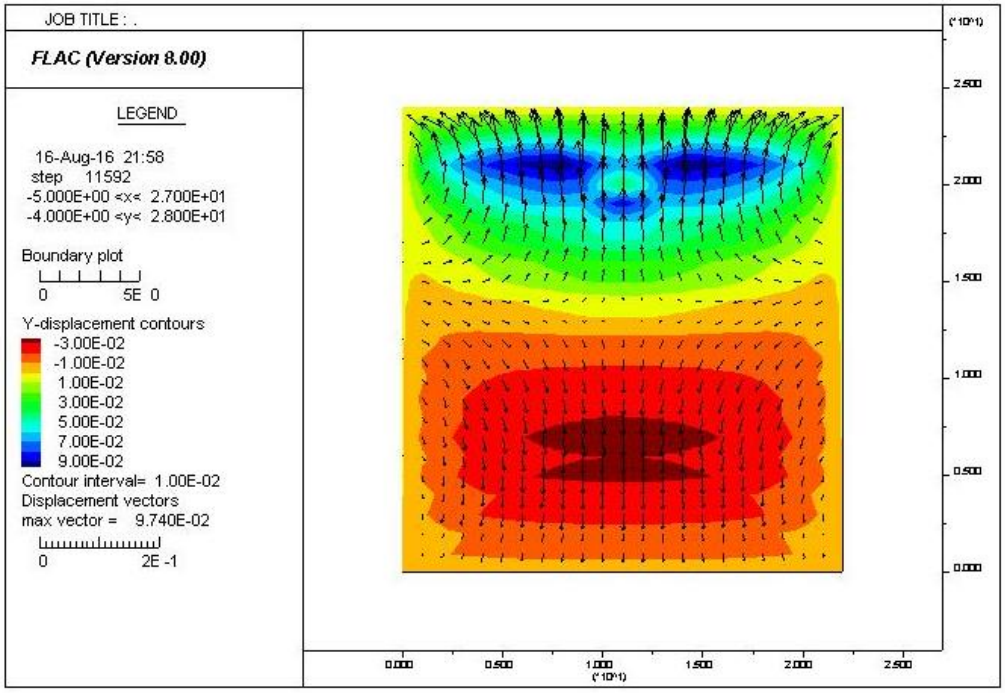

Figure 100. Box Test 4 – Y Displacement Contours with Displacement Vectors

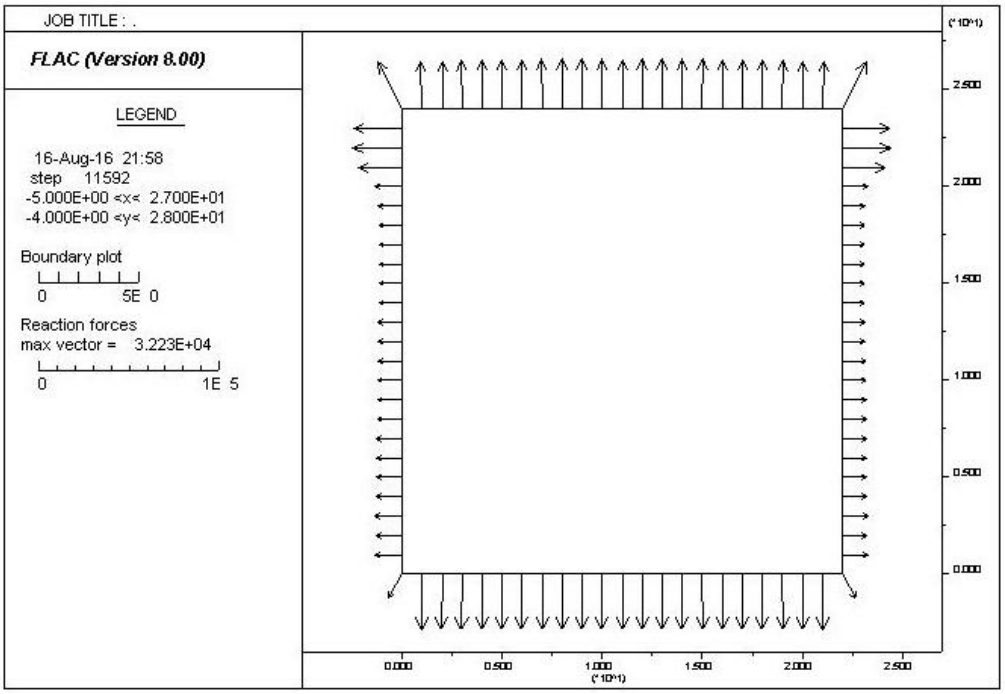

Figure 101. Box Test 4 – Reaction Forces

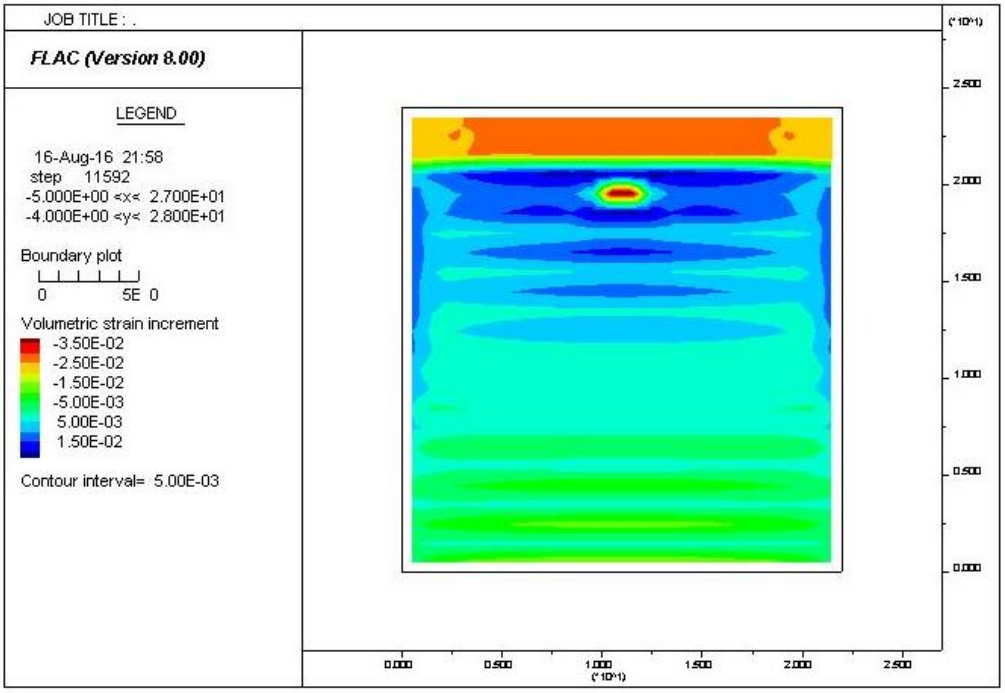

Figure 102. Box Test 4 – Accumulated Volumetric Strain

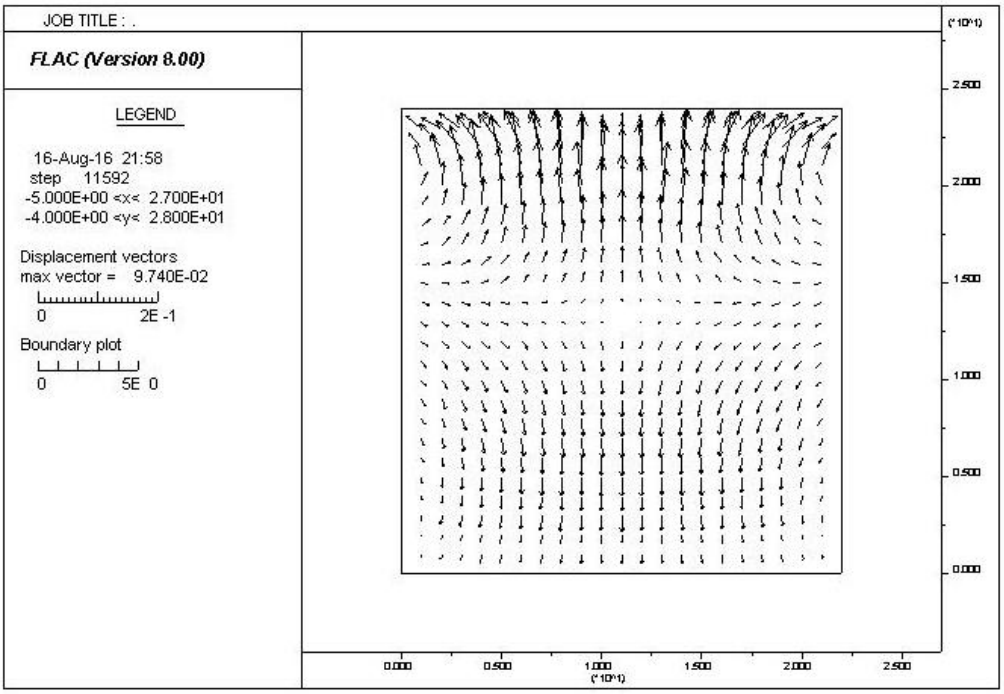

Figure 103. Box Test 4 – Displacement Vectors

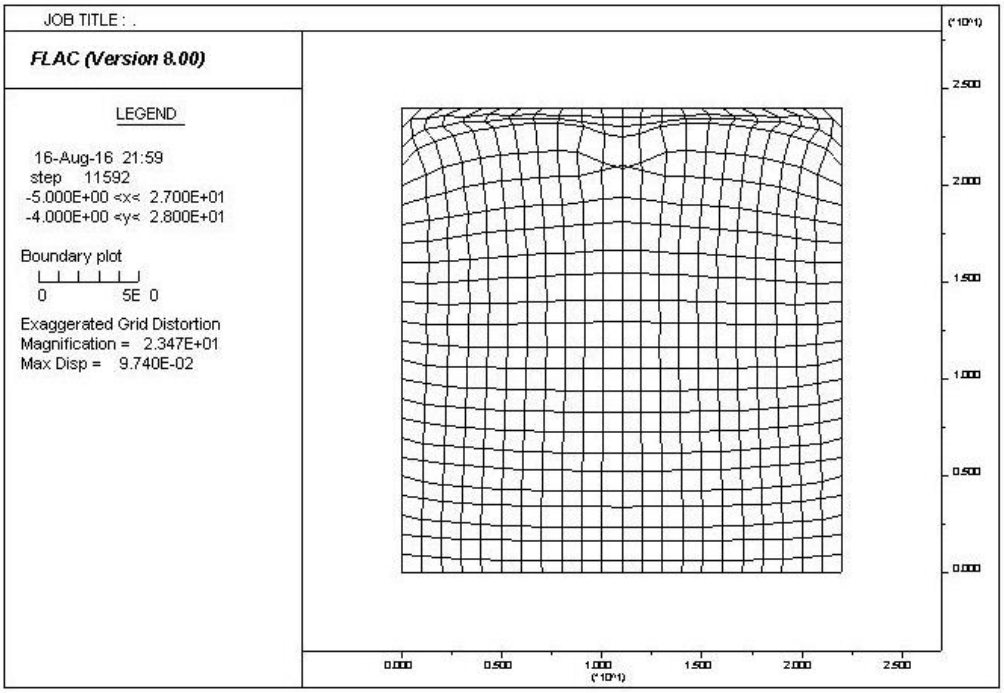

Figure 104. Box Test 4 – Magnified Grid Distortion